FLOW IN AGGREGATE - BINDER MIXES

MARCH 1969 - NUMBER 8

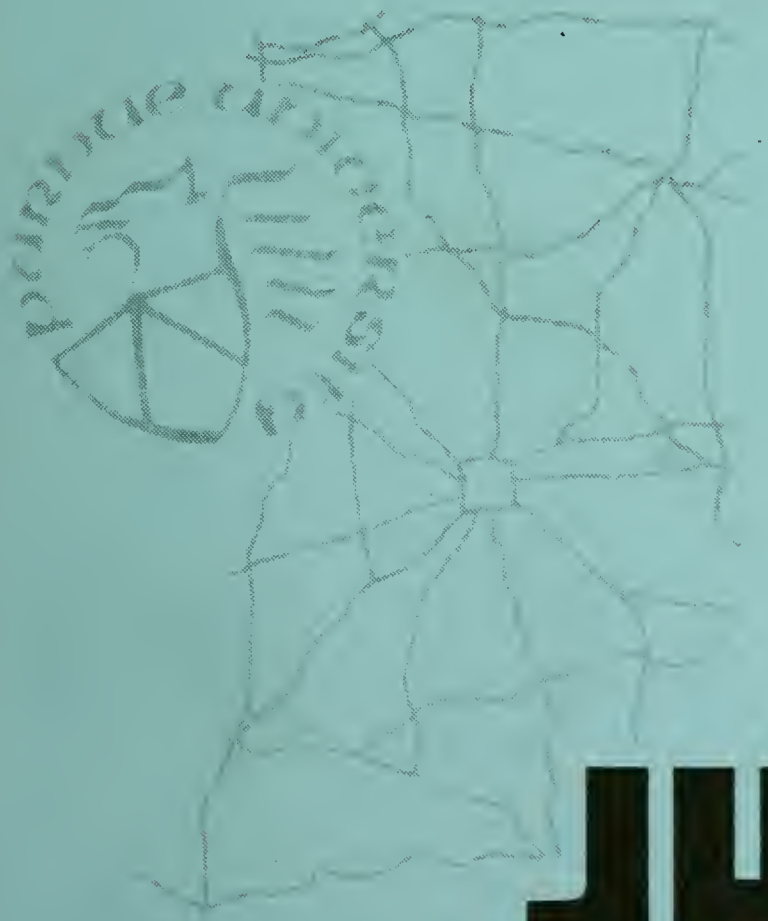

BY

EGONS TONS

JHRP

JOINT HIGHWAY RESEARCH PROJECT

PURDUE UNIVERSITY AND

INDIANA STATE HIGHWAY COMMISSION

Final Report

FLOW IN AGGREGATE - BINDER MIXES

by
Egons Tons
Graduate Instructor in Research

Joint Highway Research Project
Project: C-36-6X
File: 2-4-24

Prepared as Part of an Investigation

Conducted by

Joint Highway Research Project
Engineering Experiment Station
Purdue University

in cooperation with the

Indiana State Highway Commission

and the

U.S. Department of Transportation
Federal Highway Administration
Bureau of Public Roads

Purdue University
Lafayette, Indiana
March 21, 1969

Final Report

FLOW IN AGGREGATE - BINDER MIXES

TO: J. F. McLaughlin, Director
Joint Highway Research Project

March 21, 1969

File: 2-4-24

FROM: H. L. Michael, Associate Director
Joint Highway Research Project

Project: C-36-6X

The attached Final Report is submitted on the HPR, Part II, research project "Flow in Aggregate - Binder Mixes. The report was also used by Mr. Tons as his dissertation for the Ph.D. degree from Purdue University. Professor W. H. Goetz directed the research.

The purpose of this research was to develop concepts for a unified approach in bituminous mix design using different aggregates. The results show that the aggregate packing volume and flow asphalt concepts can be used to design mixes which behave similarly, whether they contain crushed or rounded aggregate.

The report is submitted to the Board for acceptance as fulfilling the objectives of the research project. It will also be submitted to the ISEC and the BPR for such acceptance.

Respectfully submitted,

Harold L. Michael

Harold L. Michael
Associate Director

HLM:rg
Attachment:

Copy:

F. L. Ashbaucher
W. L. Dolch
W. H. Goetz
W. L. Grecco
G. K. Hallock
M. E. Harr
R. H. Harrell
J. A. Havers
V. E. Harvey
G. A. Leonards
F. B. Mendenhall
R. D. Miles
C. F. Scholer
M. B. Scott
W. T. Spencer
H. R. J. Walsh
K. B. Woods
E. J. Yoder

ACKNOWLEDGMENTS

The author would like to acknowledge the assistance of the Bureau of Public Roads, the United States Department of Transportation, the Federal Highway Administration, and the Indiana State Highway Commission, all of whom supported this investigation.

Special thanks are due to Professor W. H. Goetz, the author's major professor, for guidance during the study and for many helpful suggestions during the writing phase. Thanks are also due to Professor V. L. Anderson for his advice in connection with the statistical design of the main experiment and the following analyses.

The author also wishes to thank the many other persons in various materials laboratories of the Purdue Civil Engineering Department who helped with measurements, data analysis, and graphing.

TABLE OF CONTENTS

TABLE OF CONTENTS (cont'd)

TABLE OF CONTENTS (cont'd)

LIST OF TABLES

LIST OF FIGURES

ABSTRACT

Tons, Egons, Ph.D., Purdue University, June 1969. Flow in Aggregate-Binder Mixes. Major Professor: William H. Goetz.

The main purpose of this research was to develop concepts for a unified approach in bituminous mix design using different aggregates. The work involved defining and measuring parameters of aggregates, analyzing the functions of asphalt, and performing laboratory experiments in the flow (non-brittle) region.

A hypothesis was proposed suggesting that aggregate gradation by packing volume instead of size is a unifying description of rock pieces. Since some types of aggregates are rounded and smooth (rounded gravel) and others are angular and rough (crushed rocks), a so-called rugosity volume was introduced to describe the roughness numerically. Packing volume of a piece of rock includes solids plus voids plus surface roughness or rugosity volume. In mix design, the rugosity is neutralized with rugosity asphalt and binding of the particles is achieved by flow asphalt.

To test the above hypothesis, three types and three sizes of rocks were used, first in dry condition and afterwards mixed with asphalt. Vibratory compaction experiments combined with tests in tension, compression, and cyclic deformation were performed and the results were evaluated by the use of regression, analysis of variance and contact area model equation. All the work was concerned with mono-volume (one-size)

rocks only. Three rates of deformation at three temperatures were used, staying largely in the flow region of mix behavior (no brittle failures).

The results show that the aggregate packing volume and flow asphalt concepts can be used to design mixes which behave similarly, whether they contain crushed or rounded aggregate. Analytic means, (using the contact area model), permit a reasonably close prediction of tensile and compressive strength. A foundation has been laid for unified mix design.

INTRODUCTION

Prediction of field service behavior of a bituminous mix on the basis of its composition or material ingredients, presents a difficult problem. In spite of this, research and experience have provided methods for practical mix designs which are adequate in most cases.

The designs used at present are essentially trial and error in nature. The type and gradation of aggregate and the asphalt grade are chosen, then a number of asphalt contents are estimated which hopefully bracket the desired optimum conditions. Next follows the making of specimens and their testing to determine the optimum mix. If the combination of ingredients does not give the specified or desired properties (stability, voids, etc.), the components in the mix have to be changed and the tests must be repeated.

At the start of this work it was assumed that there is a need for a more general or analytical approach to mix design. Such an approach should provide a quantitative and systematic means of characterizing the ingredients of a mix and should provide for predicting how the mix will respond to external forces when all of the ingredients are combined. The design should be applicable to different types of aggregates and not tied to some selected criterion such as "residual voids." Such a design approach should open the way to the formulation of a variety of mixes with controlled properties to suit varied present and future applications.

There may be several ways of solving the problem of general mix

design. Interesting and powerful statistical methods are available for exploration and optimization of multivariate systems using different levels and combinations of ingredients. In order to achieve generality, however, the variables have to be defined quantitatively. Consequently, there is no surprise in the conclusion that bulk tests and mathematical models for mix response in bulk are only valid for the particular mixes investigated unless the proper parameters of the ingredients of the mix are known quantitatively and are properly represented.

An attempt appears to be in order to measure and describe numerically the ingredients of a bituminous concrete as well as its physical structure. Since a large proportion of a mix is occupied by the aggregate phase, an important first step would be to study and define various aggregate properties singularly and in bulk. To start with, a simple, one-size system could be used with particles of such physical "size" that the defined parameters could be measured relatively easily and accurately. Next, a binder can be introduced and the mixes can be tested under defined conditions and evaluated using theories developed in the area of bituminous concrete and in the fields of other materials.

PURPOSE AND SCOPE

The specific objectives of this research were:

a. To define and measure useful mix-design parameters for aggregates.

b. To define and analyze the function of asphalt in a mix.

c. To predict test values for aggregate-asphalt mixtures from composition parameters.

The initial hypothesis involved the assumption that, in order to achieve a more uniform approach in mix design, different types of aggregate, such as crushed limestone and rounded gravel, should be graded in such a manner that under identical circumstances the number of particles and their "size" distribution would be identical in a given unit volume. When asphalt is added to rock particles, part of it will become bound to the valleys of the rock surfaces; the other part will be participating in the flow of a mix under load. The amount of the bound or stagnant asphalt should vary with different types of rocks and should permit a mix design based on similar proportions of "solid," void-filling, and flow asphalt.

The work involved a literature review on aggregates and various flow models, theoretical prediction, statistical design of an experiment, laboratory testing, and analysis and comparison of test results with preconceived models and theory. Three different rocks, three rock sizes and three asphalt film thicknesses were used. Both tension and compression tests at three rates of deformation and at three temperatures were employed. A limited number of cyclic tests was also performed.

LITERATURE REVIEW

Because of its varied nature, it was found desirable to subdivide the literature review into four sections: uncoated aggregates, aggregates in mixes, flow in porous media, and miscellaneous references.

Uncoated Aggregates

A number of significant studies have been made to characterize pieces of rock. The main factors of apparent importance seem to be the following: (a) particle geometry (sometimes called shape or sphericity); (b) angularity or roundness; and (c) surface roughness or texture. There are two recent and informative summaries by Gronhaug (1)[1] and Mather (2) based on about two hundred references which discuss the various parameters. A limited number of these references is included in the Bibliography. In the work reported here, the main emphasis was placed on a quantitative approach in the description of particle geometry, volume, surface roughness, sliding friction, and packing in bulk.

Particle Geometry

Four primary factors seem to affect the shape of an aggregate particle: (a) type of rock; (b) geologic history; (c) type of crushing; and (d) sizing operation (1) (4) (5) (6).

A number of qualitative terms are used to picture a piece of rock (rounded, irregular, flaky, rods, discs, blades, equidimensionals).

1. Numbers in parenthesis refer to references in the Bibliography.

There have been attempts to quantify particle dimension by a so-called sphericity factor, S (7) (8):

$$S = \left(\frac{\pi/6\ d^3}{\pi/6\ R^3} \right)^{\frac{1}{3}} = \frac{d}{\ell} \qquad (1)$$

Here d is the diameter of a sphere of the same volume as the rock piece, and ℓ is the long dimension of the particle. Further improvement in defining the geometric shape of a particle is achieved by using three descriptive diameters, namely; long (ℓ), short (s), and medium (m) (9) (10) (11). For instance, in ASTM Designation C 125 (11), the ratios of ℓ/m (ℓ/w) and m/s are adopted to classify rock pieces into four categories ranging from "flat" to "elongated." The values of the ratios for differentiating between the various classes are set arbitrarily.

The measurement of three "diameters" on a rock piece suggests the geometric form of an ellipsoid. However, the possiblility of using an ellipsoid has apparently not been greatly explored. Mackey (12), in connection with his work on radii of curvature measurements, uses the concept of a perfect ellipsoid and the degree of departure from this shape.

In work with particles in bulk, the effect of aggregate shape has been investigated by a number of researchers. Since the shape factor is hard to separate from other elements such as angularity, surface roughness and material properties, it is difficult to judge the true influence of particle geometry on mass density and other properties. This confusion may account for apparent contradictions as summarized by Gronhaug (1) and Mather (2).

Angularity or Roundness

Angularity or roundness is often described in qualitative terms such as angular, subangular, subrounded, rounded or well-rounded (13). Another more quantitative way of describing roundness is to take the ratio of the average radius of curvature (r) of the corners (n) to the radius of the maximum inscribed circle (R) of the rock piece (14) (15) (16):

$$\text{Roundness} = \frac{1}{n} \sum \frac{r}{R} \qquad (2)$$

Since in the case of crushed angular pieces, the radii of curvature are very small and difficult to measure accurately, actual angles of the sharp edges can be determined to supplement the radii of the rounded-off corners (12).

In addition to the above direct methods of measuring angularity, experimental determinations have been made using masses of particles for relative comparisons. These include refined sieving through calibrated openings, measurements of voids in bulk, measurement of angle of repose, and others (1) (2). The results are unreliable because angularity usually is confounded with particle shape and roughness. Furthermore, the measurement of angularity, as such, cannot be used directly to calculate or predict the behavior of particles in bulk. These effects have to be determined experimentally.

Surface Roughness

The existence of surface roughness or texture of aggregate surfaces is easy to see but hard to measure. One way to express roughness quantitatively is by using mean surface and deviation from it (17). There are several publications on surface texture and finish, including devices

and methods for measurement (13) (17) (18) (19) (20). There is no definite agreement on classification of roughness except in qualitative terms such as rough, smooth, furrowed, grooved, scratched, ridged, pitted, dented, striated, frosted, etched, etc. Comparison of actual surface area of polished with rough limestone, showed that the surface area of the rough rock was about three times greater than that of the polished rock (21). Blanks (22) has pointed out that there are two kinds of surface roughness: abrupt and undulatory.

Bikerman (26) has developed a simple quantitative method for measuring surface roughness on smooth, level areas. He coated flat, sawed, rock plates with asphalt, scraped the excess down to the stone, and used the amount of asphalt left as an indicator of surface roughness (and absorption).

Angularity and Roughness Combined

Intuitively, the shape or geometry of an aggregate piece seems to be a separate parameter. There is some question, however, whether angularity and roughness do not overlap, especially in the case of crushed rock. Gronhaug (1) proposes to combine angularity and texture (roughness) into one term: form. Another, possibly unifying, term would be rugosity (17). Here the adjective "rugged," which stands for rough, uneven, jagged, ridged, or wrinkled, applies to irregular pieces of aggregate; but the concept can also encompass some of the surface voids of the rock.

Sliding Friction and Compaction

If all aggregate pieces were ideal, smooth, one-size spheres and if they were packed in a simple cubical arrangement, the voids (porosity) in

the mass would amount to about 47.6 percent; in the densest tetrahedral packing the void value would be reduced to 26.0 percent. For randomly packed spheres and irregular particles, the voids vary between these two extremes.

During packing of rocks, either by gravity flow or by some other mode of densification such as vibration, some relative movement between pieces takes place. The actual contact area between two pieces (rough or smooth) is small, no more than about 0.01 percent of the apparent contact area (23). For two hard rock pieces:

$$F = W \frac{s}{y} \qquad (3)$$

where

F = force to drag one particle along the surface of another,

W = load on the particle (contact),

s = shear resistance, and

y = yield value of the rock.

The ratio s/y should be nearly independent of the nature of the rock itself, since s and y tend to vary together (23). Thus, for rocks with clean surfaces, the force F should be dependent on the load only. In other words, the masses of different one-size rock pieces subjected to identical load W (compaction) should respond in a similar manner.

The velocity in free fall, neglecting air friction, is (27):

$$V = (2\,gx)^{\frac{1}{2}} \qquad (4)$$

where

V = velocity of particle,

g = gravitational constant, and

x = distance of fall.

Therefore, if two masses of particles are "poured" from identical heights into a container, their velocities will be about the same regardless of the individual particle mass.

D'Appolonia (25) suggests that in vibration compaction (sinusoidal) the peak acceleration in g's is important and, in order to get noticeable compaction, acceleration above one g is necessary. A useful equation for relating frequency and amplitude to acceleration is (25):

$$f^2 = \frac{a_g}{.102A} \qquad (5)$$

where

f = frequency, cps,

a_g = acceleration in g's, and

A = peak amplitude, inches.

Parameters Affecting Flow in Mixes

It is evident that the properties of the aggregate will influence greatly the reaction of a bituminous concrete mix to various forces. In the literature reviewed here, research on plain rocks has been concerned primarily with describing the individual pieces of rock, rather than with bulk behavior. On the other hand, literature on bituminous mixes deals primarily with graded systems in which the various parameters are confounded. One of the recent literature reviews in this area has been done by Benson (28).

Aggregate Size and Gradation

A graded mix can have almost an infinite variety of rock sizes spaced between its largest and smallest particle fractions.

One of the early studies on gradation was done by Fuller and Thompson

(29). They were interested in the best sizing approach for portland cement concrete mixes and the emphasis was placed on achieving maximum density. The best curve for aggregate gradation resembled a parabola. The parabolic curve could be approximated by an elliptical portion running from about 7 percent passing the No. 200 sieve to one tenth of the diameter of the maximum size piece, and a straight line to the maximum size. The equation of the elliptical portion of the curve is:

$$(y - 7)^2 = \frac{b^2}{a^2}(2ax - x^2) \qquad (6)$$

where

y = percentage of weight smaller than a given diameter,

x = diameter of a particle, and

a and b are constants to be determined experimentally for a particular material.

Additional studies (30) (31) have extended the work of Fuller. The following is the most often seen simple equation for a maximum density curve:

$$P = 100\left(\frac{S}{M}\right)^K \qquad (7)$$

where

P = percent passing the particular sieve,

S = sieve size opening,

M = maximum size of aggregate, and

K = value depending on type of aggregate (0.5 is often used).

Subsequent work on aggregate size and grading for bituminous mixtures has indicated that some of the most unconventional and irregular grading curves have produced "better" mixes on the road than those graded by Fuller's criterion (32) (33) (34). On the other hand, there are also field reports showing that mixes using gradations with humps in the curve

are not performing well under traffic (35) and that flow resistance (stability) of an asphaltic mix can be unpredictably affected by changes in grading (34) (36).

It is apparent that gradation of aggregate affects the total surface area of the rock pieces to be coated with asphalt (37). The larger the particle size, the smaller the area per given weight of aggregate. This relationship has been recognized for a long time in mix design.

Aggregate Shape

Aggregate shape is often discussed comparing natural aggregates, such as gravel, with crushed aggregates, such as processed limestone. In published data on bituminous mixes, shape often means geometry and angularity combined. At the same time, the investigations have usually included texture or surface roughness.

The shape of the coarse aggregate does not seem to be of much importance in the compacted mix, as far as flow resistance is concerned, unless this fraction reaches a certain influential limit. This limit is a function of the type of gradation used, the material, and other variables (38) (41) (42). The shape of fine aggregate in dense-graded mixes has been found significant. Increase of angularity of the fine aggregate is generally accompanied by increase in "strength" and changes in other properties of the mix (38) (39) (40) (41) (43) (44).

While a mix is being compacted, particle shape reportedly affects the orientation of the individual rocks (45).

There are publications which do not agree with the above summary statements (46) but such conflicts seem understandable since a simple division of particles into "angular" and "rounded" is based on a qualitative

judgment which cannot always give comparable results.

Finally, there is another factor which has been brought out by Lee (47) in a study comparing Marshall stability values of mixes containing either "flaky" or "cubical" aggregates. Using a sieve gradation, Lee found that a pound of mix contained more "flaky" than "cubical" particles. All the other research reviewed did not take into account the number of the particles in a unit volume of mix. This is one of the important projections in the hypothesis for this study.

Aggregate Texture

The authors whose work was reviewed in the previous section are also responsible for most of the studies on the effect of the texture of aggregate on the properties of mixes. There is general agreement that increased surface roughness inhibits the flow in a mix, and therefore higher stability-strength values are obtained in comparison with mixes containing smooth-surface aggregates (39) (43) (48) (49) (50) (51). The explanation lies in the assumed higher friction between the aggregates (48) (49) (50). Furthermore, rough and angular particles have a higher inter-particle void space in bulk than smooth ones (43) (39). Such mixes require extra asphalt for workability because part of the asphalt is lost in "pits and crevices" and does not participate in flow (37).

Miscellaneous Factors

Another factor which affects flow in bituminous mixes is the binder. There is general agreement that asphalt can be classified as a linear viscoelastic material (52) (53) (54) (55). The viscosity of asphalt depends on temperature and physico-chemical composition (52).

In addition to the rocks and asphalt, a mix contains voids; that is, a gas phase. The present mix design procedures (56) use the relative volume of voids as one of the criteria in the design. In general, high and low void content are associated with low flow resistance of the mix, with maximum "strength" occurring at an intermediate void content. This concept may be valid for the usual compression-shear types of tests. On the other hand, mixes have been produced with only two phases, the rock and the binder, without voids. Certain experiments have achieved flow resistance in voidless mixtures several times higher than in mixes containing a measureable void content (57) (58) (59) (60).

Comparisons to Flow in Porous Media

Since asphalt and the smaller aggregate particles associated with it is displaced and flows between the larger particles when a mix is subjected to load, there may be some similarity between the flow of asphalt in a bituminous mix and flow in porous media (especially in low-void mixes). The literature concerning this flow was reviewed briefly.

It would appear that the more porous the composite, the more easily liquid can permeate it. Several researchers (61 to 68) have investigated this topic and have come to two different opinions. One group says there is no general correlation between porosity and permeability and that two composites with the same porosity can be of different permeability (67) (68). Others, however, have found some correlation (64) (65) (66). Mavis (64), for instance, claims that permeability K and porosity P have the following approximate relationship: $K = P^6$. In general, the studies seem to indicate that while an approximate relationship may exist for a given type of porous material, general agreement is lacking.

Structure-Permeability

Attempts have been made to correlate permeability using a given liquid with structure of the composite forming the porous media (69) (70). Structure may be defined here as "pore size distribution" within a given material. This distribution is usually measured by capillary pressure. There is some question whether this technique can indicate the true pore size distribution, especially in an aggregate composite such as bituminous concrete.

Grain Size Distribution and Permeability

The distribution of grain size in a given mix is relatively easy to determine, and the idea of correlating grain size distribution with permeability has attracted several investigators (71) (64) (72) (73). The most important conclusions appear to be: (a) materials with different mineral composition but the same gradation, may not have the same permeability; (b) the permeability of one-size granular aggregates is often similar.

Grain Size-Angularity-Permeability

In addition to grain size, angularity of the aggregates and its effect on packing and orientation of grains can be considered. Again the difficulty here is how to define and measure angularity and so far no definite conclusions have been reached (74) (75).

There may be other similar approaches in the literature involving the same parameters under different names; only the most outstanding were mentioned in this brief summary on experimental efforts to characterize permeability. It is possible to assume or invent new parameters and

perhaps eventually, by trial and error testing, to arrive at a more significant and general solution to predict permeability. On the other hand, it may be more advantageous to start with theoretical considerations which could attach significance to these parameters. The simplest way to try to establish correlations theoretically is by representing the porous media (graded crushed rock, plus sand, plus filler) by theoretical models which can be treated mathematically. Trial and error will show which model fits best. If a proper model is found, it can be substituted for the actual porous media. Some of the models are discussed below.

Models for Permeability

The motion of a fluid can be described if the position of every material point of the fluid is known at a given time. There are three kinds of physical conditions which have to be satisfied: (a) the continuity condition, (b) rheological equation of state, and (c) Newton's Third Law of Motion. In addition to these, initial and boundary conditions are to be taken into account.

For the steady-state flow of viscous, incompressible fluids, the Navier-Stokes equation of motion is appropriate. For shorthand purposes it is written in vector form:

$$\bar{v} \text{ grad } \bar{v} + \partial\bar{v}/\partial t = \bar{F} - (1/\rho) \text{ grad } p - (\eta/\rho) \text{ curl curl } \bar{v} \qquad (8)$$

where

$\bar{v}$ = local velocity-vector of a point of the fluid,

t = time,

$\bar{F}$ = the volume-force per unit mass,

p = pressure,

η = viscosity of the fluid, and

ρ = density of the fluid.

The boundary conditions require V = 0 at the wall of the container.

The structure of the Navier-Stokes equation and the boundary conditions make the analytical solution rather cumbersome. Attempts have been made to use simple models to circumvent the difficulty (76) (77).

The Navier-Stokes equation can be solved exactly for a straight circular tube. One form of the solution is the so-called Hagen-Poiseuille equation (76):

$$Q = \left(\frac{\pi}{8}\right)\left(\frac{\Delta p}{h}\right)\left(\frac{a^4}{\eta}\right) \qquad (9)$$

where

Q = the rate of liquid flow through the capillary,

p = pressure drop between the two ends of the capillary,

h = length of the capillary,

a = radius of the capillary, and

η = viscosity of the liquid.

This equation can be developed further using Darcy's law and arriving at a coefficient of permeability K, dependent upon porosity and average pore size diameter. It is known that a model built on this equation does not correctly represent the connection between permeability and porosity. It is of interest only from a qualitative point of view, indicating that if one could call a space between two rocks of the skeleton a capillary, the flow between capillaries would be greatly influenced by the distance by which they are separated and to a lesser extent by viscosity of the fluid, length of the pass, and pressure.

One can also assume that the capillaries are varied in diameter (serial type of model). The problem here is to decide and measure the

value of the capillary radius.

Hydraulic radius is often mentioned in the literature. A possible measure of hydraulic radius is the ratio of the pore volume to the surface area and a general equation may be as follows:

$$K = C \frac{m^2}{F(P)} \tag{10}$$

where

K = permeability,

m = hydraulic radius,

F(P) = porosity factor, and

C = dimensionless constant.

Attempts to utilize the hydraulic radius approach (78) (79) (80), have met with varying success.

Koseny's theory is also a widely used explanation for permeability as conditioned by the geometrical properties of a porous medium (81). The model consists of a porous medium of an assemblage of channels varied in cross-section but having a definite length. The Navier-Stokes equation is applied and solved. The equation is as follows:

$$q = \frac{c\, P^3}{\eta\, S^2} \text{ grad } p \tag{11}$$

where

q = amount of flow in unit time,

c = geometric factor,

(c = 0.5 for circle; c = 0.5619 for square;
c = 0.597 for triangle; c = 0.66 for strip)

P = porosity,

η = viscosity,

S = specified surface area of "tube", and

p = pressure.

Comparing this equation with Darcy's Law, permeability can be expressed as:

$$K = \frac{c\ P^3}{S^2} \qquad (12)$$

But the channels may not be straight and therefore the Koseny equation is often extended introducing a "tortuosity" factor T,

$$\text{grad p reduced} = \frac{1}{T} \text{ grad p} \qquad (13)$$

showing that the pass is T times longer than a straight pass through a given layer. From this follows:

$$K = \frac{c\ P^3}{T\ S^2} \qquad (14)$$

Other modifications of the Kozeny equation have been attempted, for example by Carman (83) and Sullivan (84). For them, too, the apparent difficulty is the method for determining S, c and T by independent means.

Disordered "Model" Approach

Although Darcy's law and some of the previously discussed models have been partially successful, it is difficult to visualize how they could reasonably reflect the flow of asphalt and finer particles within an irregular rock skeleton. We are dealing here with a disordered rather than an ordered porous composite, and it is questionable whether the Navier-Stokes equation is valid under such conditions. The nature of the composite has led to attempts to predict the flow by applying statistics and a model of disorder.

Hubbert (85) was apparently the first to apply statistics to flow through porous media. His considerations are based upon the concept that

the microscopic flow velocity of each fluid particle is proportional to the acting force. Childs (86) used a theory of pore size distribution.

Taub (87) developed equations of flow based on the Maxwell-Bolzman distribution function of gases. Density, pressure, and velocity are defined according to kinetic theory.

Scheidegger (88) (89) applied statistics to porous media more systematically. As a starting point, he used Einstein's theory on the Brownian motion. The flow of each particle point is assumed to be a statistical process and the differential equation is formulated in terms of probability distribution function for each point. To account for the fact that individual "particles" in the fluid do not move along the streamline, Sheidegger introduced the "dispersivity" factor D. The relationship between D and other factors affecting flow at time = t_o is given by the equation:

$$P \frac{\partial p}{\partial t} = \text{lap} \left[P\rho D + \text{div} \left(\rho \frac{K}{\eta} \text{ grad } p \right) \right] \qquad (15)$$

where:

P = porosity,

p = pressure,

ρ = density of fluid,

K = permeability, and

η = viscosity.

If D = 0, Equation 15 reduces to Darcy's Law.

Equation 15 can also be simplified by introducing "a" as a "catch-all" constant for a given porous medium.

Then:

$$D = \frac{\rho a}{\eta^3} (\text{grad } p)^2 \qquad (16)$$

The difficulty with Scheidegger's equation is the need to measure or determine with reasonable accuracy and confidence the value of D, the dispersivity factor. In addition, porosity P, viscosity η, and permeability K have to be known. It is also questionable whether a completely disordered approach is appropriate. Scheidegger himself suggests that the true description of porous media lies somewhere between the ordered and disordered state.

At this stage of development the permeability models are not easy to apply to bituminous concrete and further theoretical work is necessary.

Contact Area Model and Theory

The simplest unit in bituminous concrete may be visualized as consisting of two idealized rocks glued together with a drop of asphalt. It is assumed that the two small areas of the rocks facing each other are flat and parallel to each other, and that the asphalt drop between the two rocks will have the shape of a thin cylindrical disc with radius r and thickness h_o. Under these ideal conditions the asphalt acts as an adhesive and the "strength" of this adhesive joint is a function of both the radius and the thickness of the film between the rocks.

This concept leads to the theoretical and experimental work done by Stefan (102). He used a Newtonian liquid between two parallel discs. The mathematical derivation of Stefan's theory has been more clearly presented and interpreted by Bikerman (17) (103) and Majidzadeh (109). For two parallel plates or discs with a radius r, immersed in a Newtonian liquid with viscosity η and separated by a distance h, the force required to separate them at a rate $\frac{dH}{dt}$ is:

$$F = 1.5\eta \frac{\pi r^4}{h^3} \frac{dH}{dt} \tag{17}$$

If the two parallel discs are not immersed but contain a drop of liquid the volume of which is smaller than the volume between the surfaces, then the above equation becomes:

$$F = 1.5\eta \frac{V^2}{\pi h^5} \frac{dH}{dt} \tag{18}$$

where V is the volume of the adhesive material between the plates.

If the material is non-Newtonian, the relationship can be expressed using Scott's formula (105):

$$F^n = \frac{(2n)^n \, k(n+2) \, V \frac{3n+1}{2}}{(3n+1)^n \, \pi \frac{n+1}{2} \, h \frac{5n+5}{2}} \tag{19}$$

where n is a constant for a material and k is related to viscosity. Both are related with shear rate $\dot{\gamma}$ and shear force τ through the equation:

$$k\dot{\gamma} = \tau^n$$

The above theory assumes that a cylindrical plug (or any other shape) of liquid or semiliquid placed between two plates will exhibit flow towards the center of the disc when the plates are separated. The outside edges of the disc will distort in a parabolic fashion and shear forces will develop in addition to tensile forces.

The horizontal flow between two discs occurs because external load creates a pressure difference in the material. If for some reason gas cavities are generated inside the liquid, the above equations are no longer valid. Also, if the rate of deformation is so fast that no laminar-shear flow can take place, rupture will occur in tension. This is because the work to cause the liquid to flow by overcoming viscous

resistance is greater than the work required to create new surfaces (106). In such a case the liquid between the plates starts to behave like a solid and other theories, such as potential energy, are more appropriate (107) (108).

The flow of asphalt between two smooth parallel surfaces has been recently investigated by Majidzadeh and Herrin (109) and by Marek and Herrin (110). Because of the importance of these two papers for the present study, each will be briefly summarized.

The paper by Majidzadeh and Herrin provides a good review of literature in the area of adhesive films subjected to tensile strain. Also, experimental work was performed using one-inch diameter aluminum cylinders with a 72 penetration asphalt film of a thickness between 10 and 1000 microns. The rates of extension varied between 0.005 and 1.0 inch per minute and test temperatures were between 32 and 113 F. In terms of relevance to the present study, Majidzadeh and Herrin's most important conclusions are:

a. It appears that the hydrodynamic or Stefan's theory can be used to predict the tensile strength of thick films. In thin films the asphalt fails predominantly in tension (cohesion).

b. Three types of failure were observed depending on test conditions; namely, by flow and necking, by brittle fracture or tensile rupture, and by an intermediate mechanism accompanied by cavity and filament formation during extension.

c. The amount of deformation (not strain) at failure was practically constant regardless of film thickness and did not vary significantly with rate of extension and temperature.

The work by Marek and Herrin (110) is an extension of that done with Majidzadeh. They used asphalt cements in film thicknesses between 20 and 600 microns. The other variables were approximately the same as those reported from Majidzadeh's work except for improved equipment and techniques. Some of Marek and Herrin's conclusions are:

a. The consistency of the asphalt has an influence on film strength.

b. The limit of film thickness at which flow failure occurs is a function of temperature, rate of deformation and asphalt consistency.

c. The amount of deformation before failure appears to be dependent on film thickness up to a certain limit, beyond which increased film thickness no longer affects deformation at peak force.

As will be seen in later chapters, the work of both Majidzadeh, Marek and Herrin was very useful for developing analyses and explanations for this research.

THEORETICAL CONSIDERATIONS

The literature review supplied two basic types of background needed in this research: (a) suggestions for characterizing uncoated aggregate particles, and (b) the contact area model for explaining flow in mixes. Then an attempt was made to add to these ideas so as to have a specific hypothesis involving a predictable response on which to base the experimental work. This involved considerations of uncoated rocks, single and in bulk, the aggregate-binder composite, and a prediction of a region of flow.

Uncoated Rocks, Single and in Bulk

With reference to uncoated rocks, single and in bulk, consideration was given to particle volume of the piece itself, the volume it occupies when in association with other pieces, referred to as packing volume, the packing density of perfect ellipsoids, and grading by sieve size and by packing-volume "size."

Particle Volume

The bulk volume of a number of particles in a container is, among other things, a function of the volumes of each of them. To start with, it is assumed that the volume which a particle occupies in a mass of other particles largely determines the density and the voids in bulk and therefore this volume is important as far as the response of the composite to various forces is concerned. The problem at hand is to attempt to define

the volume of a particle, especially if it is irregular in shape as well as rough.

In order to define the volume of any particle, it is convenient to have a geometric form which lends itself to numerical description and analytical manipulation. As pointed out in the literature survey, the measurement of long, medium and short dimensions of a particle is not a new idea. Since in the field of aggregates there are practically no cubes, spheres, rods or other regular shapes, why not try to fit an ellipsoid for all types of particles?

The volume of an ellipsoid is:

$$V = \frac{\pi}{6} \ell \, m \, s \qquad (20)$$

The equation for surface area of an ellipsoid is more complicated and a prolate spheroid is often used as an approximation.

Packing Volume of a Particle

All particles possess some kind of surface roughness. The peaks or asperities of the roughnesses are spaced randomly. Therefore if two pieces of crushed limestone are in contact with each other, the peaks and the valleys will not mesh like two carefully cut gears. Instead, the particles will touch one another at the high spots and only a small portion of the areas will be in contact (23). As a result, the volume which a piece of rock occupies in a mass of other particles encompasses not only the volume of solids and internal voids, but also the volume of the dips and valleys of the particle surface which may be called "outside voids" (Figure 1). These outside voids are primarily a function of the rugosity of the surface. As used in this study, the term "packing volume" when

applied to a particle, is that volume which the particle occupies in a mass of particles, or:

$$V_p = V_s + V_i + V_o \tag{21}$$

where

V_p = packing volume of a particle,

V_s = volume of solids of the particle,

V_i = volume of internal voids, and

V_o = volume of outside voids or surface irregularities.

The packing volume can be pictured as a volume enclosed by a dimensionless, flexible membrane stretched along the surface of a rock (Figure 1).

In the laboratory, it was proposed to measure packing volume by heating rock and asphalt to 300 F (simulating bituminous mix temperature), immersing the heated rock pieces in the heated asphalt for thirty minutes to allow for penetration of surface voids (an attempt to simulate mixing and high temperature storage time), then removing the coated rocks from the asphalt and dipping them into ice water before removal of the excess asphalt coating to achieve a "membrane" condition. After the coated rocks had cooled, they were to be taken out and the excess asphalt removed down to the asperities of the rock piece. As a scraping tool, a razor blade, as used by Bikerman (26), was to be tried. Finally the actual packing volume, V_p, can be obtained by weighing the scraped rock piece in air and water:

$$V_p = \frac{W_t - W_w}{G_w} \tag{22}$$

where:

W_t = total weight, rock plus asphalt, in air,

W_w = weight in water, and

G_w = unit weight of water.

The weight of a rock piece to give a certain desired packing volume for practical application can be derived as follows (Figure 1):

$$V_p = V_s + V_v + V_a \tag{23}$$

$$V_p = \frac{W}{G_{s+v}} + V_a \tag{24}$$

$$W = G_{s+v} (V_p - V_a) \tag{25}$$

where

V_v = internal and surface voids unfilled with asphalt,

V_a = volume of asphalt after scraping,

W = weight of dry rock piece,

G_{s+v} = specific gravity of solids plus voids including those under the asphalt coating,

V_p = packing volume, and

V_s = volume of solids of the particle.

The volume of asphalt, V_a, will depend on the surface area "A" and surface roughness "R" of the rock piece. Therefore Equation 25 can be rewritten:

$$W = G_{s+v} (V_p - AR) \tag{26}$$

where

$R = \frac{Va}{A}$ or the volume of asphalt on the rock piece after scraping, divided by the smooth "membrane" surface area of the rock. The equation for G_{s+v} is:

$$G_{s+v} = \frac{W}{\frac{W_t - W_w}{G_w} - \frac{W_a}{G_a}} \qquad (27)$$

where

W = weight of the rock piece (or pieces),

W_t = weight of the rock piece + asphalt in air,

W_w = weight of the rock piece + asphalt in water,

W_a = weight of asphalt,

G_a = unit weight of asphalt, and

G_w = unit weight of water.

The value G_{s+v} is constant for a given aggregate piece provided a certain procedure is followed just as in any test for specific gravity of aggregates. However, if two laboratories use two different methods and obtain two different G_{s+v} values, Equation 26 still holds, since rugosity, R, changes in unison with G_{s+v} (Figure 1). A knowledge of G_{s+v} may be useful for obtaining rugosity, R, factors without resorting to scraping.

As mentioned in the literature review, for a given aggregate the surface rugosity, R, is higher for larger pieces as compared to smaller ones. During crushing operations cracks propagate along the path of least resistance, leaving fine surface roughness superimposed on longer undulating roughness. The smaller the rock, the less the inclusion of larger undulations and the smaller should be the rugosity factor R.

Packing Densities of Perfect Ellipsoids

Packing densities and voids (porosity) for perfect spheres under certain configurations have often been used for comparison in particle

studies. The volume of a sphere is $V_s = \pi/6\ d^3$, and that of an ellipsoid $V_e = \pi/6\ \ell\ m\ s$. For the case of one-size smooth spheres in simple cubical packing, the porosity n = 47.6%. If, instead, ellipsoids of given ℓ, m and s values are placed in a similar manner:

$$n = 1 - \frac{\pi}{6}\ \ell\ m\ s\left(\frac{1}{\ell} \times \frac{1}{m} \times \frac{1}{s}\right) = 0.476 \qquad (28)$$

For spheres in a cubic-tetrahedral packing, n = 39.5 percent and for ellipsoids in similar arrangement,

$$n = 1 - \frac{\pi}{6}\ \ell\ m\ s\left(\frac{1}{\ell\sqrt{3}} \times \frac{1}{m} \times \frac{1}{s}\right) = 0.395 \qquad (29)$$

Finally, in the densest tetrahedral packing for spheres n = 26.0 percent. The packing for ellipsoids is similar:

$$n = 1 - \frac{\pi}{6}\ \ell\ m\ s\left(\frac{1}{\ell\sqrt{2}} \times \frac{1}{m} \times \frac{1}{s}\right) = 0.260 \qquad (30)$$

From these calculations it is apparent that dense, loose and intermediate regular packing of perfect equidimensional ellipsoids gives voids (porosities) identical to those in ideally packed spheres.

So far, consideration has been given to the shape (ellipsoid) and rugosity (surface roughness) of the particle. It should be pointed out that rugosity as measured by scraping may also be influenced by angularity (the more angular the rock, the higher the rugosity). Sharp corners of rock, however, are not accounted for in the packing volume concept.

The void content (or porosity) of a mass of small or large one-volume particles should be the same, regardless of the type of rock and shape of particle, just as it is with ideal spheres. Thus the ratio of the number of small particles, N_1, to the number of large ones, N_2, should be indirectly proportional to their packing volumes V_1 and V_2:

$$\frac{N_1}{N_2} = \frac{V_2}{V_1} \tag{31}$$

$$N_1 V_1 = N_2 V_2 \tag{32}$$

When packing or compacting different kinds of particles, identical procedures are necessary to obtain comparable results. For example, when a mass of rocks is "poured" into a given mold or container, the rocks must be deposited from a similar height and within an identical time interval (12). If vibratory compaction is used, the peak acceleration must be the same (25).

Finally, it should be pointed out that the porosity, or voids, as considered here, is not the absolute porosity of the bulk since the basis of the "solid" volume is packing volume, which includes surface roughness or surface voids. One-volume rounded gravel and crushed stone may have identical packing porosities in a mass, but the amount of liquid, such as water or mercury, needed to fill the aggregate voids is greater in the case of crushed limestone because of its greater rugosity.

Grading by Sieves and Packing Volume

Grading by sieves alone does not assure good control of particle packing volume. The volume of an ellipsoid is $V = \pi/6\ \ell\ m\ s$ and the medium and short dimensions are primarily responsible for passage through a square-holed sieve. If m and s are equal and the sieve hole size is H, the volume V of the rock passing it is:

$$V = \ell \left[\frac{\pi}{6} s(2H^2 - s^2)^{\frac{1}{2}} \right] \tag{33}$$

If s and H are fixed, this volume is $V = \ell k$, where k is a constant. This shows quantitatively that aggregates passing a given sieve (assuming identical m and s values) will have uncontrolled volumes directly proportional to the length ℓ of the rock piece (Figure 2). Thus the particle volume distribution should be different for different rocks of identical sieve size. However, for a given aggregate, it should be possible to use sieve grading to predict volume grading through correlation factors.

Aggregate-Binder Composite

The primary purpose of this work was to search for a means of characterizing mix components to make possible a unified method of designing a mix for use. The secondary purpose was to develop and test models with which to explain the mechanism of flow in an aggregate-asphalt composite. The packing volume approach promised to contribute to the first, and the contact area theory to the second goal.

Stagnant and Flow Asphalt

As pointed out earlier, the packing volume of an aggregate piece includes not only the solids of the rock but also the inside voids and surface valleys and crevices (Figure 1). The asphalt in the surface valleys and crevices cannot easily move around or flow when the mix is subjected to load-deformation. This asphalt can be called stagnant or immobile; but in order to connect it with the parameters of the rocks, it has been designated as rugosity asphalt. It was assumed that each type of rock needs a certain specific amount of rugosity asphalt to fill the surface voids and that:

$$V_s + V_{iv} + V_{ra} = V_p \qquad (34)$$

where

V_s = volume of "solids" of the rock piece,

V_{iv} = volume of internal voids of the rock piece,

V_{ra} = volume of rugosity asphalt on the rock, and

V_p = packing volume of the rock piece.

In order to have active binder which participates in flow when load is applied, additional "film" -- a quantity of asphalt -- is needed to complete the mix. Here the additional asphalt has been called binding or flow asphalt (Figure 3). It is realized that the two layers of asphalt do not have a distinct line of demarcation when a mix is made and that mixes containing only the rugosity asphalt and no binding asphalt will not necessarily fall apart. The rocks coated with just the rugosity asphalt still have asphalt to asphalt surfaces at the contact points. Capillary forces probably contribute to attraction of some of the rugosity asphalt to the contact areas. However, if binding or flow asphalt is present, it is assumed that very little of the rugosity asphalt will be dislocated.

Prediction of "Strength" Using Contact Area Theory

When the contact area theory (basically Stefan's theory) is used to predict the flow resistance of a bituminous concrete, it becomes necessary to make a number of simplifying assumptions (Figure 4). At the beginning, it is assumed that

a. the contact areas are circular,

b. the two faces of the contact areas are smooth and parallel to each other,

c. the asphalt plug between the two surfaces is cylindrical with radius r and height h_o, and

d. the asphalt is Newtonian.

This simple model provides a good insight for the problem at hand.

Equation 18 for the case of non-immersed round discs was as follows:

$$F = 1.5\eta \frac{V^2}{\pi h^5} \frac{dH}{dt}$$

If the rate of deformation is constant and the volume V of the material between the plates is fixed, and the viscosity of the asphalt is also constant, the equation reduces to:

$$F = \frac{K}{h^5} \tag{35}$$

This indicates that the film thickness h is of extreme importance with respect to the force F required to pull the discs apart or to push them closer together (Figure 4). What Equation 18 does not show clearly is that there is an equally important factor hidden in V^2. This is the radius r of the asphalt plug. It may be best shown by integrating Equation 18:

$$Fdt = 1.5\eta \frac{V^2}{\pi h^5} dH \tag{36}$$

between the limits h_o and h_1 in tension, so that

$$Ft = \frac{3}{8} \eta \frac{V^2}{\pi} \left(\frac{1}{h_o^4} - \frac{1}{h_1^4} \right) \tag{37}$$

If h_1 is considerably larger than h_o, it can be neglected and Equation 37 reduces to

$$Ft = \frac{3}{8} \eta \frac{V^2}{\pi h_o^4} \tag{38}$$

Since

$$V = \pi r^2 h_o \tag{39}$$

Equation 38 becomes

$$Ft = \frac{3}{8} \eta \frac{\pi r^4}{h_o^2} \tag{40}$$

Finally, by changing total force F to force f per unit area we obtain

$$ft = \frac{3}{8} \eta \left(\frac{r}{h_o}\right)^2 \tag{41}$$

This equation shows that not only is film thickness important, but so is the radius or lateral dimension of the film. In fact, film thickness, according to Stefan's theory, is a relative parameter because the force "f" or strength of the film per unit area will be identical in such extreme cases as when r = 1 inch and h_o = 1 inch as compared to r = 10 microns and h_o = 10 microns. This important relationship has not been brought out clearly in the literature surveyed and yet it is very helpful when applied to bituminous mixes. For instance, if the contact radius for two 1/4 inch rocks is 0.06 cm (r = 600 microns) and the initial film thickness is 60 microns (h_o = 60 microns), the r/h_o ratio is 10. This may be compared with the r/h_o ratio of 8.5 for a very thick film of 1490 microns in work done by Majidzadeh and Herrin (109). In other words, at room temperature and above, Stefan's theory should help greatly to explain the behavior of bituminous mixes.

Stefan's equation is basically valid for only one contact plug between two rocks. In a one-size mix there are many contacts, but not all of them will participate to resist tension or compression force applied to the specimen.

Cubical packing is the simplest arrangement for spheres or ellipsoids in bulk. In such a case it is easy to calculate the number of rocks M stacked up on top of each other in a given length specimen; also the number of one-size spheres per layer horizontally (L) for a given diameter is simple to calculate. The number of contact points in this packing is six per sphere (or ellipsoid) and if there is an asphalt plug at each point, only the top and bottom plugs would be pulled in direct tension and pressed in a direct compression test. Thus horizontally there would be L plugs and the force required to pull the rocks apart would be L times that for a single plug. Since the number of vertically stacked rocks would each have a "working" plug of asphalt (strictly speaking, if the number of rocks is M, the number of plugs is M-1) the effect of the vertical line of plugs would be to reduce proportionately the rate of gap widening $\left(\frac{dH}{dt} \right)$ between any two rocks. Thus, the modified Stefan's equation for a specimen with cubical packing is:

(See Appendix 1 for derivation)

$$F = \frac{10.73}{10^6} \eta \times \frac{r^4 h_o^2}{(h_o + \Delta h)^3} \times \frac{L}{M} \times \frac{dH}{dt} \qquad (42)$$

where

F = the total force,

η = viscosity of asphalt,

r = average radius of contact area for the rocks,

h_o = average "film" thickness between particles,

Δh = change in average distance between particles,

L = number of rocks - horizontally,

M = number of rocks - vertically, and

$\frac{dH}{dt}$ = rate of deformation.

The above equation assumes a Newtonian asphalt.

For a non-Newtonian asphalt:

$$F^n = \frac{2.25}{10^6} \times \frac{(2n)^n K(n + 2)\, V \frac{3n+1}{2}}{(3n + 1)^2 \pi \frac{n+1}{2} h^{5n+5}} \qquad (43)$$

where

n = a factor characteristic of asphalt,

K = a factor related to viscosity,

V = the average volume of the asphalt between each contact point, and

other factors are as before.

Prediction of Flow Region

From Stefan's theory, using constant rate of deformation:

$$F = g(\eta, r, h) \qquad (44)$$

This applies to both tension and compression. Majidzadeh, Marek and Herrin (109) (110) have indicated that for a given asphalt the theory is applicable only over a certain region. More specifically, Majidzadeh and Herrin (109) give a graphical illustration of this phenomenon, as shown in Figure 5. Here the film thicknesses for the flow region are high because the radius of the contact area is 1/2 inch.

In order to gain an insight into what factor is involved in determining the flow, intermediate, and brittle failure regions, Majidzadeh and Herrin's data were used. In the first trial it was assumed that the relative rate of creation of a new surface determines how the asphalt plug fails. In order to make quantitative comparisons, the parabolic neckdown

was approximated by a V-shaped deformation as illustrated in Figure 6. The ratio of surface areas A_{new}/A_{old} versus asphalt film thickness in microns was then plotted (Figure 7). This relationship did not appear to be constant for different film thicknesses. The next step involved calculations for the relative linear strain in the outside "skin" of the asphalt plug, again assuming a V-shape neckdown. These calculations gave a very interesting and helpful relationship; namely, for the 72 penetration asphalt at 77 F, the material between two circular discs will deform and fail by flow if the relative linear rate of strain in the outer "skin" of the plug does not exceed approximately 43 percent per second. This seems to apply to any film thickness used by Majidzadeh and Herrin (109). An example of a calculation is given in Appendix 2. The basic equation for calculating strain in the outer surface is derived in Appendix 3. The final equation follows:

$$\epsilon = \left\{ \frac{r^2}{h_o^2} \left[9 - \frac{6K^{\frac{1}{2}}}{a+1} + \frac{3K}{(a+1)^2} \right] + (a+1)^2 \right\}^{\frac{1}{2}} \qquad (45)$$

where

ϵ = unit strain in the outer surface,

r = radius of the asphalt plug,

h_o = thickness of the asphalt plug,

a = unit change in h, and

$K = 3(3 + 2a - a^2)$.

It is of interest to note here again that the linear strain is a function of r^2/h_o^2 (plus other factors) just as in Stefan's Equation. A graphical presentation of this equation is given in Figure 8.

From the derivations above it is apparent that for a given asphalt

the line between the flow region and the semi-brittle behavior is a function of (a) temperature, (b) the ratio r/h_o, and (c) the relative rate of widening of gap h_o. Using data from Majidzadeh and Herrin (109), values for Figure 9 were calculated and plotted. This Figure separates the flow and intermediate failure regions for one particular 72-penetration asphalt.

The most interesting and novel factor again is the r/h_o ratio. If it is decreased ten times, from 100 to 10, the expansion rate of the adhesive joint between the two surfaces can be increased approximately ten times.

For $r/h_o = 1000$ and a 10 percent per minute rate, the border point between the regions of flow and the intermediate zone is at 90 F, while for $r/h_o = 1$, it is 47 F for the same 10 percent.

Using a tension test similar to Majidzadeh and Herrin's, the flow region can be determined for any asphalt. The procedure, would, however, have to be simplified to make this determination less cumbersome.

Finally, it must be added that Figure 9 can be used for approximate estimates of the flow region for asphalts which are not too different from the 72 penetration asphalt used by Majidzadeh and Herrin, since in most applications the viscosity enters as a first power variable, including Stefan's equation. It was used for estimating the flow region in the following experiments with mixes.

EXPERIMENTS WITH UNCOATED AGGREGATES

In order to verify the packing volume hypothesis and measure the rugosity, the initial experiments were conducted with uncoated rocks. These were varied in size, shape and composition, but size distribution or grading was limited to "one-size" pieces in each case.

Aggregates Used and Parameters Measured

The reasoning developed by theoretical considerations on aggregates was tested in the laboratory using three types of rocks (crushed limestone, crushed gravel and rounded gravel) with three distinct packing volumes about one decade apart (4 cc, 0.4 cc, and 0.04 cc). The "size" of the rocks was about 3/4, 3/8 and 1/8 inches, respectively (Figure 10). In addition, comparative measurements were made using 1/2-inch smooth glass spheres (marbles). The surface rugosity and geometric parameters were measured, packing volumes were calculated, and weights for identical bulk volumes were predicted for the various rocks and sizes. Loose bulk volumes and volumes after vibratory compaction were measured and compared to check the validity of the packing volume concept.

The three aggregates were selected on the basis of differences in rugosity (crushed versus rounded) and composition (sedimentary versus mixed). These three rock types are frequently used in highway construction. The crushed gravel and the rounded gravel came from the same source.

It is apparent that one-size or one-volume particles exist only in theory. Even smooth, one-size glass spheres (marbles) do not have identical diameters. It is just as impossible to produce one-volume rock particles. Therefore the three categories of rock volumes actually refer to mean volumes with a controlled standard deviation and about equal coefficient of deviation.

The 0.04 cc (1/8 inch) rocks were obtained by dividing the fraction between the No. 4 and No. 6 sieves into portions retained on the No. 5 and No. 6 sieves. These two fractions were combined to get similar coefficients of deviation, D (standard deviation divided by the average weight of a particle, multiplied by 100), for the three types of rocks, based on weights of particles. A convenient D was found to be about 15 percent. Similar handling of the 0.4 cc and 4 cc rocks, using the appropriate sieves, gave a desired D = 15 percent in each case. Data on rocks are presented in Table 1.

Measurement of Rugosity and Packing Volume

As mentioned before and shown by Figure 1, the packing volume of particles can be measured without the numerical determination of rugosity. It is convenient, however, to know the characteristic relationship between rugosity and different particle sizes (volumes) for a given rock, because this relationship provides the basis for calculating particle packing volume and weight for "sizes" other than those used in the actual determination. The rugosity value is also needed when calculating the amount of a binder, such as asphalt, to be mixed with aggregate.

Figure 11 shows the curves for rugosity of the three rocks as they change with rock size (packing volume). The value for each point is based

on 20 rocks drawn at random from a mass. The rocks were washed, dried, weighed, and heated to 300 F in a compartmentalized container. They were then submerged for 30 minutes in 60-70 penetration asphalt at the same temperature. The coated rocks were then cooled in ice water and the excess asphalt was scraped off each piece, down to the peaks of roughness.

This scraping was done with a razor blade, applying its straight edge and avoiding use of the corners. This operation was tedious and required some patience and skill. After scraping, crushed rock and rounded gravel look very much alike except for some sharp angles of the former. The particles were weighed again in air and in water. Thus a direct measurement was obtained for the packing volume of each particle. In addition, the three dimensions, ℓ, m and s for the rock pieces were measured and their "membrane" surface areas were calculated using the simplified equation for prolate spheroids:

$$A = \frac{\pi d}{2}\left(d - \frac{\ell}{K}\sin^{-1} k\right) \qquad (46)$$

where

A = surface area of particle ("membrane" area),

$d = \frac{m + s}{2}$, and

$K = \left(\frac{\ell^2 - d^2}{2\ell}\right)^{\frac{1}{2}}$

In practice the area for each rock piece was obtained using a graph identical to Figure 12 but on an expanded scale. Using the above data, rugosity values were calculated for different sizes and kinds of rock:

$$\text{Rugosity} = \frac{\text{Amount of asphalt on rock, cm}^3}{\text{Surface area of rock, cm}^2} \qquad (47)$$

The manually measured ℓ, m, and s values used in the surface area calculations for each rock were also useful for calculations of packing volume and comparisons with values obtained by the water displacement method. Statistical difference analysis on ninety rocks measured by the two methods indicated that direct measurement using the assumed ellipsoid shape is in good agreeement with results obtained by the volume-by-water-displacement method. (For a detailed analysis, see Appendix 4). This suggests another method for measuring packing volumes of particles.

In order to determine differences in the shape of ellipsoids, comparisons were made among ℓ/s, ℓ/m and m/s ratios for various fractions of the rocks, as shown in Figures 13 to 15. The curves indicate a slight tendency for 0.4 cc rocks to have higher ratios than smaller or larger rocks of the same kind. Each point in Figures 13 to 15 is an average of ten measurements. Statistical analysis in Appendix 5 indicates that the differences are not important.

Miscellaneous Measurements

As pointed out previously, the particle volume distribution of crushed limestone and rounded gravel (or any two aggregates) is expected to be different even if taken from the same sieve-size fraction. Figure 16 gives an example of packing volume distribution curves for 1/2 inch to 3/8 inch crushed limestone and for gravel of the same size. In the case of this limestone and gravel, there is a tendency for the average volume of the limestone particles to be smaller than gravel. Each type of rock from a given quarry (effect of crushers is assumed constant), if sieved by a given procedure, should have a characteristic particle volume distribution on each sieve. Once this distribution is known, aggregates can be combined

on the basis of particle packing volume distribution using sieve grading and proportioning according to the packing volume formula.

The number of contact points in simple cubical packing and in tetrahedral (dense) packing of spheres is six and twelve, respectively. The same numbers apply to ellipsoids in similar loose and dense packings. The number of contact points for the nine groups of one-volume aggregates was determined at one particular mass density, using for detection the disturbance of the asphalt coating. The procedure involved mixing about 500 cc of rocks at 300 F with just enough 60-70 penetration asphalt to fill the volume of rugosity. The coated rocks were then placed in a container so as to obtain about equal porosities. The mass was then cooled to 0 F, the rocks were separated and the contact points counted. Figure 17 shows an example of a contact point distribution curve with an average of 7.6 points. No significant differences were found in the number of contacts in various kinds and sizes of rocks as shown in Appendix 6. It is expected that the number of contact points increases with increased compaction of the particles (24).

Identical Bulk Volumes with Identical ΣV_p of Rocks

As previously mentioned, the packing volume V_p of each individual rock can be calculated:

$$V_p = \frac{W}{G_{s+v}} + AR \qquad (48)$$

The number of particles needed to give a certain bulk packing volume ΣV_p of a mass of particles is:

$$N = \frac{\Sigma V_p}{V_p} \qquad (49)$$

The total weight ΣW of such a mass of N particles would be

$$\Sigma W = NW = \frac{\Sigma V_p}{V_p} W \tag{50}$$

or

$$\Sigma W = G_{s+v} (V_p - AR) \frac{\Sigma V_p}{V_p} \tag{51}$$

Equation 51 permits the calculation of how much by weight of a certain "size" of rock is needed to obtain a given packing volume ΣV_p for a mass of particles.

If Equation 51 holds, and if sliding friction is similar in the three rocks tested, as previously theorized, the rocks should have similar bulk volumes for identical ΣV_p. This suggestion was tested by two methods: free fall and vibratory compaction.

For the free fall test each of the three sizes of the three rocks (nine batches altogether) were prepared with identical total packing volumes of 800 cc. The dry, clean rocks were then poured from an average height of three inches and within a time interval of ten seconds to fill a cylindrical container five inches in diameter and five inches high. The resulting bulk volumes were then determined for each of the rock types and sizes by a direct measurement between the top of the calibrated container and the rock surface. Graphical comparisons are given in Figure 18. Statistical analysis showed no significant difference in the bulk volumes thus obtained.

In another series of tests a sinusoidal vibration was applied to the various rocks in bulk, with a peak acceleration of 1.5 times gravity and without surcharge. The vibrating frequency was 20 cps: the bulk-mass volumes of the rocks were measured at one, ten, one hundred and one

thousand cycles of vibration. Since the same rock samples had to be used repeatedly in these tests, the compaction was not extended beyond 1000 cycles to minimize particle degradation. The results are summarized in Figure 19 and the data are tabulated in Table 2. For convenience, porosities n_p, instead of bulk volumes, were compared. The equipment used for vibratory compaction of the rocks is shown in Figure 20.

The measurements showed that all rocks had similar densification trends. The bulk volumes and porosities n_p obtained at each of the indicated cycles were similar for a given sum of packing volumes (ΣV_p) regardless of rock type or size. This finding was as expected from the theoretical considerations.

As an additional check, half-inch marbles with R = 0 and the same ΣV_p were included in both of the above compaction tests. Marbles behaved quite similarly to the various one-size rocks.

Rock Parameters Compared

The central hypothesis was that the volume which a particle, large or small, angular or rounded, smooth or rough, occupies in a mass of other particles is an important factor as far as bulk properties under a defined compaction are concerned. The test results show that the concept of particle packing volume helps to define the characteristic space occupied by a piece of rock within a bulk. The packing volume can be calculated using Equation 24:

$$V_p = \frac{W}{G_{s+v}} + V_a$$

where G_{s+v} is defined by Equation 27.

However, when dealing with bulk density (or porosity), another type

of specific gravity for a rock piece may be useful. It is based on packing volume V_p and may be called packing specific gravity, G_p. If W is the dry weight of a rock piece and V_p is its packing volume, then

$$G_p = \frac{W}{V_p} \tag{52}$$

Numerically, G_p is lower than all of the commonly used specific gravity values because the volume includes surface voids. G_p is constant for one given volume of rock, but varies with rock size and type since surface voids are determined by surface roughness and surface area, and these depend upon the rock size and type.

From Equation 52 a weight-volume relationship for a number of particles taken together is:

$$\Sigma W = G_p \, \Sigma V_p \tag{53}$$

If a given total packing volume ΣV_p (say ΣV_p = 1000 cc) of any of the nine individual rock-size groups were desired and designated as

$$\Sigma V_{p1} \; ; \quad \Sigma V_{p2} \; \ldots\ldots \; \Sigma V_{p9} \tag{54}$$

then the total weight ΣW needed to give these constant volumes, can be calculated using Equation 53. It is apparent that in general:

$$\Sigma W_1 \neq \Sigma W_2 \neq \ldots \Sigma W_9 \tag{55}$$

If identical free fall or vibratory compaction is employed to densify the above nine batches of rock, the bulk volume V_B will be equal or:

$$V_{B1} = V_{B2} = \ldots\ldots\ldots\ldots\ldots V_{B9} \tag{56}$$

Weight per unit volume of these particles will be different depending on G_p and on the type of compaction. At this stage of development the

packing volume concept permits the calculation of "one-size" rock weights which will produce identical bulk volumes under identical compaction.

Laboratory findings support the general line of theoretical considerations discussed previously. Angularity did not prove to be a distinctive feature, although some of it is taken into account by the rugosity factor R. Shape did not have a noticeable influence. Nothing can be said about the effects of ℓ/s ratios larger than 3.4 since none of the rocks used in the tests exceeded this value.

EXPERIMENTS WITH MIXES IN TENSION AND COMPRESSION

In order to verify the applicability of (a) the packing volume concept with stagnant and flow asphalt, and (b) the contact area-strength theory, a series of experiments on compacted one-size mixes was performed. Both tension and compression tests were used.

Choice of Variables

In the tension and compression tests, the following variables were used:

Rock type - rounded gravel, crushed limestone

Rock "size" - 0.04 cc, 0.4 cc, 4 cc

Asphalt "film" - 10, 20, 30 microns

Rate of deformation - 0.3, 3, 30 %/minute

Temperature - 60, 80, 100 F

In the work with uncoated aggregates, rock types used included crushed gravel. However, since the rugosity values of the crushed gravel and crushed limestone were found to be quite similar (Figure 11), only the crushed limestone and the rounded gravel were used in work with mixes.

The three rock volumes of 0.04 cc, 0.4 cc and 4 cc correspond to approximately 1/8, 3/8 and 3/4 inch sizes when graded by square opening sieves. As in the case of uncoated aggregates, these sizes were chosen to allow for direct measurement of rugosity, radii, and packing volume of the rock pieces. They also represented approximately the coarse aggregate fraction as used in practical mixes.

The asphalt film thicknesses chosen were 10, 20 and 30 microns. Film thickness as defined here is obtained by taking the volume of flow asphalt (rugosity asphalt excluded) and dividing it by the total "membrane" area (Figure 3) of the rock surface. The 10-micron lower limit was chosen as the thinnest practical film and the maximum of 30 microns was set because the asphalt from thicker films showed a tendency to flow downwards in a specimen during compaction. "Film thickness" rather than "asphalt content" was used to simplify and unify the contact point "strength" analysis.

Constant rate of deformation instead of constant rate of loading was used to facilitate careful seating of the specimens and to avoid preloading before testing. This was very important at higher temperatures when the specimens were "weak." Also, the application of "strength" analysis was simplified by this approach. The actual magnitudes of the rates were selected to be in or near the flow region as approximately defined by Figure 9. There was also a limitation in the testing equipment as to the lowest possible rate of deformation.

The three temperatures of 60, 80 and 100 F were also selected so as to stay in or near the flow region of the asphalt at the contact points. An attempt was made to go above 100 F, but the one-size mixes were rather weak and were hard to handle without damaging them.

Other variables which were kept constant will be discussed in the next section.

Specimens, Equipment and Measurements

Altogether six distinct batches of rock were mixed with asphalt:

CL-0.04 (0.04 cc Crushed Limestone)

RG-0.04 (0.04 cc Rounded Gravel)

CL-0.4 (0.4 cc Crushed Limestone)

RG-0.4 (0.4 cc Rounded Gravel)

CL- 4 (4 cc Crushed Limestone)

RG- 4 (4 cc Rounded Gravel)

The mixes were prepared by a standard procedure. Each batch of aggregate had a total packing volume of 565 cc (sum of the packing volumes of individual particles, or ΣV_p). The actual packing volumes and the coefficients of deviation for each batch were similar to that described in the uncoated aggregate section.

One 55-penetration asphalt was used in all mixes. Characterizing data on this asphalt are given in Table 3. The asphalt and the aggregate were placed separately in an oven at 280 F and heated for about two hours. Next a precalculated amount of asphalt (Figure 24) was added and mixed by hand in a 2-quart bowl for one minute. The mix was then placed in an unheated (75 F), 12-inch high by 4-inch diameter split mold which was previously lined with a silicone-coated aluminum foil. The specimen was then put on a vibratory table and compacted using a frequency of 20 cps and 1.5 g's maximum accceleration, just as in the experiments with uncoated aggregates (Figure 21). The standard number of cycles for compaction was 1,000, with one exception which will be discussed later.

The specimens were compacted without a surcharge on the top and therefore levelling and smoothing of the upper surface after vibration was

necessary. This was accomplished by 50 light tampings with a 2-inch diameter, 1,400 gram tamper, dropped each time from a 3/4-inch height. The compacted specimens were almost exactly four inches in diameter and four inches high.

After cooling for two hours at 75 F, the specimens were taken out of the molds. Hard asphalt (15-20 penetration) was used to glue a 3/8 x 4 x 4 inch aluminum plate to each end of the specimen. Then a cardboard jacket was wrapped around the specimen and adjustable spacers were placed at all corners of the plates to keep the specimen from deforming laterally and vertically, as shown in Figure 22. The specimen was then cured for twelve hours at 75-80 F. Before testing, each specimen was placed for at least two hours in air at the test temperature.

In all tests the specimens were "seated" between the testing machine heads with restraints on so as to avoid damage. The lower test head or table was adjustable by hand and was used in conjunction with the load indicator on the testing machine to establish full contact between the two plates of the specimen and the two test-head surfaces of the testing machine. Four screws were placed at each end to firmly tie the specimen to the testing system. The spacers and the cardboard were removed when the test was run.

Specimens were seated and fastened in the same way regardless of the type of test. In other words, the capping and seating was identical in all cases. It follows that the constraints imposed upon the specimens by the plates were similar in all tests.

The electrohydraulic system used for applying the prescribed constant rate of deformation to each specimen consisted of a testing frame with a

1000-pound hydraulic actuator (jack), a 1000-pound load cell, a hydraulic pump and an electronic control console with two-channel strip chart recorder. One of the channels was used for recording the force (output) while the other registered the prescribed rate and type of deformation (input).

The value for maximum force (peak load) was obtained by direct scaling from the load-time chart. The energy values were calculated by taking a number of evenly spaced force readings in an interval of time and multiplying the average of these readings by the distance travelled.

There were no essential differences in the method of performing the tension and compression tests, except for the "pull" and "push". The specimens were fastened in a similar manner and all tests were run to at least 2.5 percent axial deformation. This was the highest limit that could be obtained at the slowest rate of deformation with the equipment used.

In order to obtain insight into solid-asphalt-void relationships for each specimen, the height of each specimen was measured at four points to the nearest 1/100 inch and the total volume was calculated. Since the volumes of asphalt and of the rock were known, actual air voids in the specimen could be determined.

After testing, the specimens were placed in a solvent (benzene) and the rocks were recovered by cold extraction. These same rocks were used again since the production of a new batch for each specimen would have been very time consuming.

Trial Experiments

In order to establish an efficient procedure for the forming and testing of specimens and to obtain an idea whether certain fixed factors, such as compaction, were proper for tension and compression specimens, trial tests were performed. These tests were also set up to indicate the magnitudes of various interactions between the factors used in this experiment.

As a preliminary step in the experiments with mixes, a 2^5 factorial experiment in tension was performed using the two types of aggregates and the high and low levels of each of the other factors. The results indicated that some of the three-way and perhaps even higher interactions of the factors may be rather large (significant). This was taken into account in the design of the basic experiment.

It was also ascertained that it took up to six hours to change the temperature in the walk-in chamber in which the specimens were tested. Therefore each test temperature should be viewed as a block within which randomization can be applied.

The same trial experiment indicated that the rounded gravel mixes had a peak "strength" in tension higher by ten percent or even more than limestone mixes. Since it is known that bituminous mixes in tension are sensitive to void content, the void measurements were compared. The gravel mixes had slightly lower void content for the standard 1000 cycles vibratory compaction. By trial and error it was found that by reducing the compaction to around 100 cycles for the gravel mixes, a void similar to that of limestone mixes (using 1000-cycle compaction) was obtained. The small differences in strength then disappeared.

Tests in compression showed that the 1000-cycle vibratory compaction gave similar results, as far as force is concerned, for the two rocks. Thus it was decided to compact the gravel specimens for tension tests for 100 cycles and all others for 1000 cycles. In other words, the tension specimens were made so as to contain equal voids for the comparable gravel and limestone rocks. Compression specimens, on the other hand, all had equal compaction.

Design of the Basic Experiment

As outlined at the beginning of the section, two types of rocks were included in both the tension and compression tests. Since there was no way to describe them numerically, two qualitative levels for rocks were used. The other factors had three quantitative levels each.

The main purpose of the basic experiment was to show that with the help of the packing volume concept and "neutralizing" rugosity, mixes containing gravel and limestone rocks can be made to have similar resistance to flow under a given load. Statistically speaking, the first goal was to show that the means for "strength" of the mixes containing the two different rocks are the same.

The second goal was to illustrate also the effects of other factors. Since it is known that factors like temperature and rate may introduce quadratic terms in descriptive equations, three levels were introduced in the design.

The response variable (y) was the peak force ("strength") for each specimen. In addition, the energy consumed to 2.5 percent axial strain for each specimen was measured and used as a second type of response variable.

If a full 2 x 3 x 3 x 3 x 3 factorial experiment were performed, adding about 15 specimens for replicates, the total number of specimens to be made and tested would have been about 180 for the tension series with the same number for the compression series, or a total of 360 specimens. Since this is a formidable number of specimens for this type of research, an attempt was made to find a more efficient statistical design. The one which was finally adopted was a so-called composite design developed by Box (111). The treatment combination for one temperature block is outlined in Table 4. This design required 90 basic specimens plus 15 replications for each type of test. As Table 4 shows, the design consists of a 2^n factorial plus intermediate points. Analysis of variance can be made on the factorial part and regression analysis on the whole set. The five duplicates in each block were to be used to test whether the higher interactions are large (significant) or small.

As mentioned before, the randomization for each type of test over the whole field was impractical because of difficulties with test temperature control. Instead three completely randomized blocks were used, 60, 80 and 100 F. This really is a split plot design.

The mathematical model for the Peak Force and the Energy to 2.5 percent extension or compression was:

$$\begin{aligned} y_{1234} = {} & \beta_o x_o + \beta_1 x_1 + \beta_{11} x_{11} + \beta_2 x_2 + \\ & + \beta_{22} x_{22} + \beta_{12} x_{12} + \beta_3 x_3 + \beta_{33} x_{33} + \\ & + \beta_{13} x_{13} + \beta_{23} x_{23} + \beta_{123} x_{123} + \\ & + \beta_4 x_4 + \beta_{44} x_{44} + \beta_{14} x_{14} + \beta_{24} x_{24} + \end{aligned}$$

$$+ \beta_{124}x_{124} + \beta_{34}x_{34} + \beta_{134}x_{134} +$$

$$+ \beta_{234}x_{234} + \beta_{1234}x_{1234} \qquad (57)$$

where

x_1 = size of aggregate,

x_2 = asphalt film thickness,

x_3 = rate of deformation,

x_4 = temperature, and

β's = coefficients.

Force and Energy Comparisons

The results obtained in the tension and compression tests are presented in three ways: first, by graphical comparisons, second, by analysis of variance and third, by regression equations.

Graphical Comparisons for Force

Examples of force-deformation curves replotted from the strip chart recorder are given in Figures 25 to 28. They illustrate the general similarity in shape and magnitude between curves for specimens made from the two rock types. The maximum force values for tension and compression are tabulated in Tables 5 and 6. There are six blocks altogether, each containing thirty basic readings plus five replications. The grouping of the data was done in such a way that both analysis of variance (ANOVA) and regression can be made. The coding of the specimens was as follows:

Rock Type: Gravel = 0 Limestone = 2

Rock Size, cc: 0.04 = 0 0.4 = 1 4 = 2

Asphalt Film, Microns: 10 = 0 20 = 1 30 = 2

Rate of Deformation, %/min: 0.3 = 0 3 = 1 30 = 2

Temperature, F : 60 = 0 80 = 1 100 = 2

Thus, for example, Specimen 0121 in Table 5 would be gravel, 0.4 cc size, coated with a 30-micron film and tested at a rate of deformation of 3 percent per minute. The temperature is omitted here, since the force is given for various temperatures. If the above specimen was tested at 100 F, the code would simply be extended to 01212.

Since the comparison between gravel and limestone mixes is so important to the objectives of this study, the average force data for each temperature in tension and compression are presented in Figure 29. These comparisons were obtained by taking one particular temperature in Table 5 and averaging the 15 force values of the "0" rocks (gravel) and 15 values of the "2" rocks (limestone). It is apparent that the gravel and the limestone mixes averaged to be of the same "strength" as suggested by the original hypothesis.

There are a number of ways to make other graphical comparisons of the force values and other variables. Some of them are discussed below.

Figures 30 to 32 show how the force is affected by the highest and the lowest levels of rock size, film thickness and rate of deformation, respectively. The average values plotted were obtained by using only the first eight force numbers of each rock type and the three temperatures in Table 5. This gave an average of 24 specimens for each bar graph.

Figures 33 through 36 return to the comparisons between gravel and limestone, but the plots are made using all three levels of each of the variables compared; namely, flow-binder film thickness, particle packing volume, rate of deformation, and test temperature. The averages are

based mostly on three specimens only. The eye suggests that there may be some differences between limestone and gravel mixes in certain plots, but data analysis shows that the over-all averages are similar for the two rocks.

The general trends in the tension and compression test results appear to be quite similar. There may be some differences in the optimum asphalt film thickness for the two tests (Figure 33). The aggregate size also may affect the maximum force values somewhat differently in the two types of tests (Figure 34). However, more work would have to be done to determine this accurately.

The most interesting curve in this series is obtained when the average force values for all thirty specimens in each temperature block are compared as shown in Figure 37. The compressive force turns out to be about three times higher than the tensile and the two curves are approximately parallel. This suggests that similar mechanisms are operative within a mix during each type of test. This indeed appears to be the case as will be seen later in connection with the contact area and "strength" calculations.

It should be added that the general trends of curves for maximum force in tension agree closely with trends reported for the testing of a dense-graded mix in reference 114.

Graphical Comparisons for Energy

The values for energy needed to strain a given specimen up to 2.5 percent are listed in Tables 7 and 8. The tabulation technique is identical to that for force values in Table 5. It should be noted that a strain of 2.5 percent is rather high and, especially in tension, well

beyond the so-called failure strain peak force (114).

The comparisons in Figure 38 show average energy values for limestone and gravel mixes. The difference between gravel and limestone specimens appear to be slightly larger as compared to the average force differences for the two rocks as shown in Figure 29. However, as will be seen later, the statistical analysis does not indicate significance in these differences.

Figures 39 to 42 show the effect of other variables on the energy consumed to deform a specimen. The results are similar to those discussed in graphical comparisons for force.

Figure 43 shows the compression and tension energies to be different approximately by a factor of 3, similar to the force relationships.

Figure 44 presents a summary of force and energy results which indicates that they vary similarly with temperature change.

Table 9 gives a tabulation for calculated voids in each specimen. The average voids for each test and rock size are given in Figure 45. As previously discussed, the gravel specimens for compression tests had a slightly lower void content than the limestone specimens.

Analysis of Variance (ANOVA)

The final ANOVA summaries for each of the temperatures and for the low and the high levels of the various factors are given in Appendices 7 and 8 for the force and energy measurements, respectively. The five replicates in each temperature block were used for the estimate of the "pure" error. This, in turn, was applied to check whether some of the higher interactions were too large and should be excluded from the error terms. Using the F test and a 5 percent significance level, in practically all

cases some of the 3-way interactions were found to be unacceptable for use in the error term. These interactions were taken out of the computations of the final F test values, but they may be real.

The analysis of variance shows that there is no significant difference in the average peak force, both in tension and compression for specimens made from the two rock types. The same applies also to energy values. This result was of course expected since the mixes were designed to be equal. Consequently the analysis supports the main hypothesis of the work, indicating the usefulness of the packing volume and rugosity concepts combined with the concepts of stagnant and flow asphalt.

The ANOVA also shows that the size of the rocks (4 cc versus 0.04 cc) and the rate of deformation (30%/min versus 0.3 %/min) produced highly significant differences in the force and energy values, while the flow asphalt increases from 20 microns to 30 microns produced less significant differences. This, of course, has been illustrated in the graphical presentations.

Regression Analysis

The analysis of variance was performed using only the high and low levels of the factors in each of the six temperature blocks. Since all of the factors except the rock type had three quantitative levels each, a regression equation for the force and energy values could be constructed. This was done using a computer and a stepwise regression program in which only the significant variables or combinations thereof are retained in the operation. The equations for force in compression and tension follow assuming the whole plot error is negligible:

$$y_t = 37.37\,x_1 + 11.23\,x_2 + 29.58\,x_3 -$$
$$- 2.427\,x_4 + 3.240\,x_{11} - 0.03756\,x_{22} -$$
$$- 2.678\,x_{12} - 0.1300\,x_{33} - 3.592\,x_{13} -$$
$$- 0.08039\,x_{23} + 0.02353\,x_{123} +$$
$$+ 0.02706\,x_{44} - 0.6200\,x_{14} - 0.1169\,x_{24} +$$
$$+ 0.03211\,x_{124} - 0.2768\,x_{34} + 0.04058\,x_{134}$$
$$+ 0.00146\,x_{234} - 0.00040\,x_{1234} + \text{error} \qquad (58)$$

$$y_c = 17.63\,x_1 + 36.56\,x_2 + 92.82\,x_3 - 6.480\,x_4 +$$
$$+ 26.79\,x_{11} - 0.1935\,x_{22} - 7.793\,x_{12} - 0.6456\,x_{33} -$$
$$- 10.25\,x_{13} - 0.7567\,x_{23} + 0.2697\,x_{123} + 0.07064\,x_{44} -$$
$$- 1.624\,x_{14} - 0.3494\,x_{24} + 0.09450\,x_{124} -$$
$$- 0.7973\,x_{34} + 0.1180\,x_{134} + 0.01030\,x_{234} -$$
$$- 0.00343\,x_{1234} + \text{error} \qquad (59)$$

where

y_t = peak tensile force on specimen, in pounds,

y_c = peak compressive force on specimen, in pounds,

x_1 = packing volume of rock in cc's,

x_2 = asphalt film thickness, in microns,

x_3 = rate of deformation, in percent per minute, and

x_4 = test temperature in F.

The above equations were obtained by the use of combined test results of both limestone and gravel. This procedure gave about 100 test values for each equation.

Strain at Peak Force

The strain applied to a specimen when the maximum force is reached was obtained from the data curves for the tension and compression tests. The numerical values are tabulated in Table 10 and a graphical comparison of averages is given in Figure 46. As can be seen, the amount of strain at peak load in both tension and compression is about the same for both rounded gravel and crushed limestone mixes, especially at higher temperatures where flow deformation (no brittleness) is predominant.

It is of interest to note that the peak load strain in tension is close to 1/2 percent, regardless of the temperature. This agrees closely with published literature on a typical graded mix (114).

In compression the peak load strain was about three times higher than in tension or similar to the relationship between the peak force in the two tests. The temperatures used in this experiment do not seem to cause differences in the "failure" strain values in compression. In the discussion of the contact area theory, an attempt is made to explain this behavior.

Analysis Using Contact Area Theory

The results discussed so far were aimed primarily at proving that two mixes composed of different rocks, graded by packing volumes, can be made to have similar flow properties by neutralizing the rugosity of a rock and then adding a prescribed amount of binding or active asphalt.

The next question is whether there is a way to predict the actual flow resistance of the mixes once the rugosity has been accounted for and the amount of binding asphalt, plus other measurable parameters, is known.

Such a prediction was attempted using Stefan's theory. The basic equation is derived in Appendix 1. The equation, again, is as follows:

$$F = \frac{10.73}{10^6} \eta \frac{r^4 h_o^2}{(h_o + \Delta h)^5} \times \frac{L}{M} \times \frac{dH}{dt} \qquad (60)$$

where all symbols are as previously shown. They are discussed individually in the sections below. It must be repeated that the use of this equation presupposes a simple and idealized model with a number of assumptions. Nevertheless, agreement between the test results and the predicted values in the flow region is quite encouraging, especially in tension.

Tension Test Analysis

The values for variables used in Equation 60 are summarized in Table 3 and Appendix 9, including one example of the calculations. Graphical comparisons between the predicted and experimental values of peak force are shown in Figures 47 to 52 and may be tested statistically.

The viscosity values are given in Table 3. Since it was not easy to define the actual shear rates encountered at the contact points of the rocks, and since the main interest was in the flow region at 100 F and 80 F, it was assumed that the asphalt exhibited Newtonian flow. Therefore a single value of viscosity for each temperature was used in the calculations.

The contact radius "r" was measured in the laboratory. This was accomplished by taking a compacted mix apart and selecting rocks at random.

By means of a magnifying glass and a ruler the approximate radii of contact points were measured to the nearest 0.01 inch. It was apparent that the size of the "r" varied and a distribution of "r" rather than a single value was obtained (Figure 54). The average "r" was used in the calculations (Appendix 9).

For the h_o, the value of two times the film thickness was used. It was assumed that there is an asphalt plug of average thickness of 2 h_o and radius "r" between the contacts of two rocks. This further implies that the surfaces of the two rocks at the contact points are flat and parallel to each other.

The value h was calculated by taking the total axial strain in the 4-inch long specimen and dividing this by the number of estimated contact points in tension along the axis of the cylinder. The packing of the rocks was assumed to be cubical. This is not unreasonable since the number of other rocks touching any one rock piece was about seven and the packing porosity was not far from that of cubical packing, also. This assumption greatly simplified all calculations.

The value L for the number of rocks in a cubical packing between the ends of the specimen was calculated by taking the length of the specimen and dividing by the average "size" of the rock pieces. In a similar manner, the number of rocks M in one layer of cubical packing was estimated by dividing the cross-sectional area of the specimen by the square of the rock diameter.

For the rate of deformation three values were used in the calculations, namely 0.3, 3 and 30 percent per minute axial deformation. These values were the ones used in the tension and compression tests.

Figure 47 shows that one of the best agreements with theory is found with the small rocks, at high temperature, with thick asphalt films and at the slow rate of deformation. This falls into the flow region where apparently even in mixes with irregular contact surfaces the asphalt exhibits mainly flow and necking behavior as in the case of thick films between plates described by Majidzadeh, Marek and Herrin (109) (110).

Since certain simplifying assumptions are involved, it cannot be expected that the theory and the results would always agree as closely as in Figure 47. Perhaps a two or three magnitude difference between predicted and actual results is acceptable under the circumstances. Figures 48 and 52 indicate general closeness to the experimental values. However, since the predicted values are generally higher than those obtained in the tests, a more complex behavior than simple flow may be starting to take place in some specimens during the test.

The predicted flow region of Figure 9 was prepared on the basis of Majidzadeh's measurements with a 72-penetration asphalt. If this figure is compared with the results shown in Figures 47 to 53, good agreement is obtained in most cases.

There are other trends which appear to be logical if the basic equation is reviewed. It is probably no coincidence that the tests in Figure 47 show the best agreement with the theory. These are the specimens with the largest number of contacts of the thickest films (30 microns) and were stretched at the slowest rate. All of these factors are favorable to flow of the asphalt in a mix instead of to film "breaking." On the other hand, in thin-film, fast-rate, low-temperature, large-rock tests there are greater discrepancies between tested and predicted values.

In general, it can be said that there is more difference between the measured and the predicted values for force as the "size" of the rocks increases. Most likely this is due to the fact that the asphalt plug between any two rocks is defined numerically not only by the thickness or height but also by the radius of the contact. Thus for the same film thickness the radius "r" will be greater for a larger rock than for a smaller one. Consequently the film will flow with more difficulty and there might even be cohesive failure within the asphalt (formation of bubbles and strings) thus reducing the actual test strength compared to the theoretical prediction.

The importance of the r/h_o ratio rather than film thickness per se is illustrated in Figure 53. Here everything has been kept constant in the experiment except that the film thickness was changed from 30, to 20, to 10 microns. If the film thickness is the main factor, the change in film thickness from 10 to 30 microns should introduce a large difference in the strength of the specimen. Yet both the laboratory tests and the theoretical calculations show little if any practical difference. One explanation may be that the decrease in film thickness is accompanied by a decrease in the contact radius "r" (Appendix 9).

Finally, it should be recalled that Newtonian behavior of the asphalt was assumed for all temperatures and rates. This may be satisfactory for 100 F and 80 F and at the slower rates of deformation, but the 60 F region and faster rates are probably not very accurately represented by this assumption.

Compression Test Analysis

The application of Stefan's theory to the compression data presented a more difficult problem than with the tension data. In the first place, the strain at the peak compressive force was around 1 1/2 percent and it is inconceivable for a 20-micron asphalt thickness at the contacts of a large-rock specimen to be compressed by such a large amount. Some other mechanism besides compression or squeezing of the asphalt plug outwards from the initial contact area must be taking place. The compressive test data obtained in the laboratory were compared with two values: (a) the theoretical compressive strength using the simple model as in tension with average contact asphalt thicknesses of 20, 40, and 60 microns ($2h_o$); (b) a shear model with the same values.

In order to set the minimum possible value, the increment Δh in the compression model was assumed to be zero and the force was reduced to:

$$F_c = \frac{10.73}{10^6} \times \eta \times \frac{r^4}{h_o^3} \times \frac{L}{M} \times \frac{dH}{dt} \qquad (61)$$

The shear resistance values were calculated by the formula:

$$F_s = \frac{2.248}{10^6} \times \eta \times \frac{dx}{dh_o} \qquad (62)$$

where

F_s = shear force in pounds,

η = viscosity of asphalt in poises, and

$\frac{dx}{dh_o}$ = shear rate in sec^{-1}.

The sliding plane was assumed to be at 45^o.

Sample calculations for shear force and compressive force are given in Appendix 9 and calculated values are plotted graphically in Figures 55

to 65. As can be deduced from these graphical presentations, there is poor agreement between the predicted theoretical compressive force values based on Stefan's theory and the experimental values. On the other hand, the theoretically calculated resistant force values, based on shear-sliding between the rock pieces, agree well with the experiment. This can be said especially for small rocks with thick asphalt films tested at a slow rate of deformation and at high temperature. These comparisons suggest that there is little if any compression and squeezing of the asphalt plug between two rocks during the compression test and that the deformation is mainly due to shear flow.

The predicted shear values can be divided into three categories: (a) below the laboratory test values; (b) about equal; (c) above. The curves of Figure 66 are presented to illustrate the three areas.

When the predicted values are below the measured results, the pure shear resistance of the asphalt may be augmented by direct particle-to-particle contact and friction. This contact can easily occur at high temperatures (100 F) when the asphalt is "soft" and also if the test is run very slowly (Area 1, Figure 66).

The other extreme takes place when the temperature is low (60 F), the asphalt films are thin, and they are sheared at a fast rate. Due to stress concentrations the film is disrupted. The result is a lower shear force in the experiment than the prediction from theoretical calculations (Area 3, Figure 66).

Between these two extremes there is an area of close agreement between the experimental and the theoretical values. These results probably represent pure shear response of the asphalt plug alone.

If the above explanations are applied to the ninety specimens represented in Figures 55 to 65, most of the predictions look satisfactory.

Tension and Compression Compared

There is one slight difference between the tension and compression specimens: in the tension series comparisons are based on equal-void specimens while the compression series is based on equal compaction. The real differences in voids, however, are not statistically significant. It was assumed that actual average film thickness still holds and that there are only slight differences in the orientation of the particles.

One of the most interesting findings is the approximate relationship between tensile and compressive peak force:

$$3 F_{tension} \sim F_{compression} \qquad (63)$$

as illustrated in Figure 43. Various justifications are possible.

First, it is known that many materials have a similar numerical relationship between tensile and shear force.

A more rigorous explanation is suggested by the behavior of a specimen tested well within the region of peak flow — one with small aggregate, high asphalt content tested at a slow rate of deformation. If the predicted theoretical shear curve is plotted and compared with a similar predicted theoretical tension curve (Figure 67), the two differ by a factor of approximately two to three, just as in the experimental results.

EXPERIMENTS WITH MIXES - CYCLIC TESTS

The main purpose of the cyclic (sinusoidal) tests was to show that comparable gravel and limestone mixes, designed with the help of the packing volume and flow asphalt concepts, will have a similar response during a repeated deformation for an identical input. The experiment was performed only at 80 F with the following variables and levels:

Type of Rocks:	Rounded Gravel	Crushed Limestone
Size of Rocks:	0.04 cc	4 cc
Cycles per Sec:	0.01	0.1

The measured response variable was average peak force.

The types of rocks and size were selected to represent the extreme values used in the tension and compression series. The frequencies of 0.01 and 0.1 cycles per second were used in order to stay close to or within the flow region. The lowest frequency was dictated by the total test time since a noticeable distortion due to gravity was observed in some of the weaker specimens if they were left without a lateral support at 80 F. The asphalt film thickness was 20 microns.

Closely linked with the decision for cycling frequency and the total test time, was the decision for the number of cycles each specimen was to undergo. Since 15-20 minutes was set as the desirable maximum test time, the total cycles to be applied to each specimen were set at 20.

The peak-to-peak strain applied was one percent of the length of the specimen. Preliminary tests had indicated that this was about the

limiting strain at which the asphalt plug at the contact points was primarily being distorted by flow, rather than by stringing and hole formation. The measured peak force during the last few cycles was usually slightly lower than during the first cycles, which supports the above reasoning.

The factorial experiment with the mentioned levels was run in duplicate. The results are summarized in Appendix 10 and illustrated in Figure 68.

The statistical analysis and comparisons show similarities between the two types of mixes, just as in the case of the tension and compression tests (Appendix 10). The load response was not symmetrical as can be seen from Figure 68. Consequently, analytical description for the force response curve was not attempted.

SUMMARY AND APPLICATION

The results obtained in the experimental work followed closely the theoretically predicted trends. Following is a summary of the main developments and of the possible usefulness of the findings.

The work was directed towards finding a unified approach for physical characterization of aggregate-binder systems so that flow resistance under varied conditions is predictable and can be explained. The investigation was carried out using three sizes of monovolume aggregates in uncoated condition as well as mixed with asphalt.

It has been accepted that sieve-graded aggregates of different shape and with different surface characteristics behave differently during handling and application. For instance, when two types of aggregates are sieved through square-hole sieves and a container of a given unit volume is filled with each of them, the number of particles in this unit-volume will not be the same. This fact was verified experimentally and the search was pursued for a better particle characterization, singularly and in bulk.

An attempt was made to find a way of equalizing the number of particles in a given unit (bulk) volume when placed and compacted under prescribed conditions. The concept of "packing volume" (elbow room) to achieve this goal for particles was proposed. The packing volume was defined as the room which a particle occupies in bulk with other particles. Packing volume was physically measured by coating a rock piece with

asphalt, removing the excess coating down to the asperities of the rock, and then determining the volume of the "coated" piece. The amount of asphalt retained in the surface crevices was called "rugosity asphalt" and its volume, "rugosity volume." The usefulness of the packing volume concept was then tested experimentally.

Various rocks of different sizes were carefully graded by packing volume and a standard size container was filled with each of the rocks, depositing each rock in a standardized manner. The number of rocks in the container for a given rock "size" was the same, regardless of the type of rock used. The packing volume concept was then applied to mixes.

When different types of rocks with similar packing volumes were mixed with the same amount of asphalt, compacted and tested at a constant rate in tension and compression tests, different resistance to flow (or "strength" values) was encountered. On the other hand, when as a first step enough asphalt was added to offset rugosity and to create equal "solid"-void relationships, and when then a given amount of so-called "flow asphalt" was introduced, the flow properties of mixes with different aggregates proved to be similar. This approach also made it possible to predict theoretically the flow resistance (strength) of the mixes.

For the "strength" predictions a contact area model was employed using the theory developed by Stefan in conjunction with adhesives. The calculated values were in good agreement in the case of tension tests but did not agree in the case of compression results. A good agreement between the experimental and predicted compressive "strength" was obtained when the shear theory was applied.

The engineering and practical significance of this work can be summarized by saying that a unified, systematic and predictable mix design

concept has been provided for a variety of aggregates.

The work presented here has also clarified some other factors and their interactions which until now were understood only partially or in a qualitative manner. Thus the emphasis on surface area of aggregate as it increases with diminishing size does not appear to be justified in asphalt mixes, since rugosity decreases with size and may cancel the effect of surface area increase on the asphalt requirement for a mix.

The use of film thickness as the determining factor in mix behavior is also questionable. The ratio of the "contact area radius" to film thickness is of more significance. This ratio can also be used to explain optimum asphalt content in mixes. At the optimum point this ratio should be at its maximum value.

Since Stefan's theory in tension considers the flow of the asphalt between two rocks as shear flow, failure of bituminous mixes in the flow region (non-brittle) appears to be in shear.

The data indicate that the maximum rate of strain in the asphalt contact plugs between the rocks defines the region where these contact plugs fail in flow, rather than due to brittleness or "stringing." This rate of strain can be predicted numerically.

Some questions arise about the procedure of grading the aggregate by packing volume. This aspect has not been investigated here but it seems likely that sieves can still be used for grading. It is expected that a given stone quarry or sand pit will have a relatively uniform product which can be characterized by sieves and correlated with packing volume. Once this correlation is known, mixes can be designed using sieve sizing.

Similar projections can be made about rugosity measurements. Rocks

from one source and crushing process are expected to have a characteristic rugosity for a given size. Once this is known, it can be taken into account when a mix is designed.

CONCLUSIONS

The objectives set at the beginning of this work were essentially attained. The conclusions are based on theoretical considerations and laboratory work with certain crushed limestone, crushed gravel and rounded gravel aggregates of three packing volumes: approximately 0.04, 0.4, and 4 cc (about 1/8, 3/8 and 3/4 inch respectively) with and without asphalt. Although several important aggregate and mix variables have been included on a fairly broad scale, it is probable that these conclusions can be applied to a wider range of aggregates and mixes than those studied. Strictly speaking, the extension of the validity of the findings beyond the specific scope of this study remains to be demonstrated.

1. Particle packing volume, the volume which a piece of aggregate occupies in a mass of other particles, is a parameter unifying the bulk behavior of coarse aggregates.

2. The packing volume of a particle is a function of the volumes of solids, internal voids, and surface roughness or rugosity of the rock piece.

3. The rugosity volume of a rock is a function of, (a) "surface area", and (b) roughness of the rock surface. The area and the roughness vary with rock size, but in opposite directions.

4. When asphalt is added to aggregates, a certain amount of it is used to fill up the surface voids or the rugosity volume, and does not participate in flow when load is applied. This is called rugosity asphalt

or stagnant asphalt and its addition completes the packing volume of each rock piece.

5. If a flow or binding asphalt is introduced in addition to the rugosity asphalt, a unified approach to mix design may be possible using different types of aggregates.

6. With the help of Stefan's theory (hydro-dynamic theory), the expected peak force for a compacted specimen can be closely predicted in or near the flow region when the flow asphalt alone is considered as the "working" asphalt.

7. Two geometric parameters which affect the "strength" of a mix are, (a) average radius of asphalt contact "plug" between rocks, and (b) the thickness of the plug or film thickness. The ratio of radius/film thickness is important, rather than the film thickness alone.

8. If the rate of strain imposed in the "necked down" surface of an asphalt plug between two rocks exceeds a certain critical limit, the asphalt plug will "fail" in cohesion (hole forming and stringing) instead of flow and "necking."

RECOMMENDATIONS

The work done so far has involved only one-size (one-volume) rocks in the coarse aggregate fraction of a mix. The next important step could be a two-size and multi-size system, including also sand-size particles. As in this work, first only dry aggregates should be considered. The most important prerequisite before "blending and testing" should be a hypothesis concerning the packing of different size particles. Since the rugosity of a rock changes with its size, a rugosity distribution instead of a single rugosity number, as in the present experiments, may become necessary to define the "elbow room" of the particles. For practical purposes it may be possible to work with an "average" or "effective" rugosity for multi-volume gradations.

If asphalt is added to the graded system, the radii of contact points as well as film thicknesses will vary from place to place and it may become necessary, once more, to work with a distribution of values rather than a single r and h, even though the "average value" method worked well with mono-volume rocks although even these did not actually have single values for the above parameter.

TABLES

TABLE 1

DATA ON AGGREGATES

	Rounded Gravel			Crushed Gravel			Crushed Limestone		
	0.04	0.4	4cc	0.04	0.4	4cc	0.04	0.4	4cc
Approximate Size, inches	1/8	3/8	3/4	1/8	3/8	3/4	1/8	3/8	3/4
Average Packing Volume, cc	3.71	0.297	0.041	3.61	0.291	0.039	3.66	0.252	0.036
Rugosity, cm	0.0026	0.0034	0.0044	0.0080	0.017	0.027	0.0077	0.016	0.025
Apparent Specific Gravity	2.67	2.67	2.67	2.67	2.67	2.67	2.71	2.71	2.71
Bulk Specific Gravity	2.54	2.54	2.54	2.54	2.54	2.54	2.66	2.66	2.66
Average Particle S.A., cm^2	0.61	2.31	12.6	0.60	2.45	12.1	0.58	2.40	12.4

TABLE 2

POROSITIES OF VARIOUS ROCKS, VIBRATORY COMPACTION

Cycles	Type of Rock									
	CL-4	CL-.4	CL-.04	CG-4	CG-.4	CG-.04	RG-4	RG-.4	RG-.04	Marb.
	41.00	41.99	41.86	40.56	41.82	40.18	40.93	41.40	40.14	40.44
	39.90	40.53	41.31	41.10	40.87	41.53	39.00	40.44	40.34	40.67
1	39.54	39.77	40.56	40.56	41.63	41.00	39.36	40.64	40.73	40.67
	39.36	40.31	40.56	40.56	42.19	40.46	39.76	41.02	39.54	40.21
	40.27	40.53	41.13	39.56	40.48	41.27	40.00	40.64	40.00	40.21
	38.61	40.53	40.56	40.38	40.28	40.18	40.54	40.44	39.14	39.04
	39.54	39.58	40.37	39.80	39.89	39.63	38.51	39.85	38.72	39.04
10	38.42	38.99	39.60	38.71	40.87	40.46	38.71	39.65	39.34	40.21
	39.36	39.58	39.79	39.65	40.28	40.18	39.51	39.85	39.02	39.80
	38.22	39.38	39.99	38.71	39.68	40.18	38.30	39.85	38.72	39.51
	37.25	37.38	37.57	37.54	38.66	38.48	36.88	38.21	37.24	38.07
	36.45	37.79	37.57	36.94	38.03	38.19	37.32	38.42	37.02	38.56
100	36.45	37.05	36.94	36.94	39.08	38.48	36.21	38.21	37.24	38.07
	36.85	37.17	37.10	37.33	38.87	37.40	36.06	38.42	37.24	38.56
	37.45	37.38	36.94	36.54	37.82	38.48	37.10	38.42	37.08	38.31
	36.45	36.96	36.50	35.28	37.29	36.06	36.20	37.00	37.24	37.50
	35.42	35.23	35.85	35.71	36.06	37.90	35.97	36.26	35.91	37.32
1000	35.21	36.11	36.72	35.71	36.95	37.60	36.20	36.92	36.14	38.31
	36.45	36.54	34.95	35.50	37.39	35.74	35.97	36.70	36.58	36.81
	35.63	35.89	35.85	35.28	36.06	36.68	36.42	36.36	37.24	37.57

TABLE 3

DATA ON ASPHALT

Viscosity at 60 F, 0.05 sec^{-1} Shear Rate, Poises	4.4×10^7
Viscosity at 80 F, 0.05 sec^{-1} Shear Rate, Poises	2.0×10^6
Viscosity at 100 F, 0.05 sec^{-1} Shear Rate, Poises	1.7×10^5
Penetration at 77 F, 100 g., 5 sec.	55
Softening Point, R & B, F	121
Ductility at 77 F, cm	100+

TABLE 4

COMPOSITE DESIGN OUTLINE ONE QUALITATIVE FACTOR AT TWO LEVELS AND 3 QUANTITATIVE FACTORS AT 3 LEVELS

Treatment Combinations		Dependent Variables																				
		x_0	x_1	x_2	x_1x_2	x_3	x_1x_3	x_2x_3	$x_1x_2x_3$	x_4	x_1x_4	x_2x_4	$x_1x_2x_4$	x_3x_4	$x_1x_3x_4$	$x_2x_3x_4$	$x_1x_2x_3x_4$	x_{11}	x_{22}	x_{33}	x_{44}
1	(1)	+	-	-	+	-	+	+	-	-	+	+	-	+	-	-	+	0	1/3	1/3	1/3
2	x_1	+	+	-	-	-	-	+	+	-	-	+	+	+	+	-	-	0	1/3	1/3	1/3
3	x_2	+	-	+	-	-	+	-	+	-	+	-	+	+	-	+	-	0	1/3	1/3	1/3
4	x_1x_2	+	+	+	+	-	-	-	-	-	-	-	-	+	+	+	+	0	1/3	1/3	1/3
5	x_3	+	-	-	+	+	-	-	+	-	+	+	-	-	+	+	-	0	1/3	1/3	1/3
6	x_1x_3	+	+	-	-	+	+	-	-	-	-	+	+	-	-	+	+	0	1/3	1/3	1/3
7	x_2x_3	+	-	+	-	+	-	+	-	-	+	-	+	-	+	-	+	0	1/3	1/3	1/3
8	$x_1x_2x_3$	+	+	+	+	+	+	+	+	-	-	-	-	-	-	-	-	0	1/3	1/3	1/3
9	x_4	+	-	-	+	-	+	+	-	+	-	-	+	-	+	+	-	0	1/3	1/3	1/3
10	x_1x_4	+	+	-	-	-	-	+	+	+	+	-	-	-	-	+	+	0	1/3	1/3	1/3
11	x_2x_4	+	-	+	-	-	+	-	+	+	-	+	-	-	+	-	+	0	1/3	1/3	1/3
12	$x_1x_2x_4$	+	+	+	+	-	-	-	-	+	+	+	+	-	-	-	-	0	1/3	1/3	1/3
13	x_3x_4	+	-	-	+	+	-	-	+	+	-	-	+	+	-	-	+	0	1/3	1/3	1/3
14	$x_1x_3x_4$	+	+	-	-	+	+	-	-	+	+	-	-	+	+	-	-	0	1/3	1/3	1/3

TABLE 4 (CONT'D)

COMPOSITE DESIGN OUTLINE ONE QUALITATIVE FACTOR AT TWO LEVELS AND 3 QUANTITATIVE FACTORS AT 3 LEVELS

Treatment Combinations		Dependent Variables																			
		x_0	x_1	x_2	x_1x_2	x_3	x_1x_3	x_2x_3	$x_1x_2x_3$	x_4	x_1x_4	x_2x_4	$x_1x_2x_4$	x_3x_4	$x_1x_3x_4$	$x_2x_3x_4$	$x_1x_2x_3x_4$	x_{11}	x_{22}	x_{33}	x_{44}
15	$x_2x_3x_4$	+	-	+	-	+	-	+	-	+	-	+	-	+	-	+	-	0	1/3	1/3	1/3
16	$x_1x_2x_3x_4$	+	+	+	+	+	+	+	+	+	+	+	+	+	+	+	+	0	1/3	1/3	1/3
17	0	+	+	0	0	0	0	0	0	0	0	0	0	0	0	0	0	0	-2/3	-2/3	-2/3
18	0	+	-	0	0	0	0	0	0	0	0	0	0	0	0	0	0	0	-2/3	-2/3	-2/3
19	d_1x_4	+	+	0	0	0	0	0	0	1	1	0	0	0	0	0	0	0	-2/3	-2/3	-1/3
20		+	-	0	0	0	0	0	0	1	-1	0	0	0	0	0	0	0	-2/3	-2/3	1/3
21	$-d_1x_4$	+	+	0	0	0	0	0	0	-1	-1	0	0	0	0	0	0	0	-2/3	-2/3	1/3
22		+	-	0	0	0	0	0	0	-1	1	0	0	0	0	0	0	0	-2/3	-2/3	1/3
23	d_2x_3	+	+	0	0	1	1	0	0	0	0	0	0	0	0	0	0	0	-2/3	1/3	-2/3
24		+	-	0	0	1	-1	0	0	0	0	0	0	0	0	0	0	0	-2/3	1/3	-2/3
25	$-d_2x_3$	+	+	0	0	-1	-1	0	0	0	0	0	0	0	0	0	0	0	-2/3	1/3	-2/3
26		+	-	0	0	-1	1	0	0	0	0	0	0	0	0	0	0	0	-2/3	1/3	-2/3
27	d_3x_2	+	+	1	1	0	0	0	0	0	0	0	0	0	0	0	0	0	1/3	-2/3	-2/3
28		+	-	1	-1	0	0	0	0	0	0	0	0	0	0	0	0	0	1/3	-2/3	-2/3

TABLE 4 (CONT'D)

COMPOSITE DESIGN OUTLINE ONE QUALITATIVE FACTOR AT TWO LEVELS AND 3 QUANTITATIVE FACTORS AT 3 LEVELS

Treatment Combinations		Dependent Variables																			
		x_0	x_1	x_2	x_1x_2	x_3	x_1x_3	x_2x_3	$x_1x_2x_3$	x_4	x_1x_4	x_2x_4	$x_1x_2x_4$	x_3x_4	$x_1x_3x_4$	$x_2x_3x_4$	$x_1x_2x_3x_4$	x_{11}	x_{22}	x_{33}	x_{44}
29	$-d_3x_4$	+	+	-1	-1	0	0	0	0	0	0	0	0	0	0	0	0	0	1/3	-2/3	-2/3
30		+	-	-1	1	0	0	0	0	0	0	0	0	0	0	0	0	0	1/3	-2/3	-2/3

TABLE 5

FORCE IN POUNDS FOR SPECIMENS
IN BASIC EXPERIMENT

Specimen	Tension			Compression		
	60 F	80 F	100 F	60 F	80 F	100 F
0000	23	1.7	.3	74	9	.7
0200	11	.4	.1	23	3	.3
0020	21	1.7	.2	78	7.5	.4
0220	9	1.1	.1	32	4.4	.4
0002	300	50	14	750	95	50
0202	160	33	4	500	83	13
0022	365	73	17	910	140	56
0222	160	35	9	585	90	24
0111	76	11	2	190	37	6.2
0211	26	5.2	1	89	13	4.3
0011	75	11	2.5	312	30	9
0121	78	8	1.7	220	35	8.5
0101	65	10	1	245	30	5
0112	250	50	14	550	145	46
0110	19	1.8	.2	50	7.5	.5
2000	18	1.0	.2	72	9	.7
2200	12	.8	.1	25	3	.3
2020	17	1.5	.2	92	7.5	.5
2220	10	.9	.1	25	3	.3
2002	270	53	13	850	100	54
2202	165	31	5	505	80	14
2022	375	70	15	940	205	70
2222	160	32	6	460	82	20
2111	75	9	1.8	193	33	6.3
2211	35	5.4	1	145	17	4.5
2011	68	9	2.5	377	27	9.5
2121	65	6	1.5	230	33	5.5
2101	60	9	1.5	230	28	6.2
2112	285	47	11	700	155	46
2110	16	2.0	.2	50	5.5	.5

TABLE 6

FORCE IN POUNDS FOR REPLICATE SPECIMENS

Specimen	Tension			Compression		
	60 F	80 F	100 F	60 F	80 F	100 F
0000	25					
0200		1.0				
0020			.2			
0220						
0002			16			
0202						
0022						
0222						
0111						
0211		7.0				
0011						7.0
0121			2.0		24	
0101	80					
0112		55		45	125	.6
0110						
2000				68		
2200						
2020				73		
2220					4	
2002	325	50				65
2202	150	29			95	
2022					230	68
2222			5.0	440		23
2111						
2211						
2011						
2121	70			190		6.0
2101						
2112			10			
2110						

TABLE 7

ENERGY IN INCH-POUNDS x 100
FOR BASIC SPECIMENS STRAINED TO 2.5%

Specimen	Tension			Compression		
	60 F	80 F	100 F	60 F	80 F	100 F
0000	198	10	.4	650	78	4.4
0200	76	2	.2	180	27	2
0200	192	14	.4	660	68	4.8
0220	44	6	.2	280	38	2.8
0002	2500	390	112	5700	760	356
0202	770	176	88	3850	700	106
0022	3250	650	132	5900	1480	416
0222	1140	200	48	4950	780	204
0111	630	100	16	1460	286	48
0211	200	40	6	830	156	36
0011	640	98	22	2540	192	78
0121	670	68	14	1940	296	70
0101	530	78	12	2100	262	46
0112	1850	420	118	4600	1160	372
0110	168	12	.4	450	50	4
2000	160	6	.4	600	74	5.6
2200	102	4	.2	230	30	2
2020	152	13	.4	720	64	4.8
2220	90	6	.2	230	28	2.4
2002	2350	390	112	5900	760	380
2202	1460	246	88	3950	660	84
2022	3200	640	132	5400	1475	455
2222	1420	276	48	3750	630	156
2111	700	86	16	1320	286	40
2211	300	40	6	1110	156	36
2011	610	84	21	2540	192	76
2121	600	50	14	1600	296	40
2101	550	70	12	1940	262	46
2112	2400	420	100	4500	1160	340
2110	140	16	.4	400	50	4

TABLE 8

ENERGY IN INCH-POUNDS x 100
FOR REPLICATE SPECIMENS STRAINED TO 2.5%

Specimen	Tension			Compression		
	60 F	80 F	100 F	60 F	80 F	100 F
0000	198					
0200		44				
0020			.6			
0220						
0002						
0202			116			
0022					580	
0222						
0111						
0211		46				
0011					210	44
0121	720		18			
0101						
0112		470			1100	
0110				400		4
2000				520		
2200						
2020				600		
2220					34	
2002	2650	430				
2202	1480	260			710	
2022						400
2222			44	3050		148
2111						
2211						
2011						
2121	800			1240		42
2101						
2112			94			
2110						

TABLE 9

PERCENT AIR VOIDS IN EACH SPECIMEN

Specimen	Tension			Compression		
	60 F	80 F	100 F	60 F	80 F	100 F
0000	30.7	30.7	30.7	33.2	33.2	32.8
0200	32.2	32.2	32.9	35.3	33.5	34.7
0020	28.8	28.8	28.1	32.1	30.1	30.1
0220	29.7	30.4	31.1	33.0	32.3	32.3
0002	30.7	32.6	30.7	32.0	33.9	32.0
0202	31.6	30.2	30.2	33.5	33.5	34.1
0022	29.7	28.1	29.5	30.1	32.1	30.1
0222	31.1	31.1	30.4	33.0	30.4	33.0
0111	32.6	32.0	32.0	30.7	32.7	33.2
0211	30.8	28.7	30.8	33.2	32.6	30.8
0011	29.6	32.9	30.3	32.9	32.2	30.9
0121	31.3	32.0	32.0	33.2	33.2	31.3
0101	32.5	31.9	31.9	33.8	34.4	33.8
0112	32.6	32.0	32.0	33.3	32.7	32.6
0110	32.6	32.0	32.6	33.9	33.3	33.3
2000	32.0	32.0	32.0	33.2	32.7	32.0
2200	33.5	33.5	32.9	32.9	33.5	33.5
2020	30.4	29.8	30.4	31.1	29.8	29.8
2220	33.0	32.3	33.6	33.0	32.3	32.3
2002	32.7	32.7	32.0	32.6	32.6	32.0
2202	33.5	33.5	33.5	33.5	32.9	32.9
2022	30.4	31.1	30.4	29.1	28.5	29.8
2222	32.7	34.8	32.7	33.6	33.6	31.7
2111	32.4	32.4	31.9	31.9	31.9	31.1
2211	34.5	30.8	30.8	33.9	34.5	30.8
2011	30.3	31.6	30.9	32.2	31.6	30.3
2121	31.2	31.8	31.8	32.5	32.5	29.9
2101	31.1	31.8	31.1	33.1	33.1	32.4
2112	31.1	31.9	31.9	31.9	31.9	30.0
2110	32.4	31.1	31.9	32.4	30.0	30.0

TABLE 10

PERCENT STRAIN AT PEAK LOAD
TO THE NEAREST 0.25%

Specimen	Tension			Compression		
	60 F	80 F	100 F	60 F	80 F	100 F
0000	2	1.5	1	.5	.25	.25
0200	1	1.5	1	.25	.25	.25
0020	2.5	1.5	1	.75	.5	.25
0220	1	1.5	.5	.25	.75	.5
0002	2.5	2.5	2.5	.75	.25	.25
0202	1	1	2.5	.25	.5	.5
0022	2.5	2.5	2.5	1.0	.25	.25
0222	1.5	1	.5	.5	.5	.25
0111	2.5	2	2	.5	.5	.25
0211	1	1	2.5	.5	.5	.25
0011	2	2	2	.75	.25	.25
0121	2	2	2	.5	.25	.25
0101	2	1.5	1.5	.5	.25	.25
0112	2.5	2	2.5	.75	.25	.5
0110	2	1.5	2	.5	.25	.25
2000	2.5	1.5	2	.5	.25	.25
2200	1	1.5	1	.25	.25	.25
2020	2.5	1.5	1	.5	.5	.25
2220	1	1	.5	.5	.25	.5
2002	2.5	2.5	2.5	1.0	.25	.5
2202	2.5	2	2.5	.75	.5	.5
2022	2.5	2.5	2.5	1.0	.75	.25
2222	1.5	1.5	.5	.75	.5	.25
2111	2.5	2.5	2.5	.75	.5	.25
2211	2	1	2.5	.75	.25	.25
2011	2	2.5	2	.75	.25	.25
2121	2.5	2	2	.75	.25	.25
2101	2.5	1.5	2.5	.75	.5	.25
2112	2.5	2.5	2.5	1.0	.75	.5
2110	2	1.5	2	.5	.25	.25

FIGURES

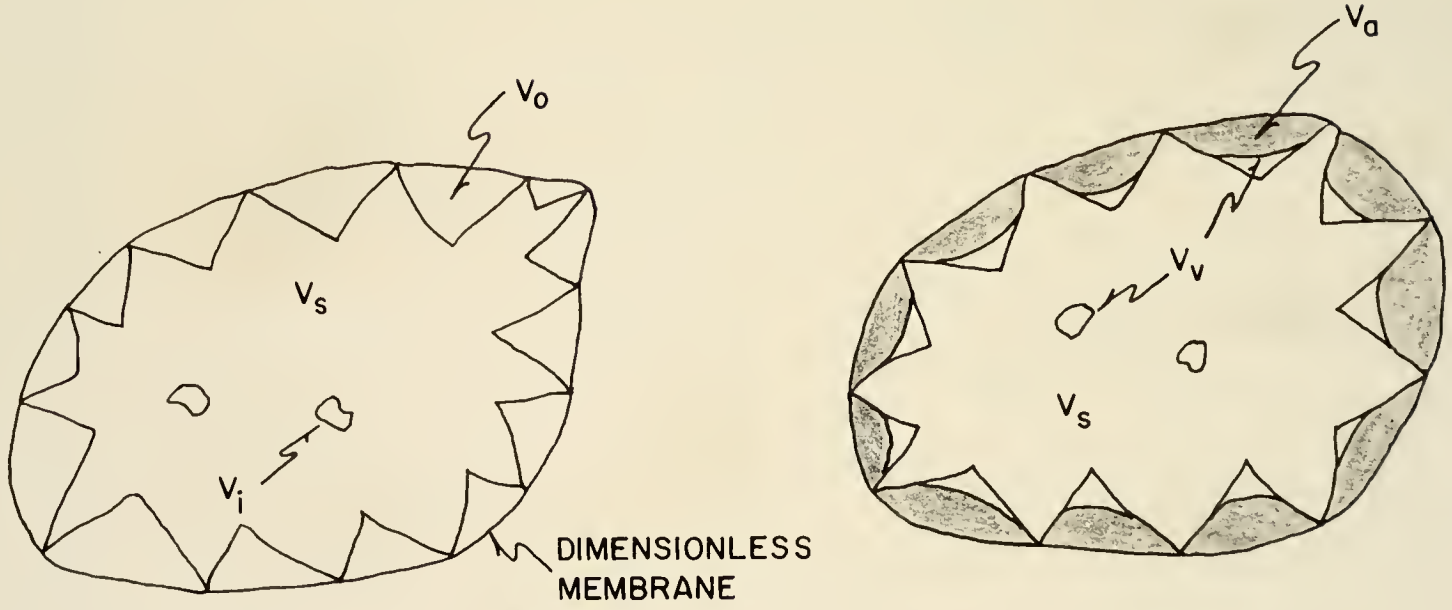

THEORETICAL

$$V_p = V_s + V_i + V_o$$

PRACTICAL

$$V_p = V_s + V_v + V_a$$

FIGURE 1 COMPONENTS OF A PARTICLE PACKING VOLUME

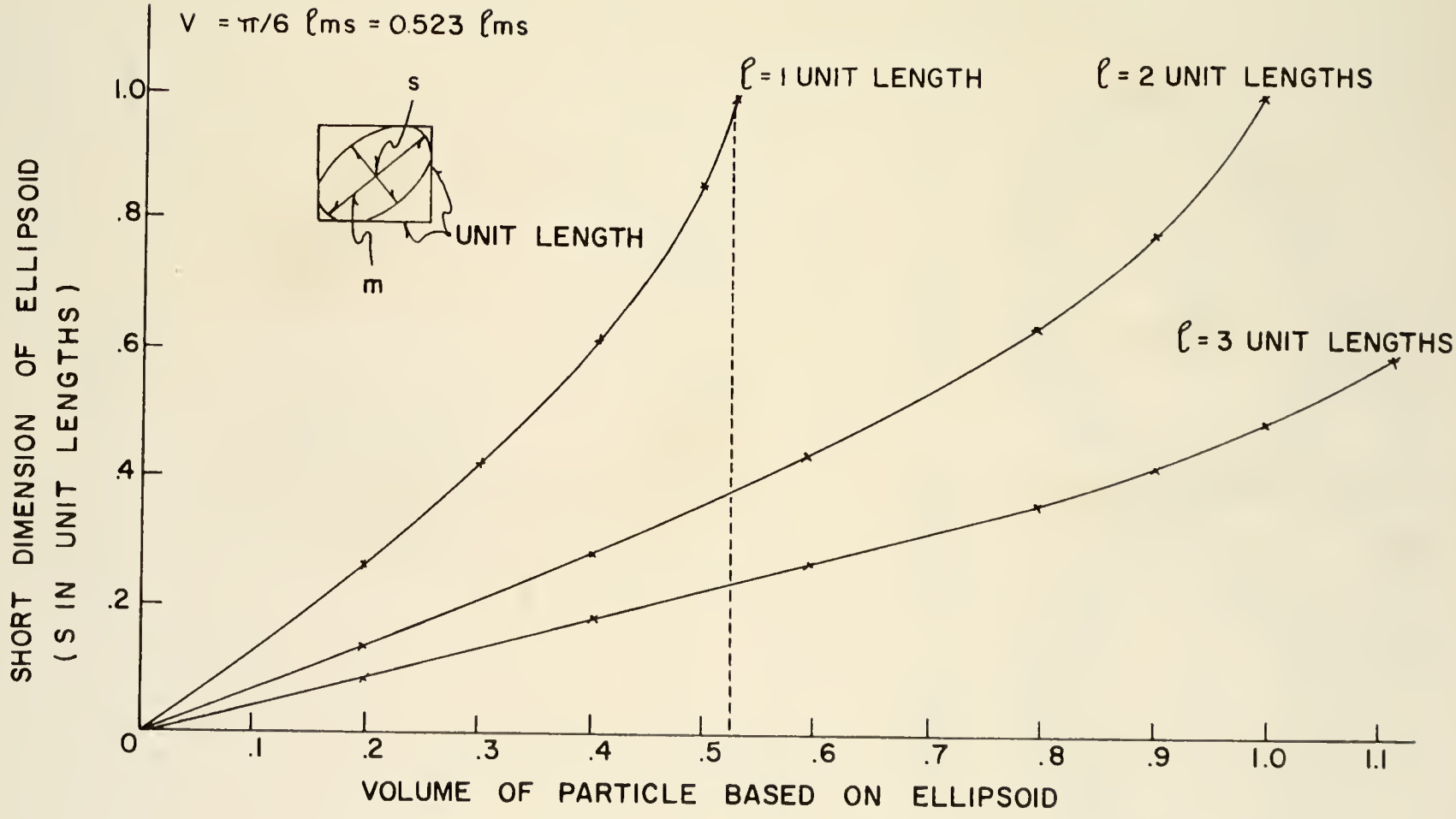

FIGURE 2 THEORETICAL VOLUMES FOR ELLIPSOIDS PASSING A SQUARE SIEVE

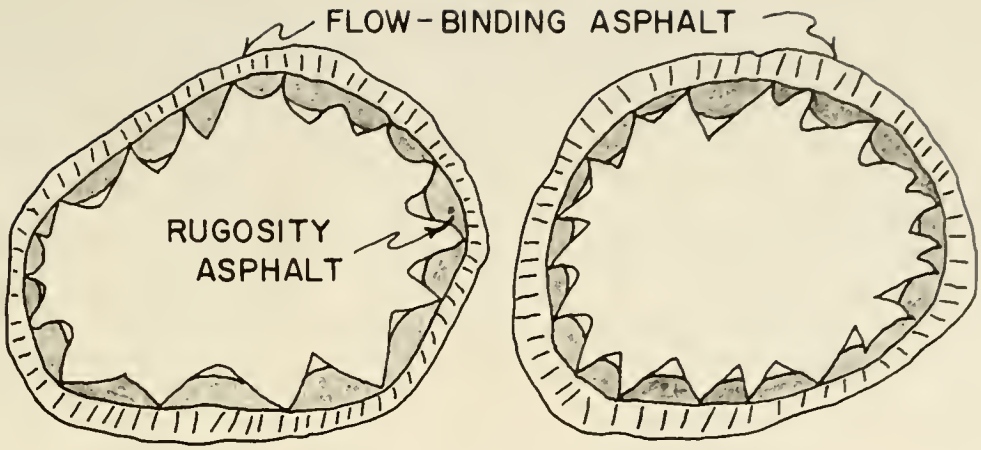

FIGURE 3 FLOW AND RUGOSITY ASPHALTS

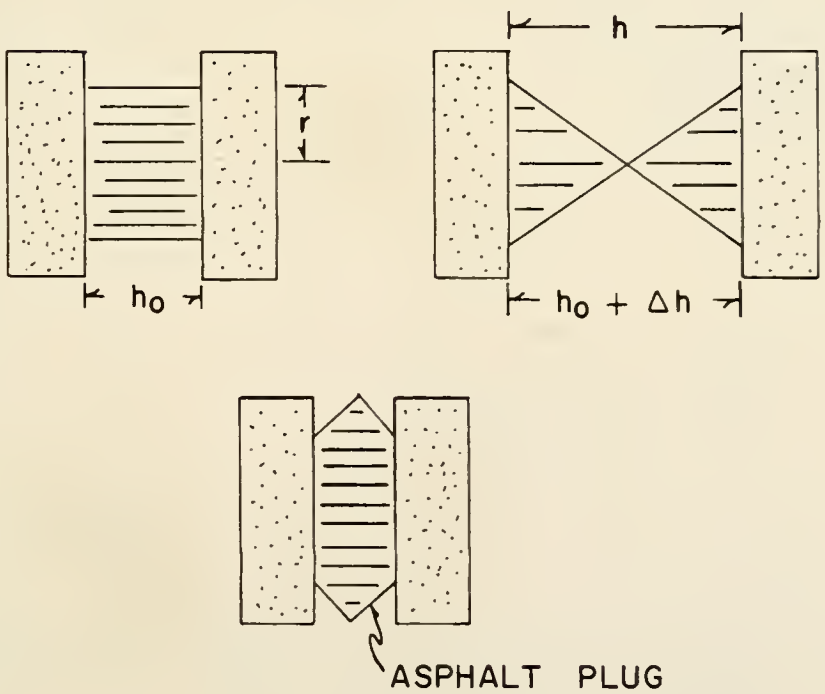

FIGURE 4 DISTORTION OF IDEALIZED CYLINDRICAL ASPHALT PLUG

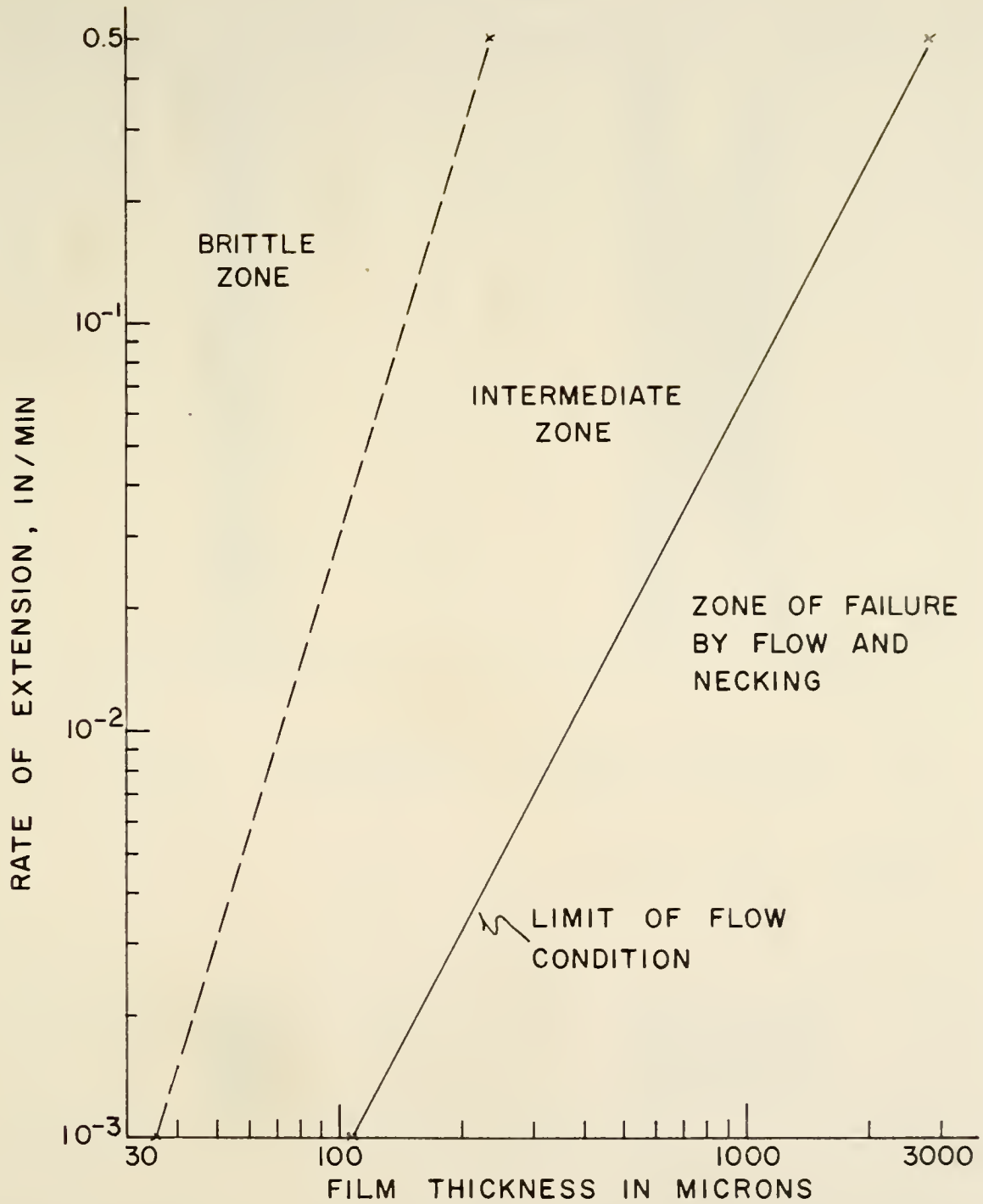

FIGURE 5 INFLUENCE OF RATE OF EXTENSION ON TYPES OF FAILURE.
(FROM MAJIDZADEH, REF. 109, FIG. 11)

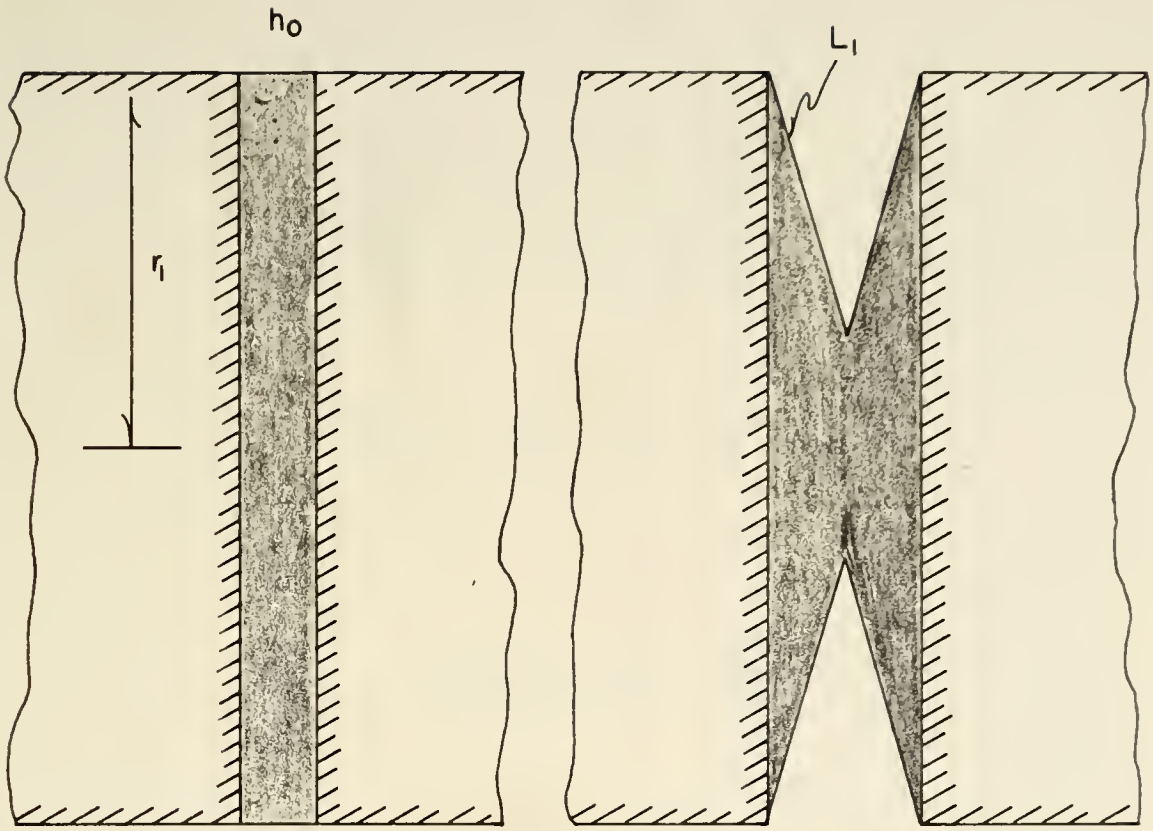

$$\frac{r_1}{h_o} = 5 \qquad \text{MAX. SURFACE STRAIN} = 100\,\frac{L_1 - h_o}{h_o}$$

$$= 100\,\frac{7.2-1}{1} = 620\%$$

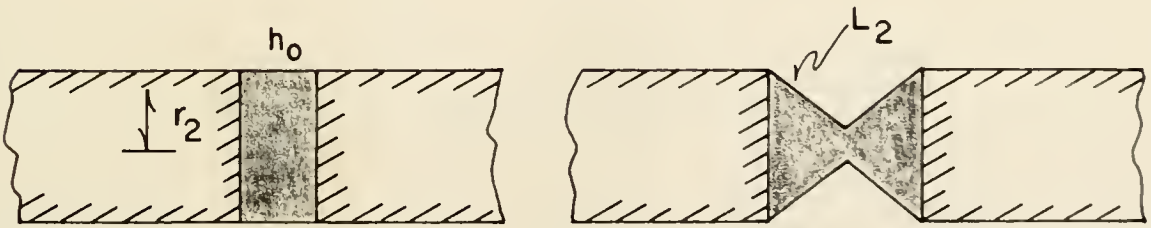

$$\frac{r_2}{h_o} = 1 \qquad \text{MAX. SURFACE STRAIN} = 100\,\frac{L_2 - h_o}{h_o} = 140\%$$

FIGURE 6 STRAIN IN SURFACE DEPENDS ON CONTACT RADIUS

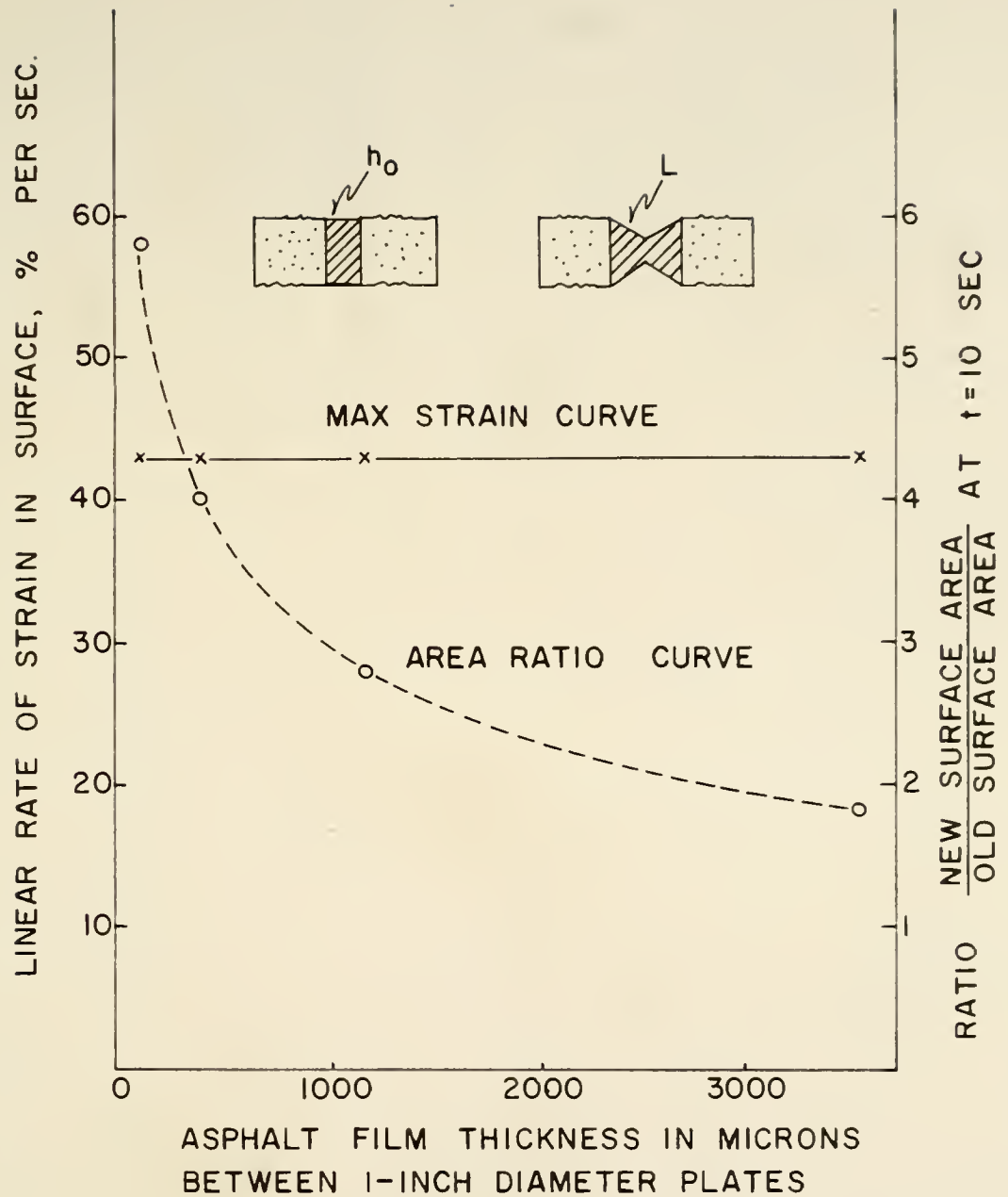

FIGURE 7 MAXIMUM ALLOWABLE STRAIN RATE FOR FLOW CONDITION FOR ONE 72 PEN ASPHALT (CALCULATED FROM MAJIDZADEH)

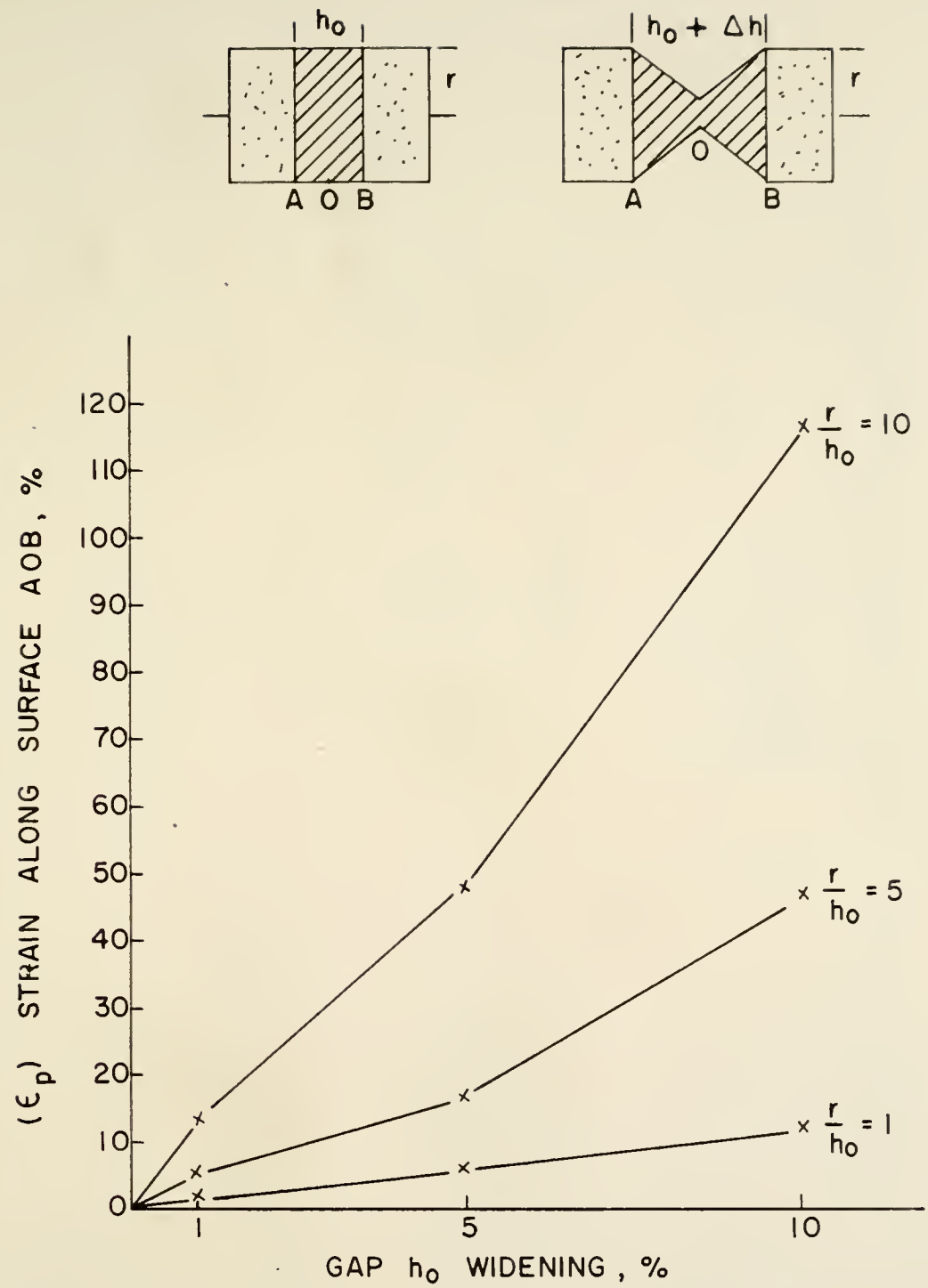

FIGURE 8 SURFACE STRAINS IN IDEALIZED ASPHALT FILMS BETWEEN ROCKS

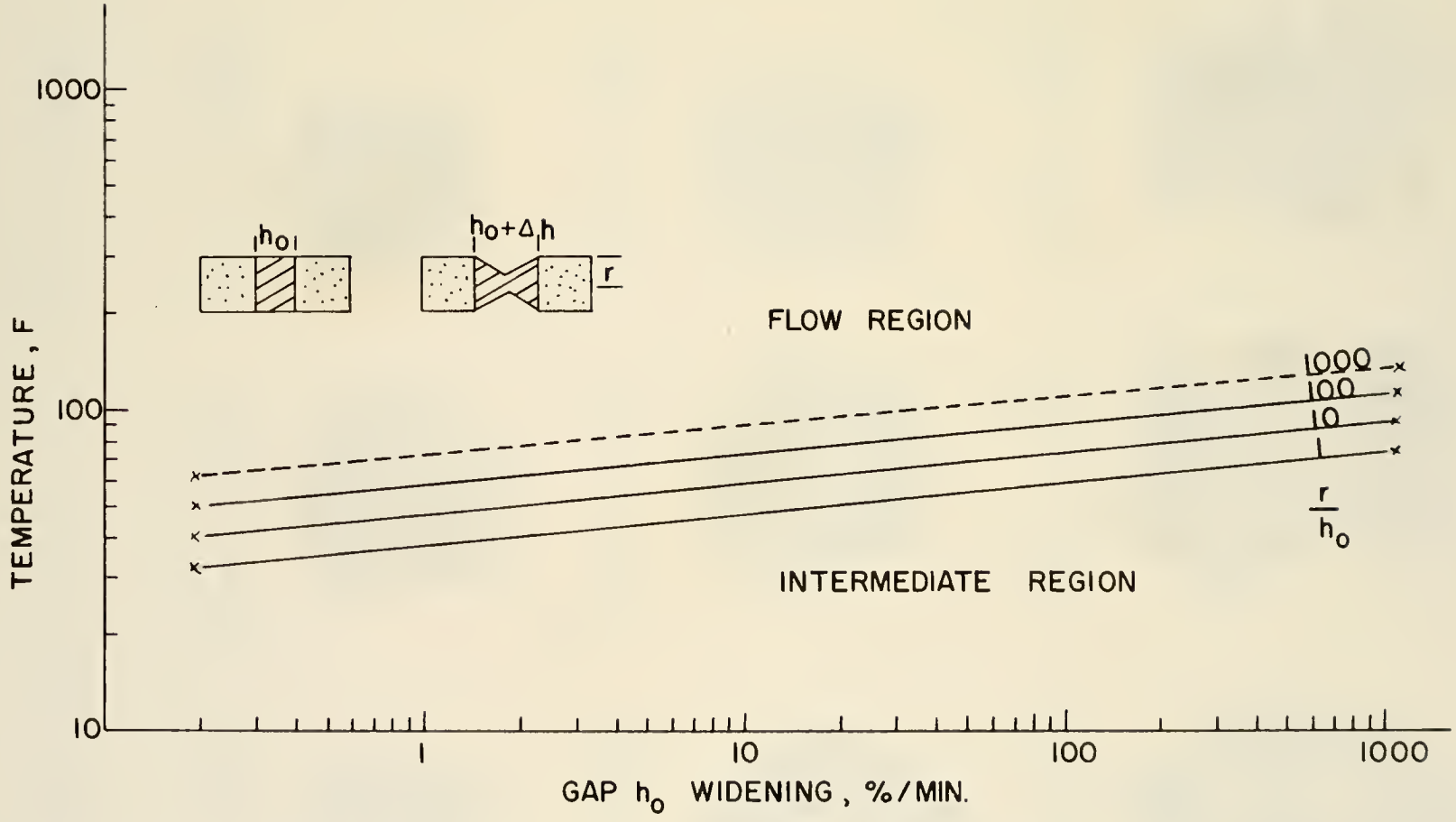

FIGURE 9 MAXIMUM RATE OF LINEAR GAP WIDENING FOR FLOW CONDITION, 72 PEN ASPHALT, USING MAJIDZADEH'S DATA

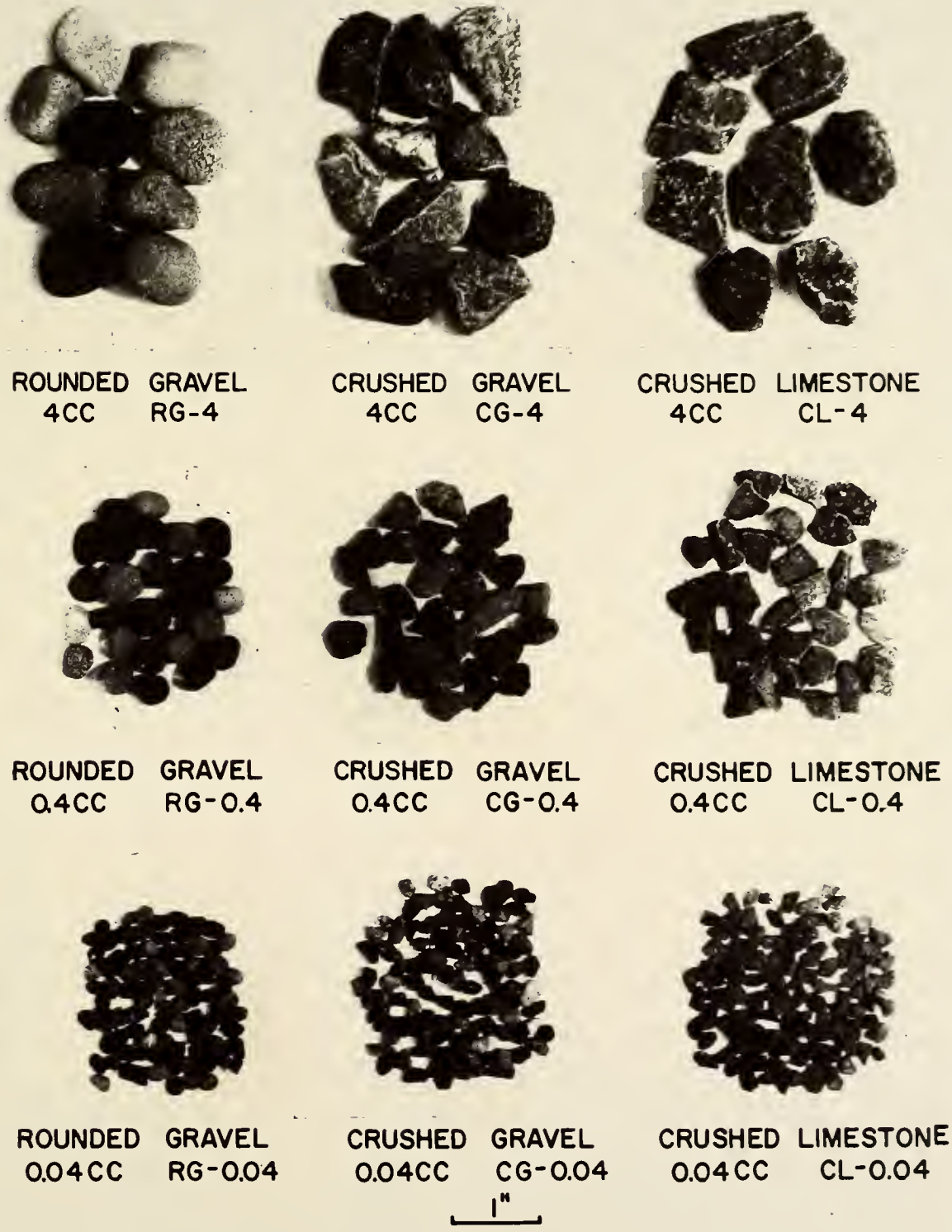

FIGURE 10 TYPES AND SIZES OF ROCKS USED IN THIS STUDY

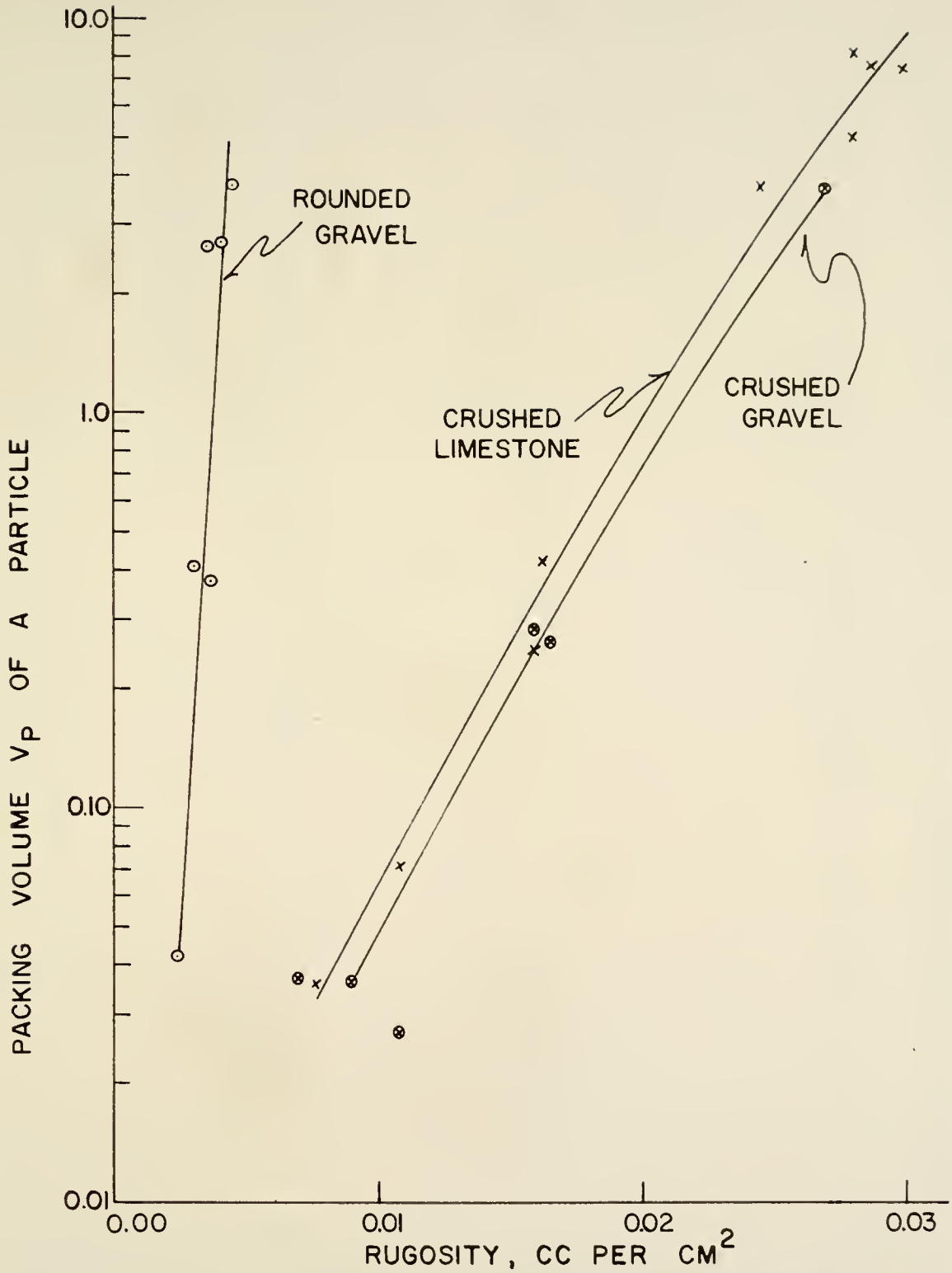

FIGURE 11 RUGOSITY VERSUS PACKING VOLUME FOR THE THREE TYPES OF ROCKS

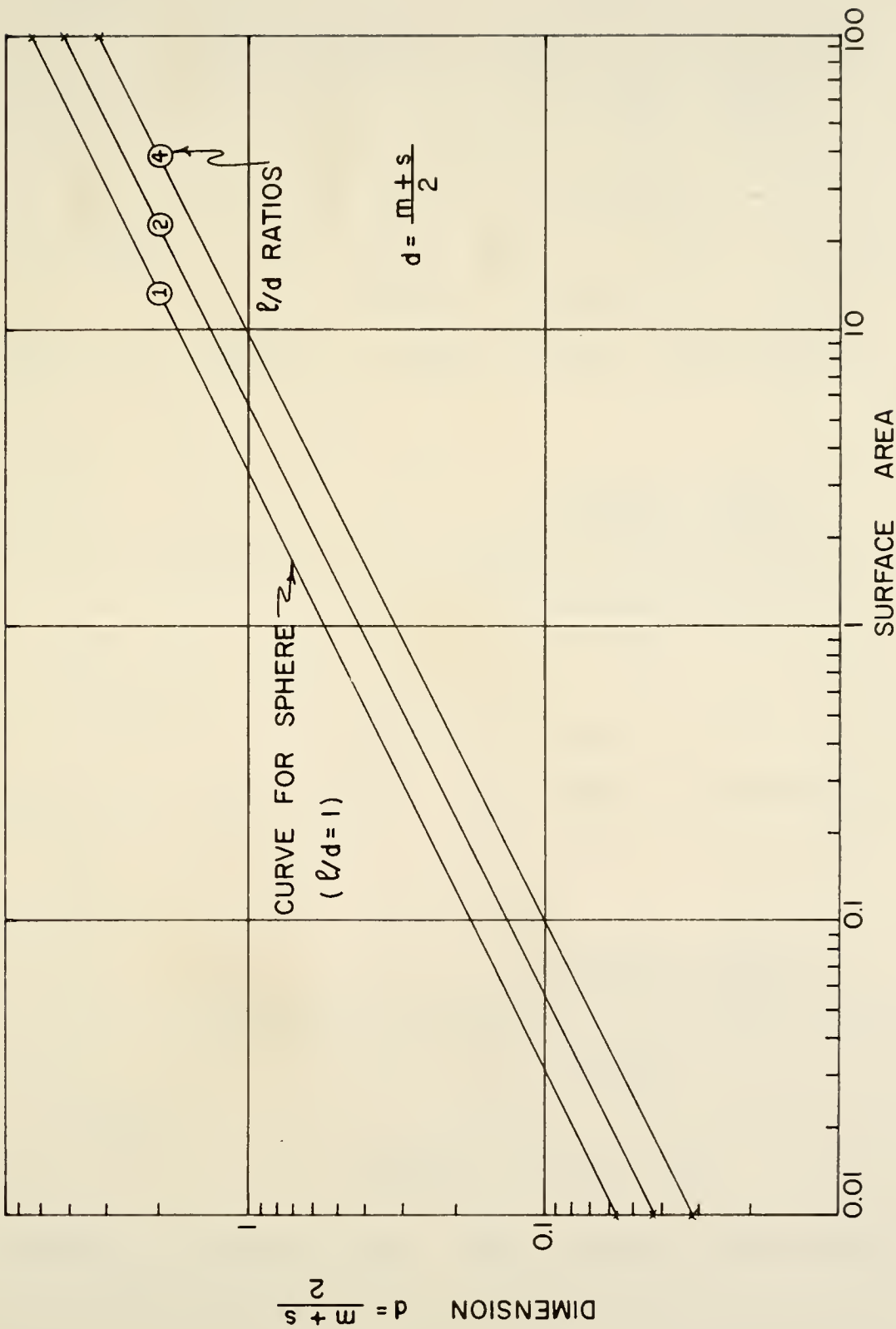

FIGURE 12 GRAPH FOR DETERMINING SURFACE AREA OF PROLATE SPHEROID

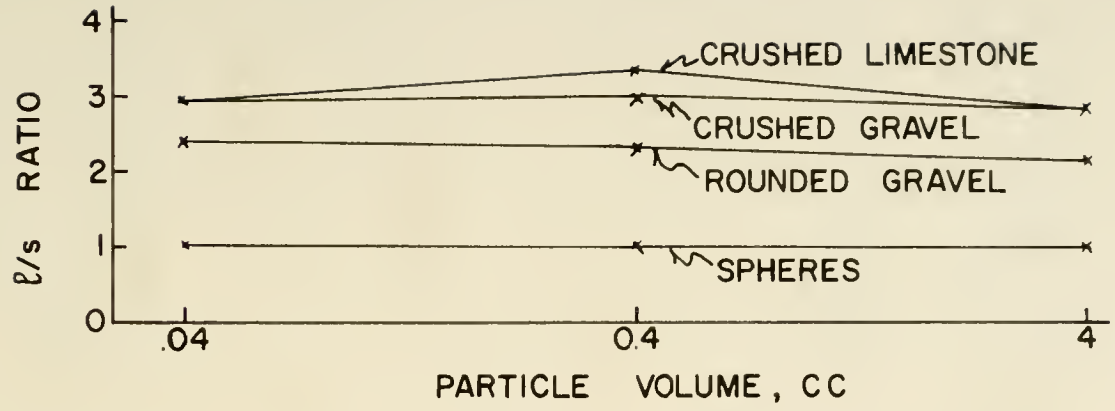

FIGURE 13 RATIO ℓ/s FOR VARIOUS AGGREGATES

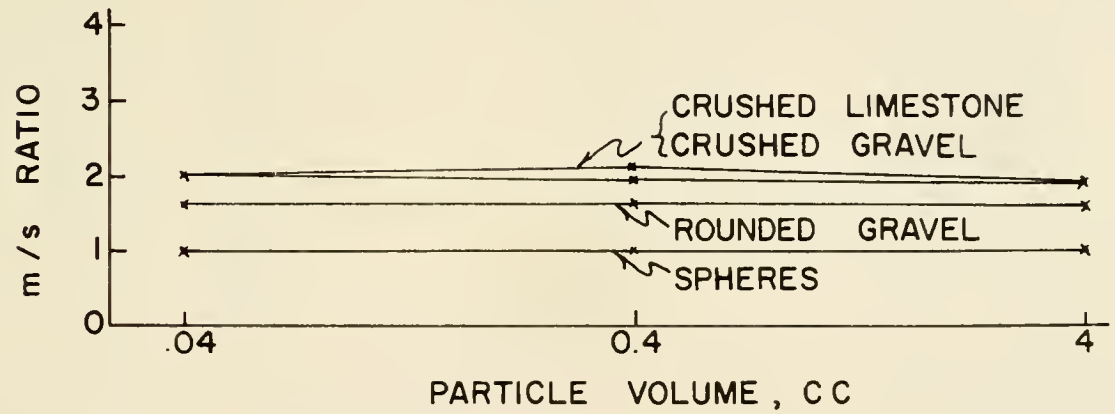

FIGURE 14 RATIO m/s FOR VARIOUS AGGREGATES

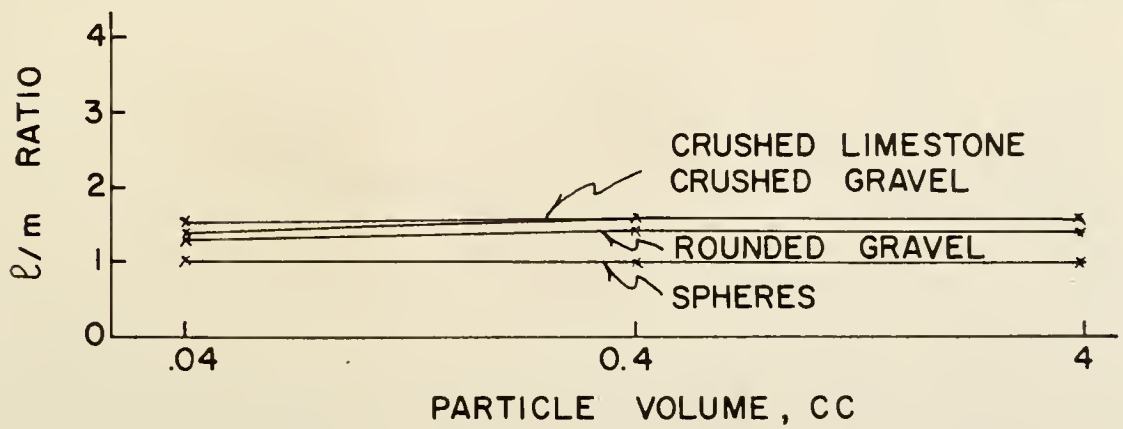

FIGURE 15 RATIO ℓ/m FOR VARIOUS AGGREGATES

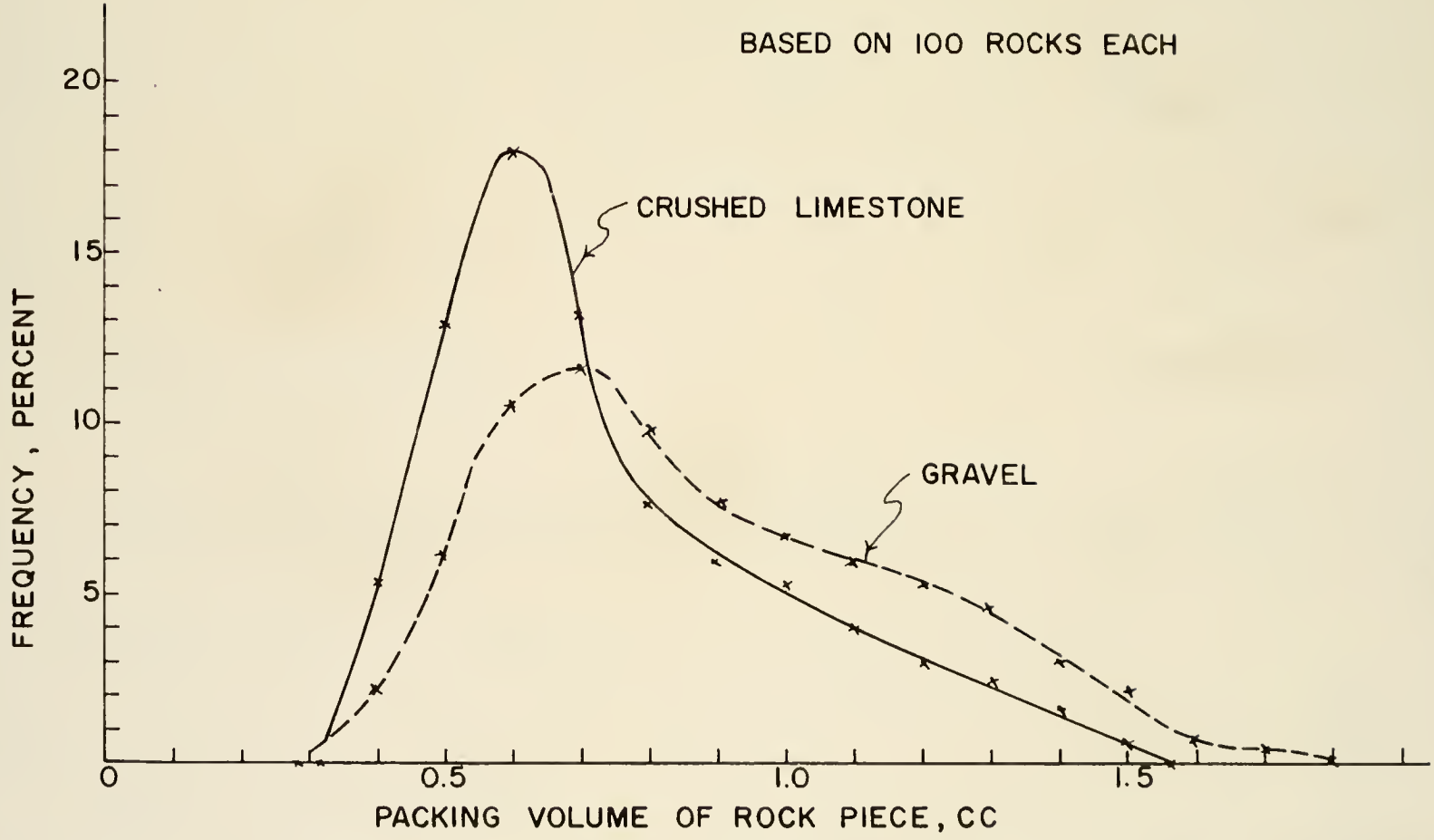

FIGURE 16 EXAMPLE OF PARTICLE VOLUME DISTRIBUTION FOR 1/2"–3/8" CRUSHED LIMESTONE AND PARTIALLY CRUSHED (ABOUT 50% PARTICLES) GRAVEL.

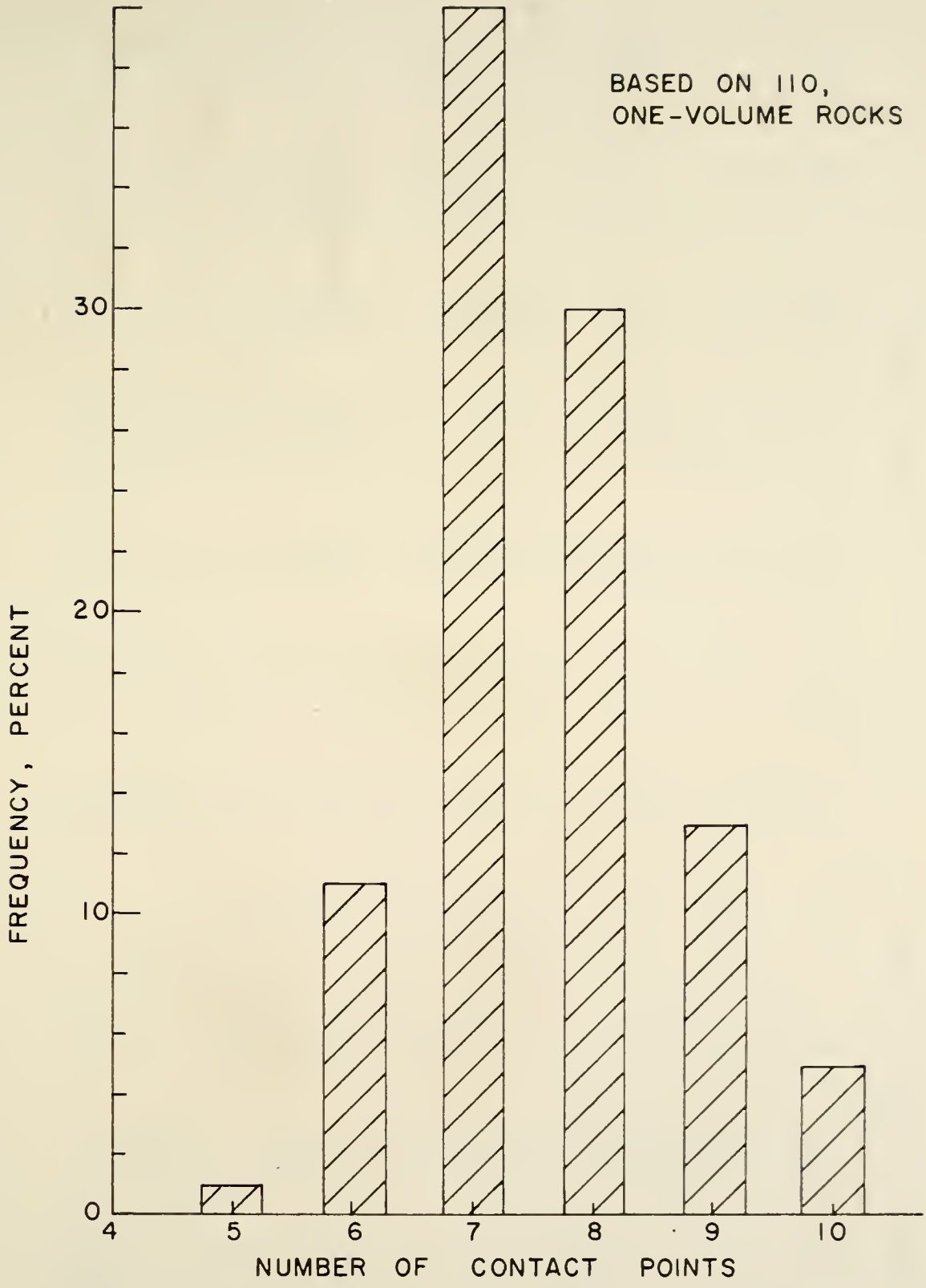

FIGURE 17 EXAMPLE OF CONTACT POINT DISTRIBUTION

FIGURE 18 LOOSE VOLUMES OF ΣV_p= 800CC, 3" DROP, 10 SEC

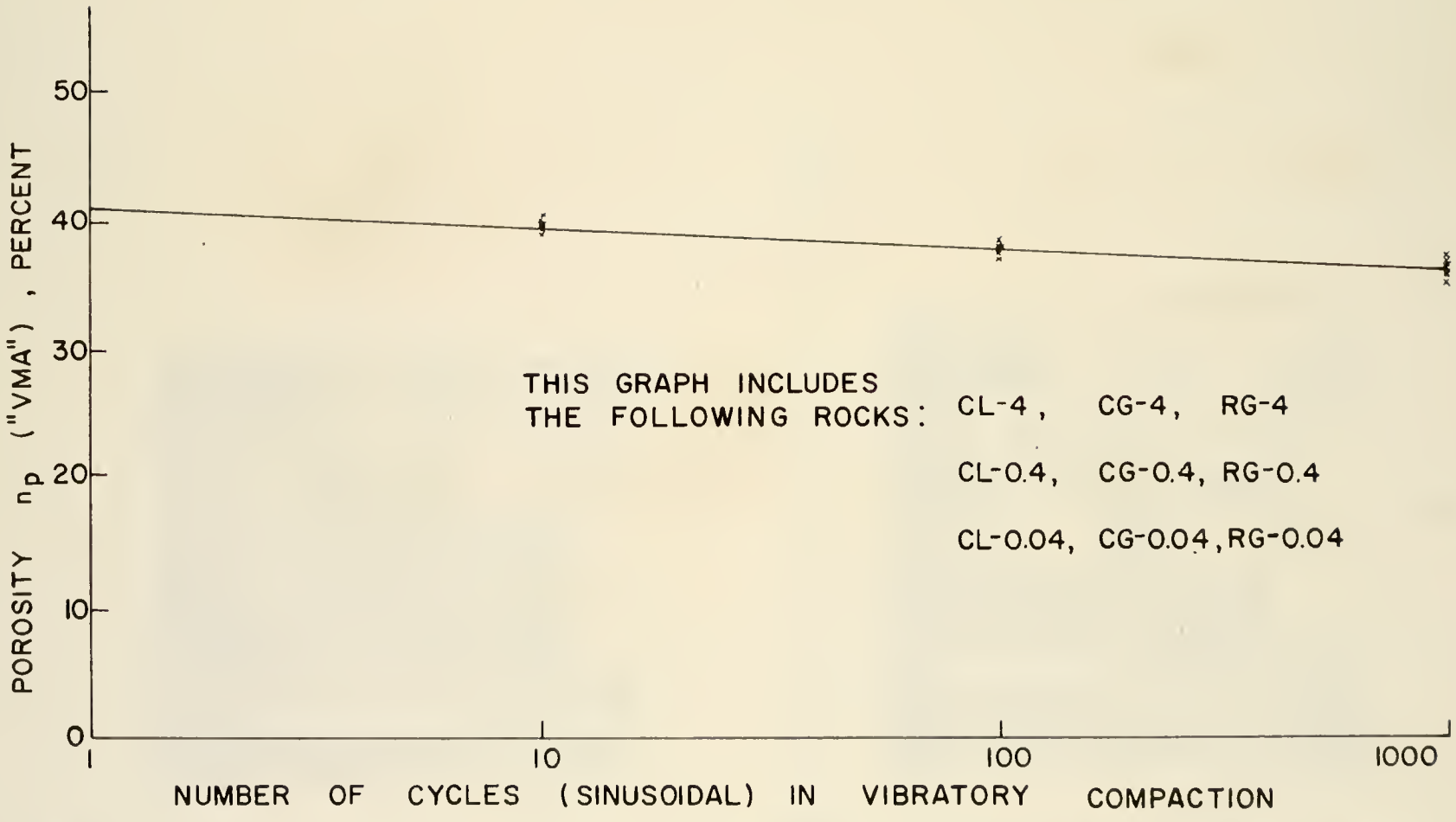

FIGURE 19 POROSITY OR VOIDS IN THE BULK AFTER VARIOUS NUMBERS OF CYCLES AT 1.5 G'S ACCELERATION. ALL ROCKS AND SIZES ARE INCLUDED.

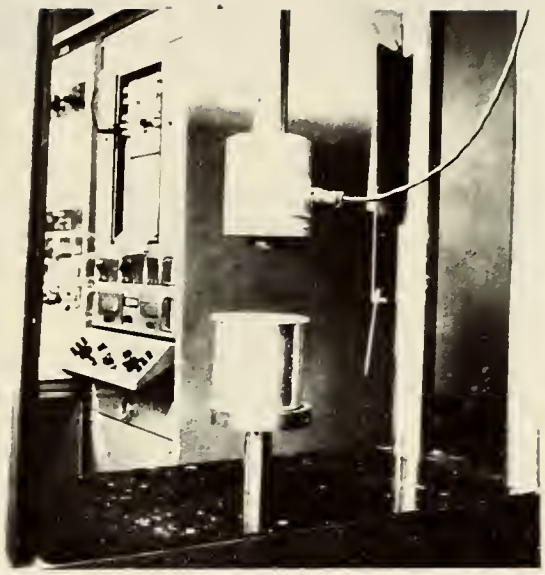

FIGURE 20 VIBRATORY COMPACTION OF ROCKS

FIGURE 21 VIBRATORY COMPACTION OF MIXES

FIGURE 22 COMPACTED AND CAPPED SPECIMEN

FIGURE 23 SPECIMEN AFTER TESTING

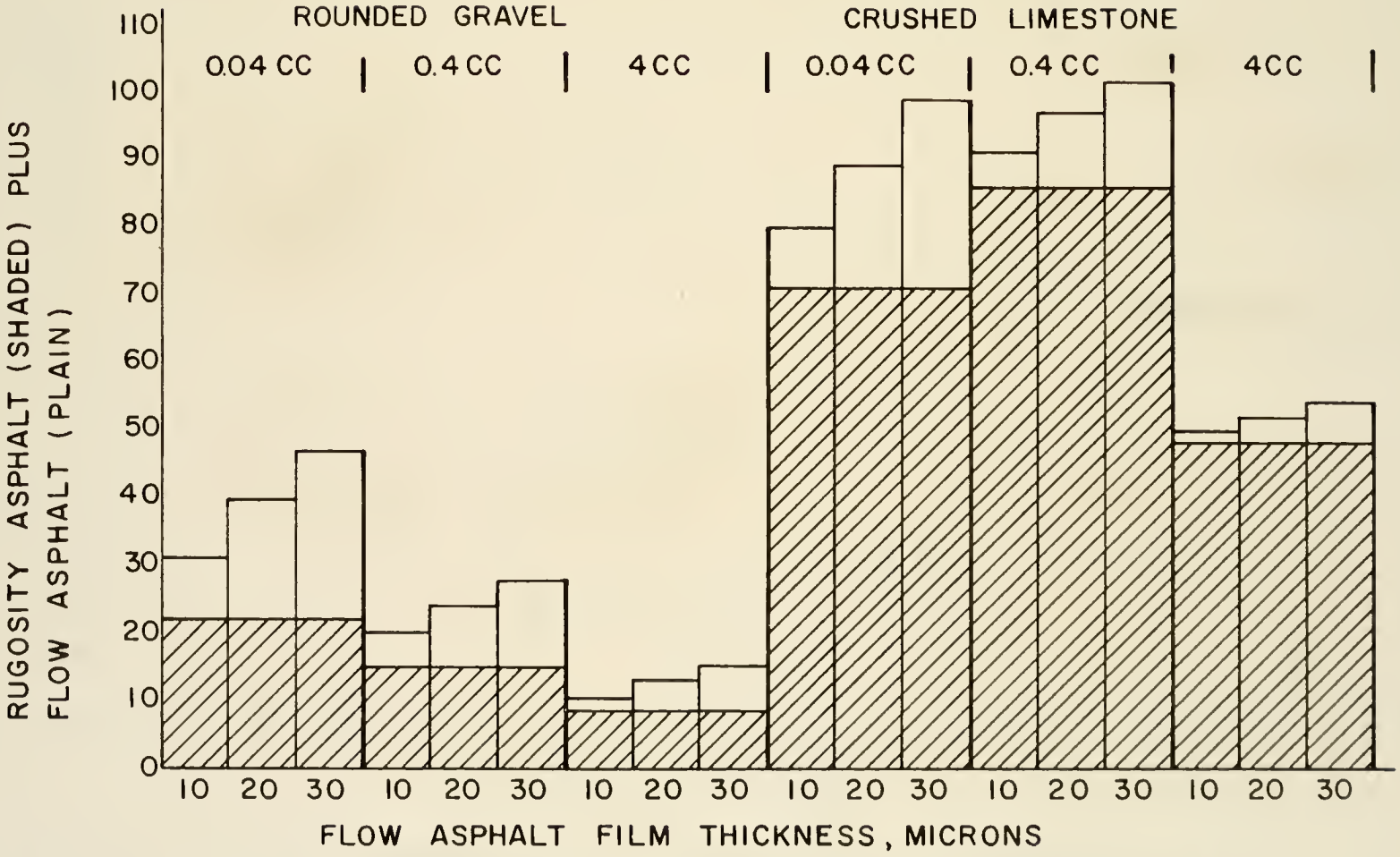

FIGURE 24 TOTAL ASPHALT IN EACH SPECIMEN (GRAMS) FOR VARIED FILM THICKNESS.

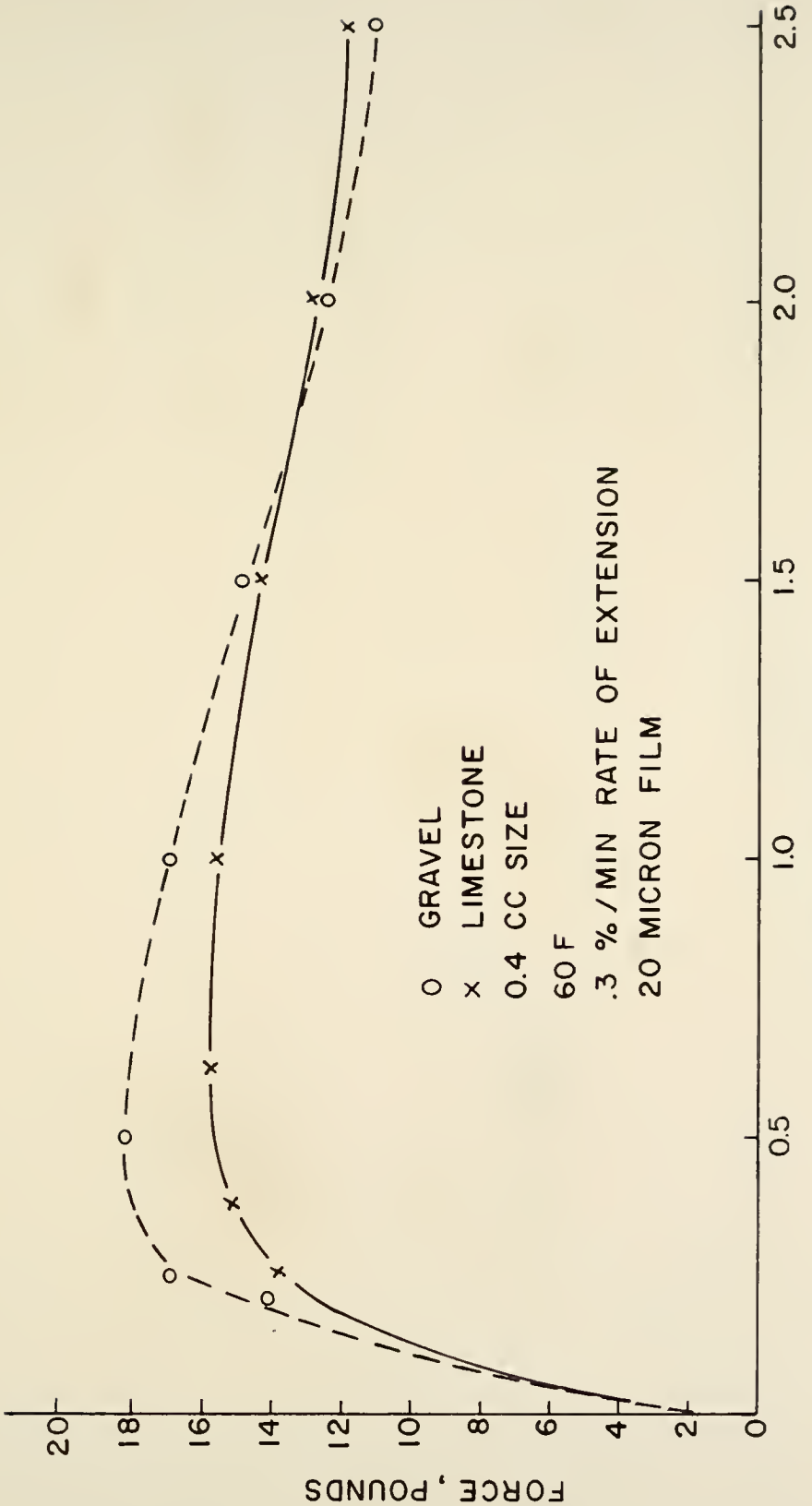

FIGURE 25 FORCE–DEFORMATION CURVES FOR COMPARABLE GRAVEL AND LIMESTONE SPECIMENS, IN TENSION, 0.4CC ROCKS

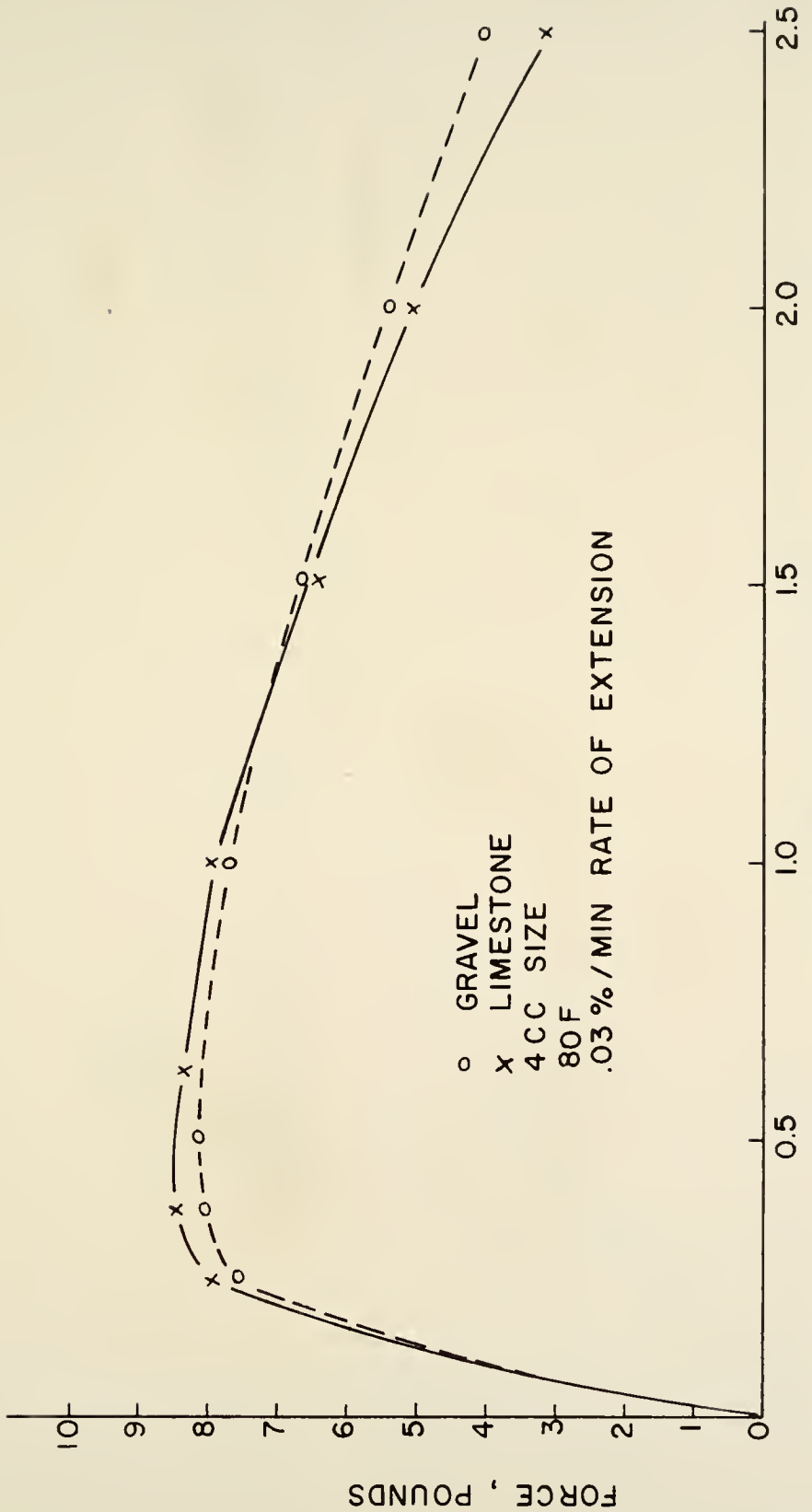

FIGURE 26 FORCE–DEFORMATION CURVES FOR COMPARABLE GRAVEL AND LIMESTONE SPECIMENS, IN TENSION, 4 CC ROCKS

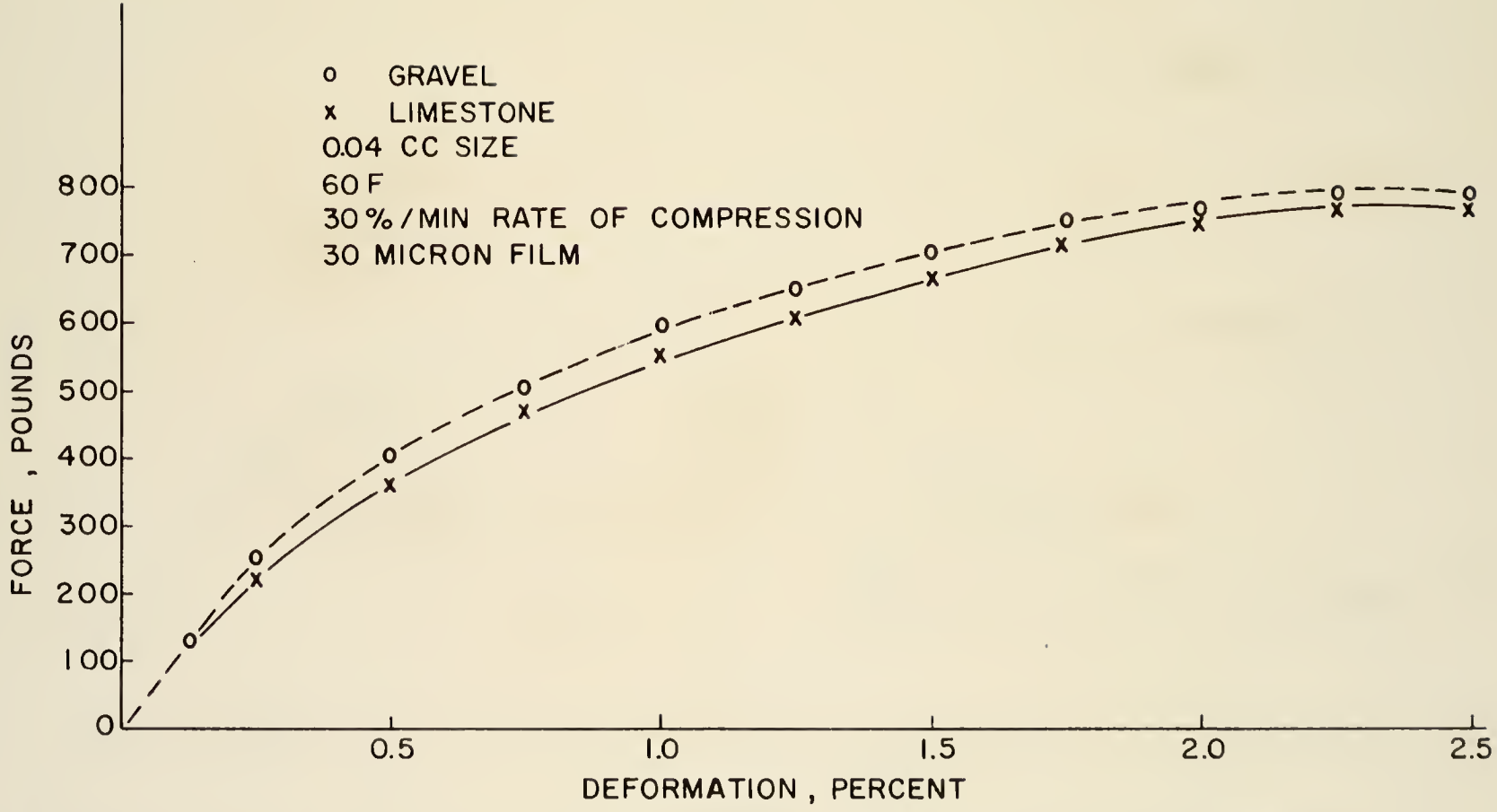

FIGURE 27 FORCE–DEFORMATION CURVES FOR COMPARABLE GRAVEL AND LIMESTONE SPECIMENS , IN COMPRESSION, AT 60 F

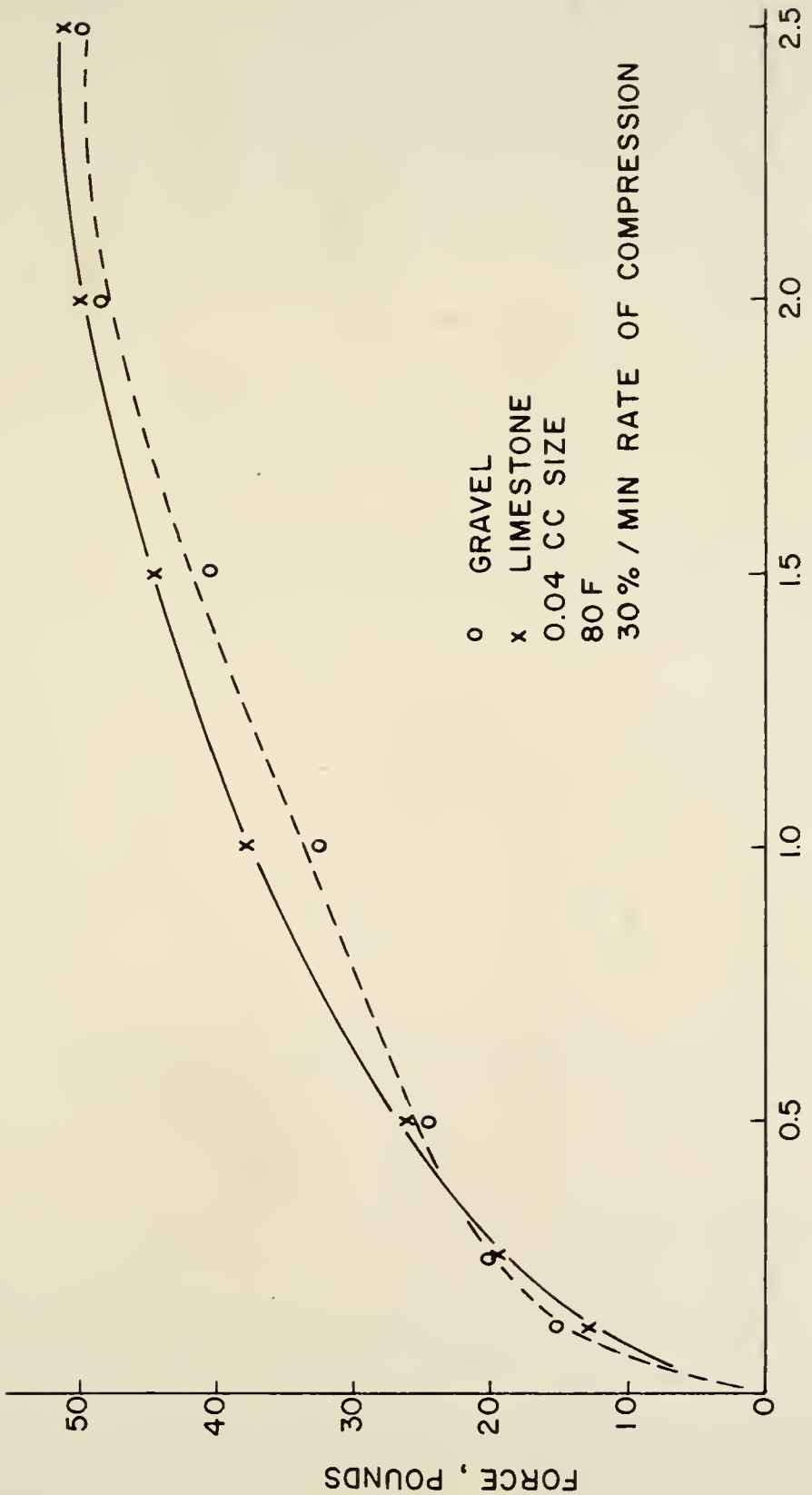

FIGURE 28 FORCE–DEFORMATION CURVES FOR COMPARABLE GRAVEL AND LIMESTONE SPECIMENS, IN COMPRESSION, AT 80 F

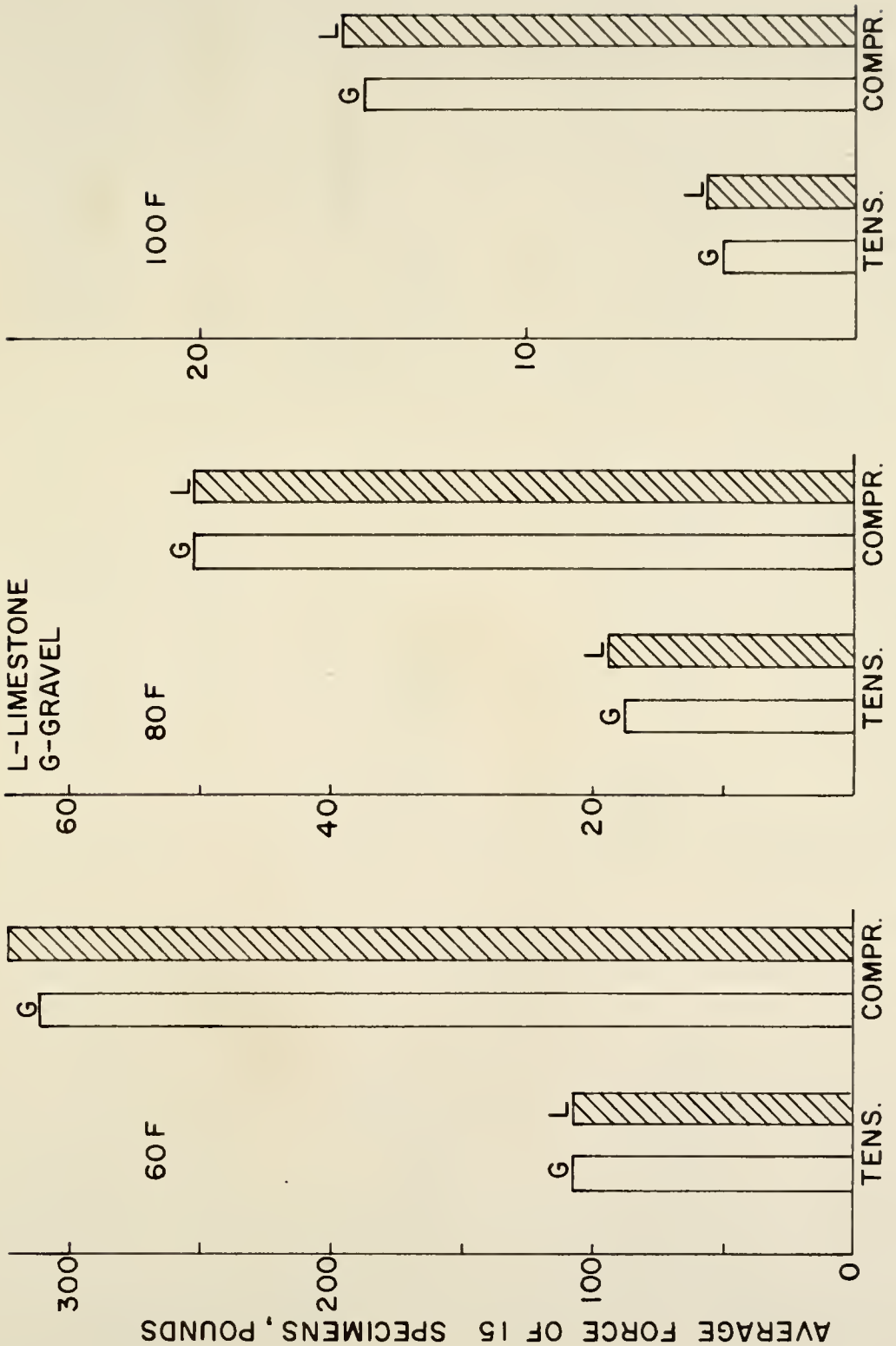

FIGURE 29 FORCE COMPARISONS FOR MIXES IN TENSION AND COMPRESSION, ALL SPECIMENS

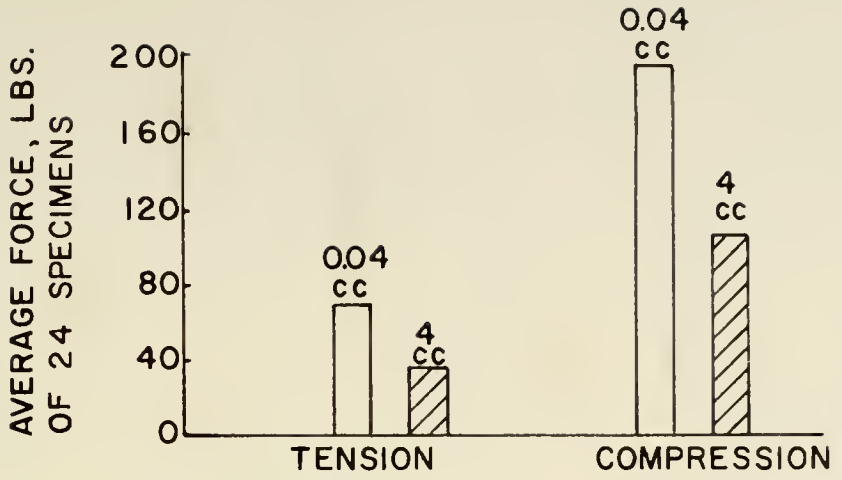

FIGURE 30 FORCE FOR MIXES - 0.04 AND 4CC ROCKS

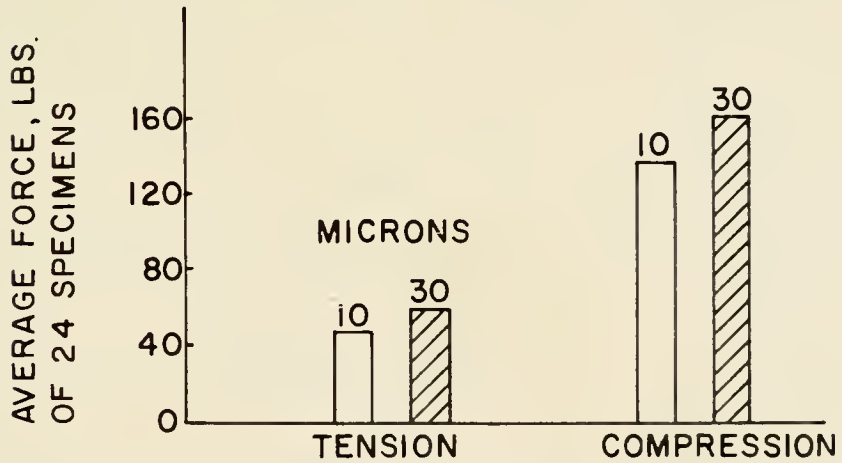

FIGURE 31 FORCE FOR MIXES - 10 AND 30 MICRON FILM

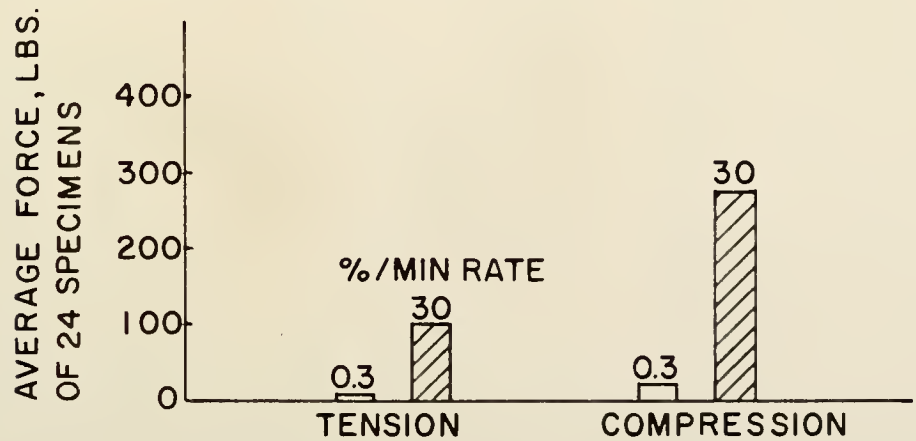

FIGURE 32 FORCE FOR MIXES - 0.3 AND 30 %/MIN

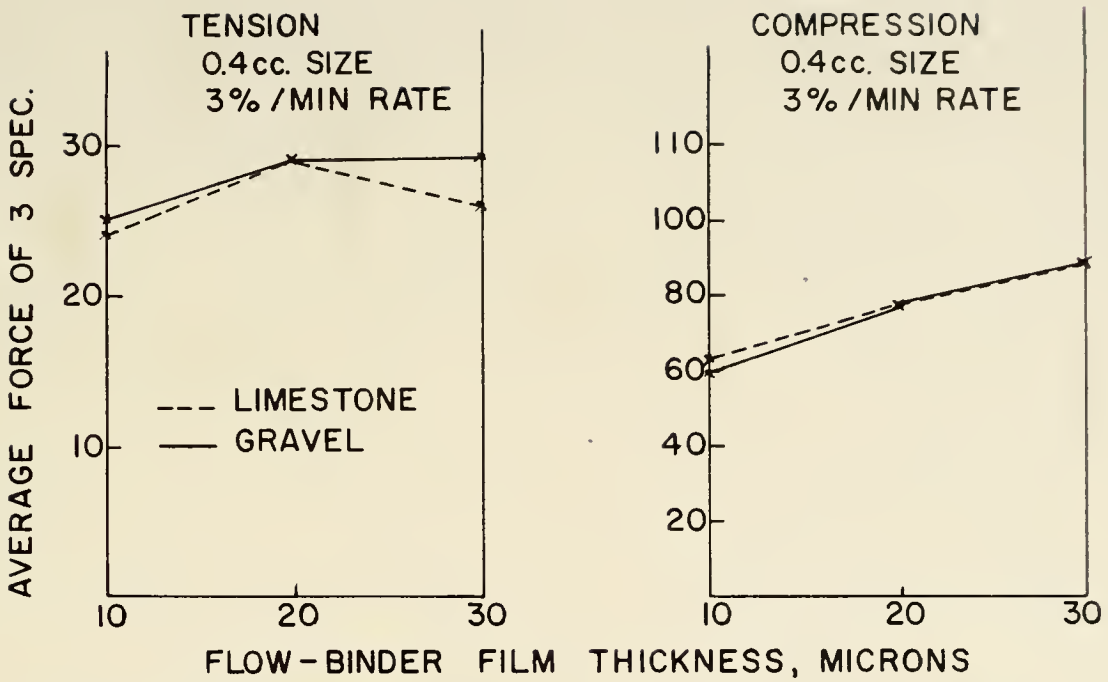

FIGURE 33 FORCE FOR 0.4cc ROCKS AND 3 FILMS

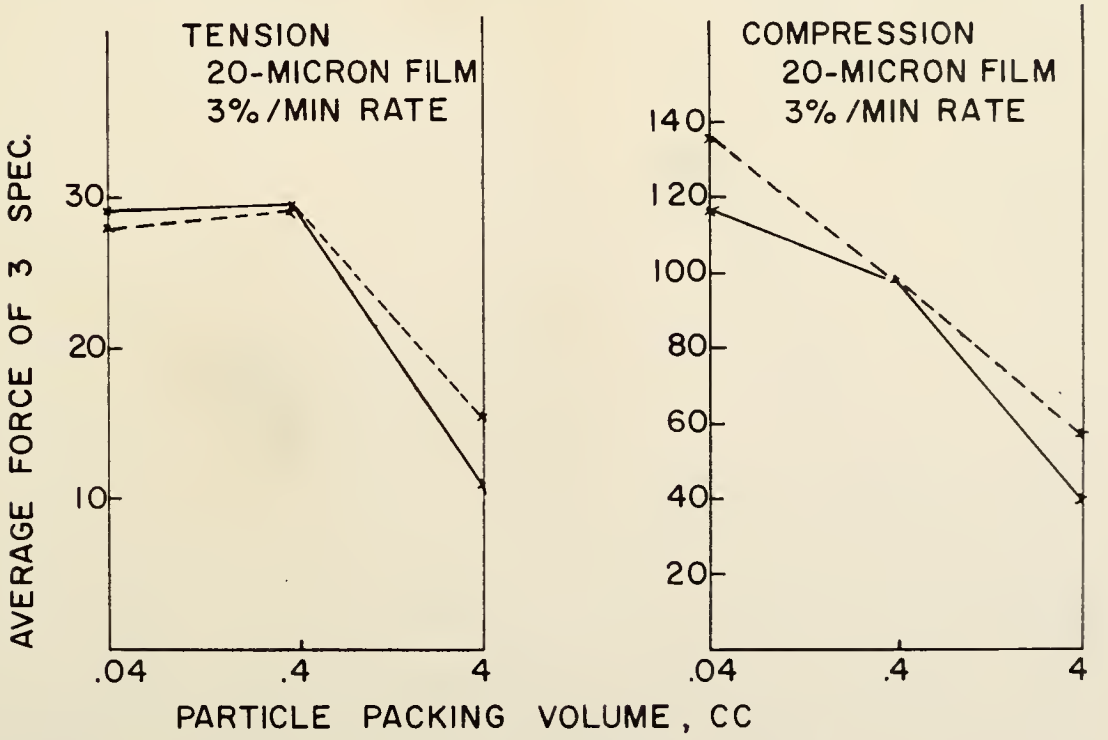

FIGURE 34 FORCE FOR 20 MICRON FILM

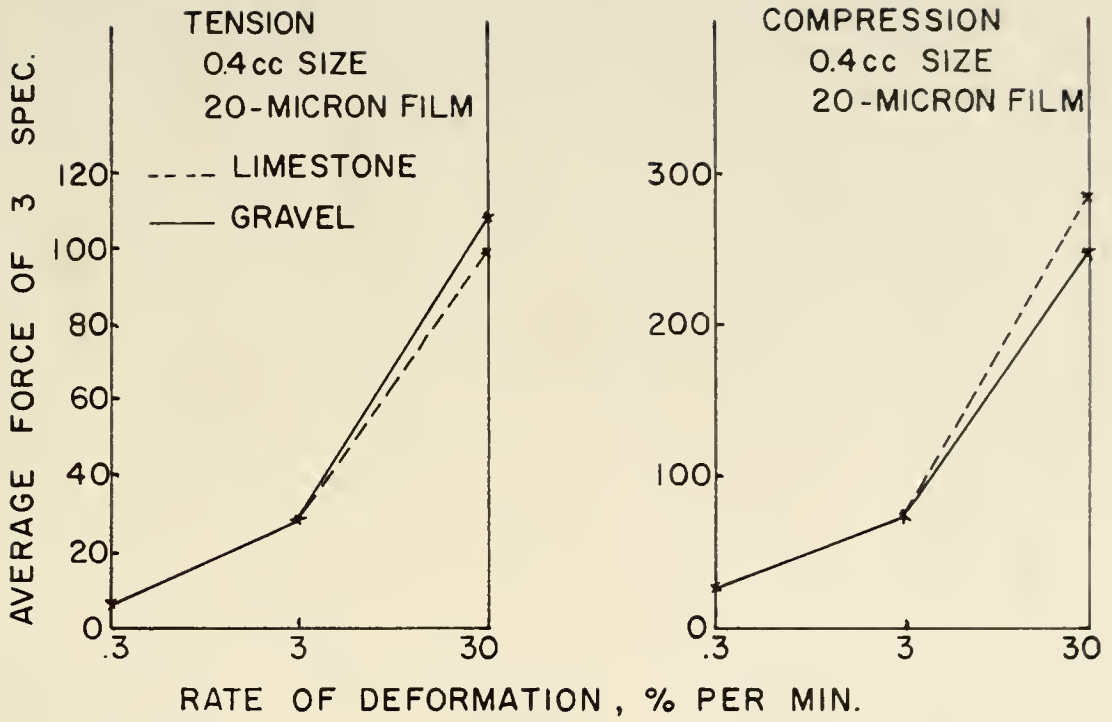

FIGURE 35 FORCE FOR 0.4CC ROCK AND 3 RATES

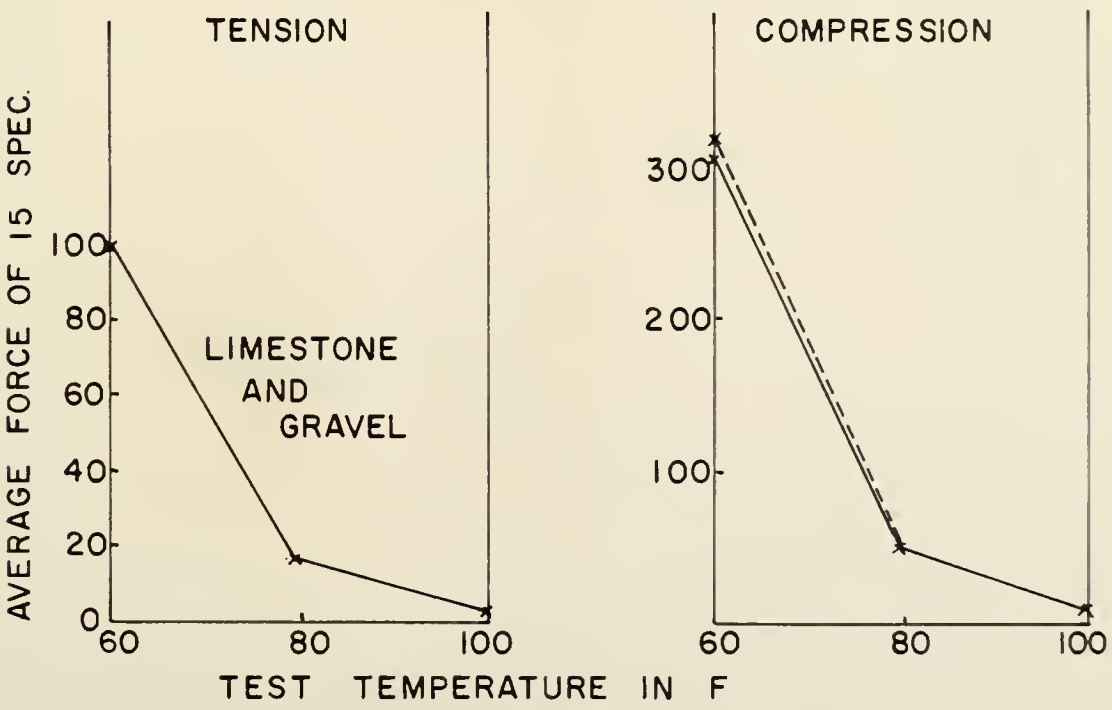

FIGURE 36 FORCE AT 3 TEMPERATURES

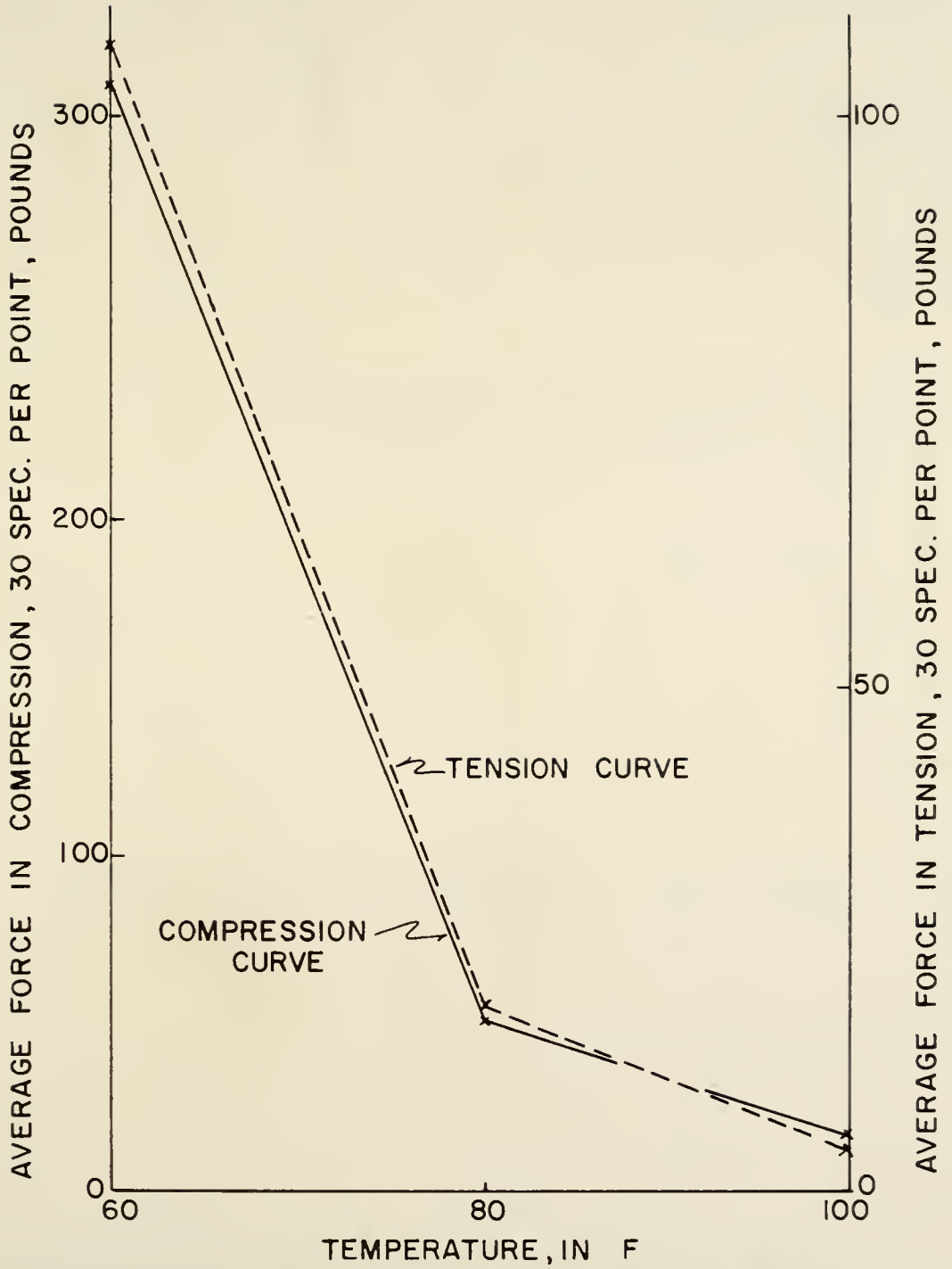

FIGURE 37 FORCE IN COMPRESSION ≈ 3X TENSION

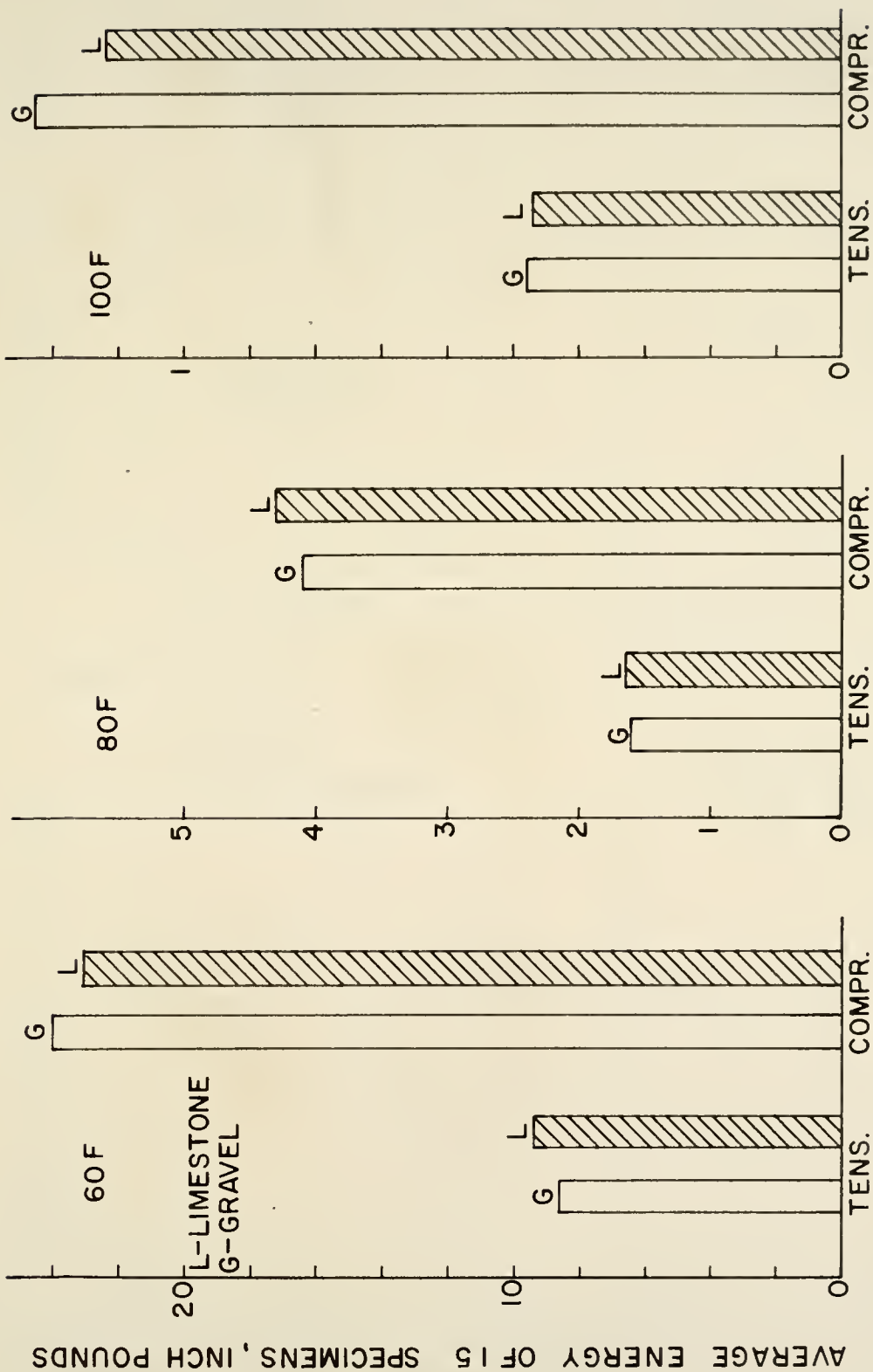

FIGURE 38 ENERGY TO 2.5% STRAIN COMPARISONS IN TENSION AND COMPRESSION, ALL SPECIMENS

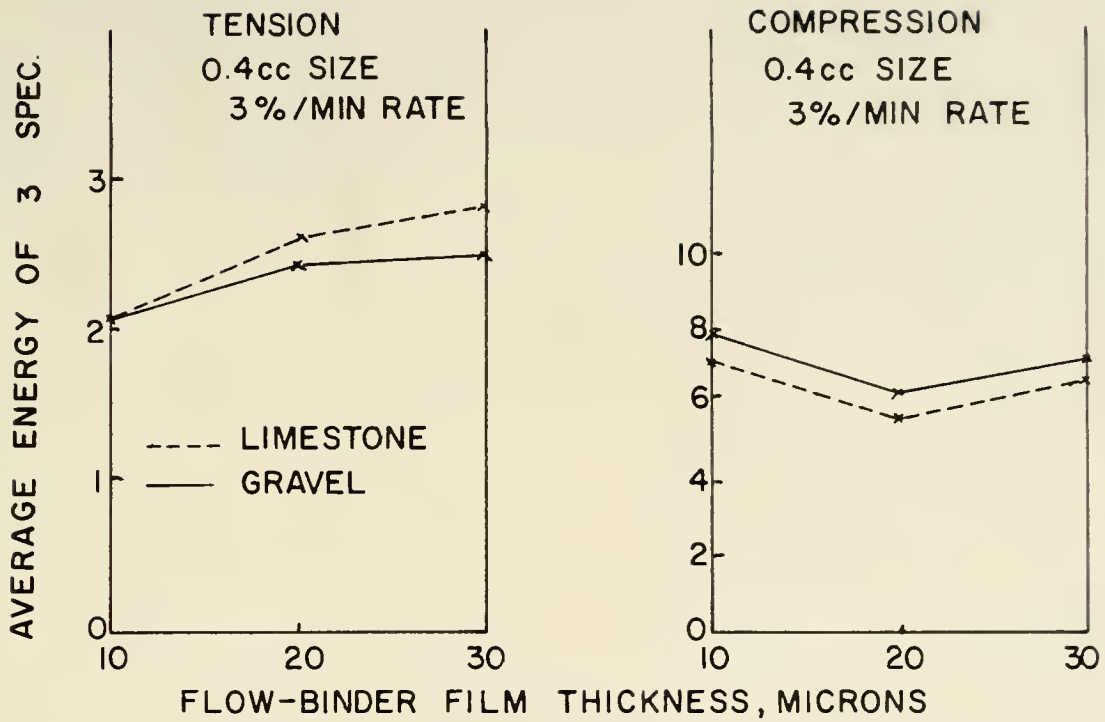

FIGURE 39 ENERGY FOR 0.4CC ROCKS AND 3 FILMS

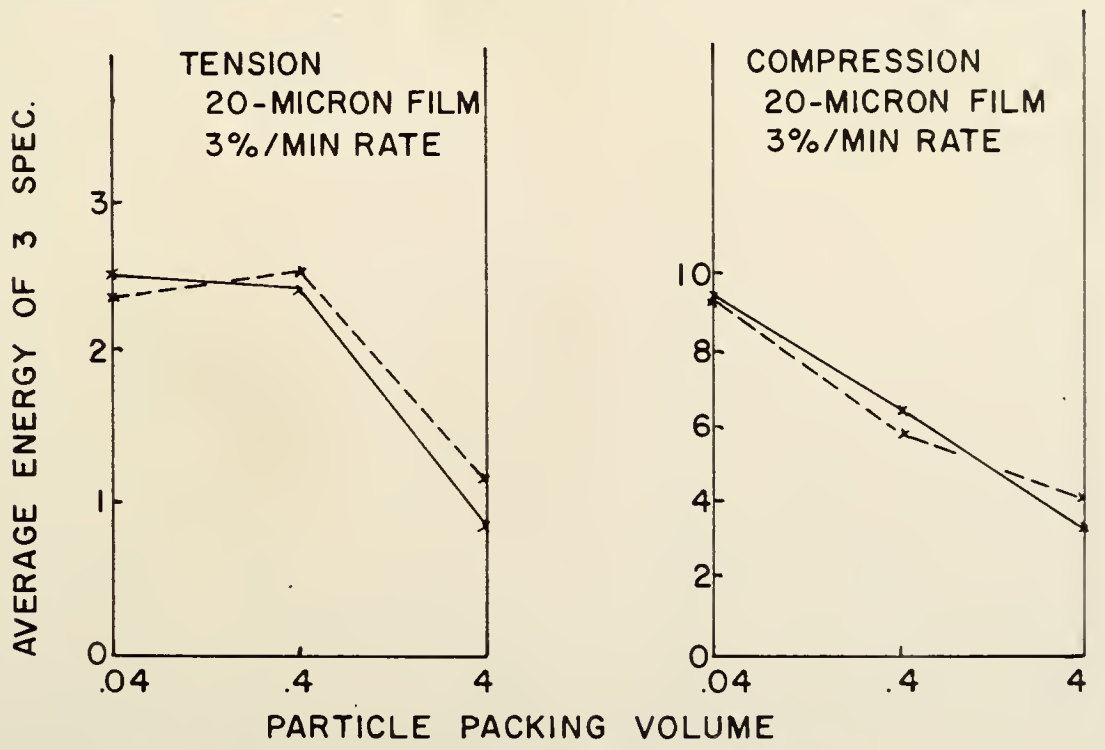

FIGURE 40 ENERGY FOR 20 MICRON FILM

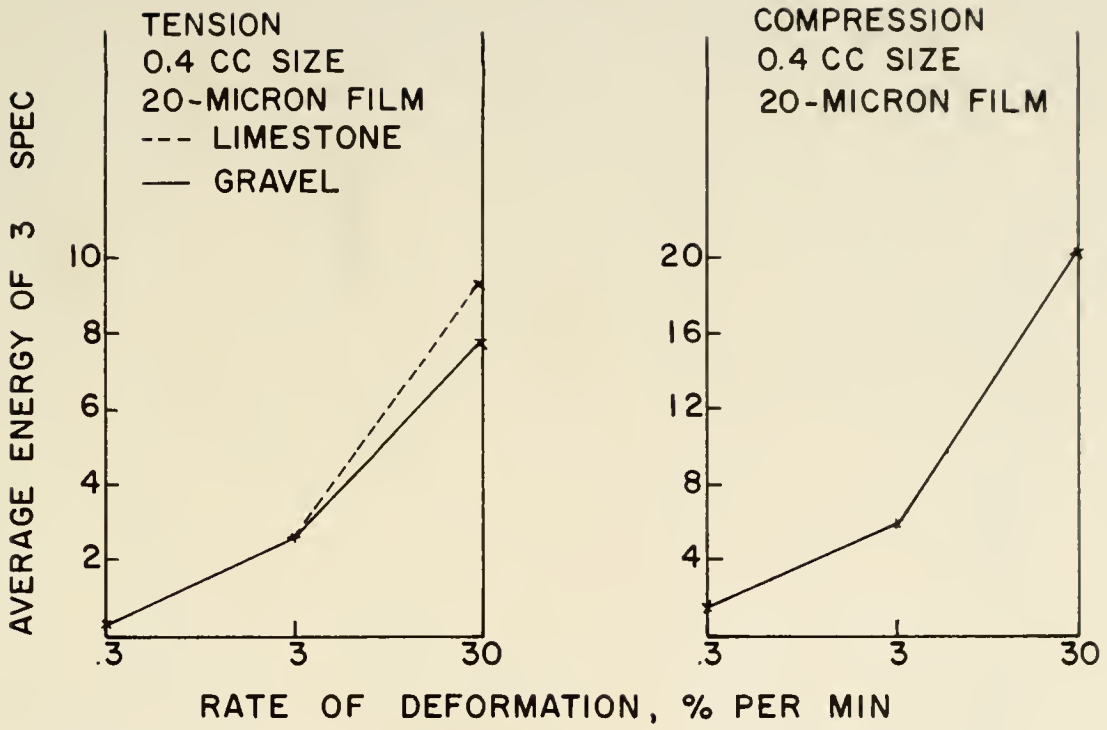

FIGURE 41 ENERGY FOR 0.4CC ROCKS AND 3 RATES

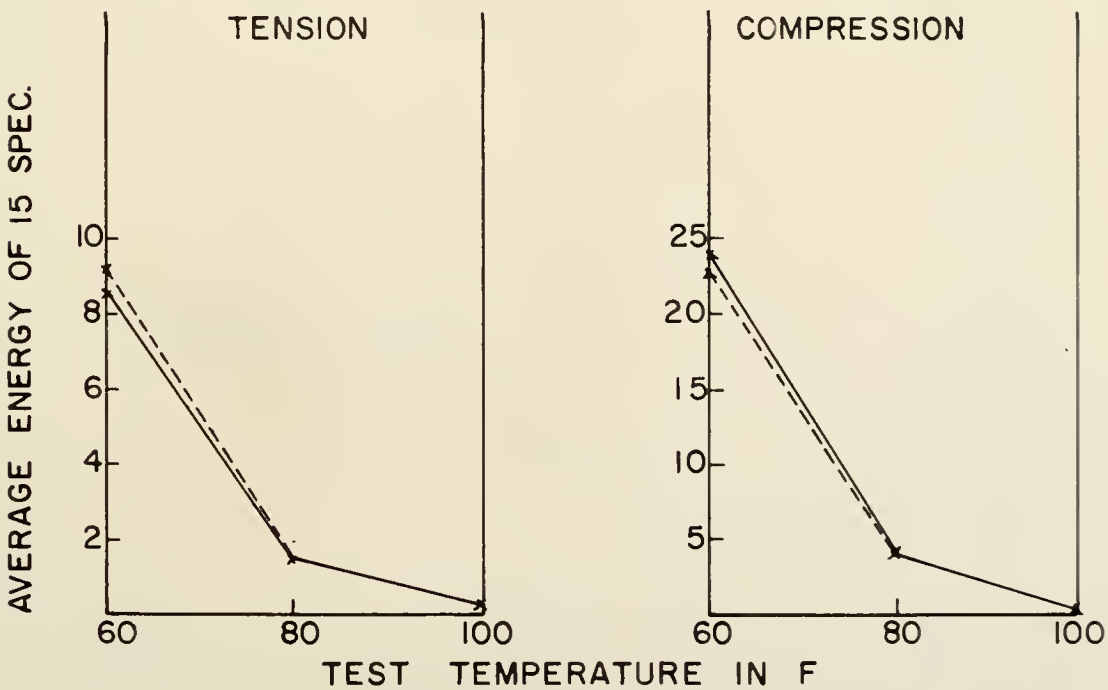

FIGURE 42 ENERGY AT 3 TEMPERATURES

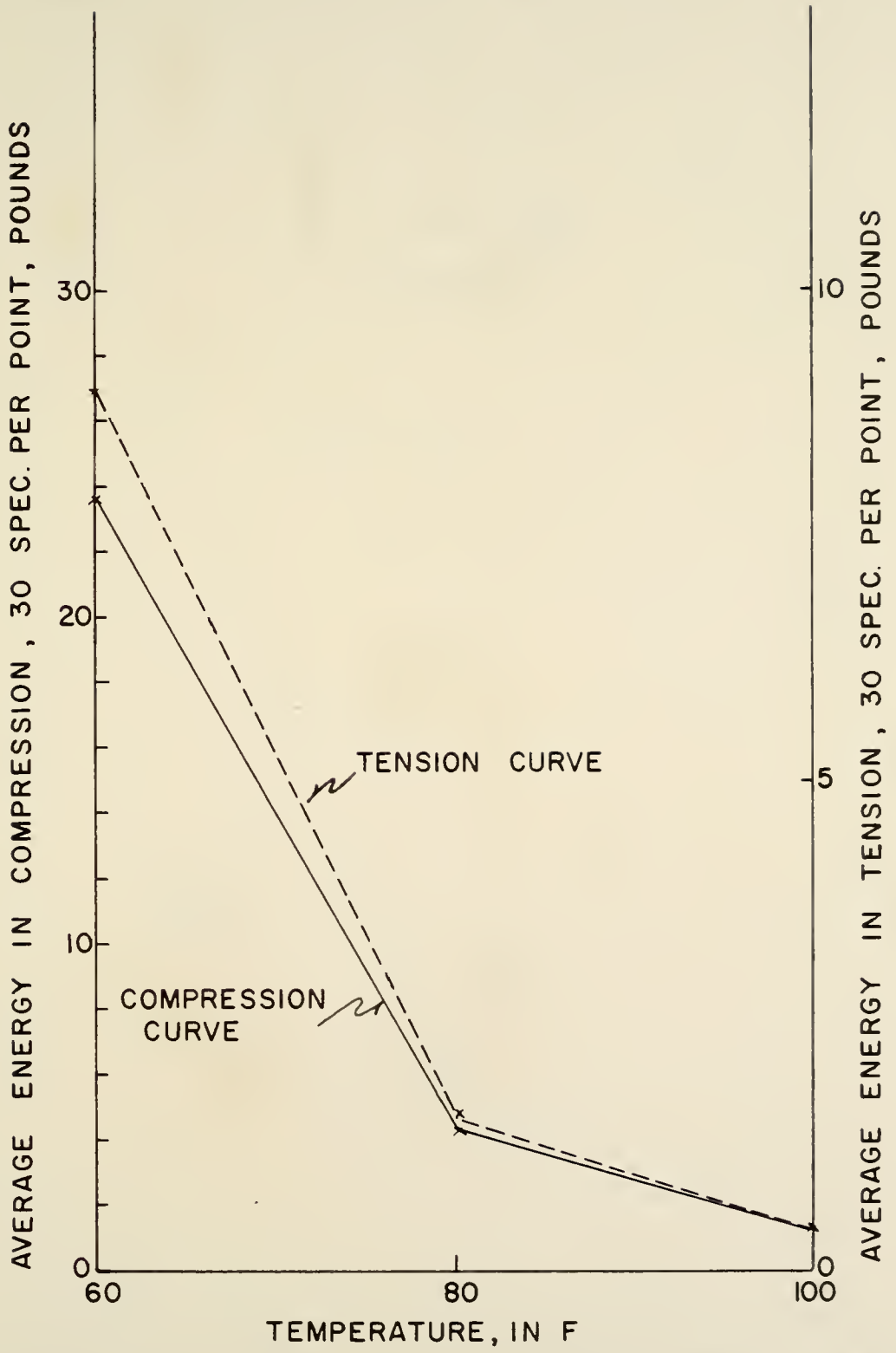

FIGURE 43 ENERGY IN COMPRESSION≈3X TENSION

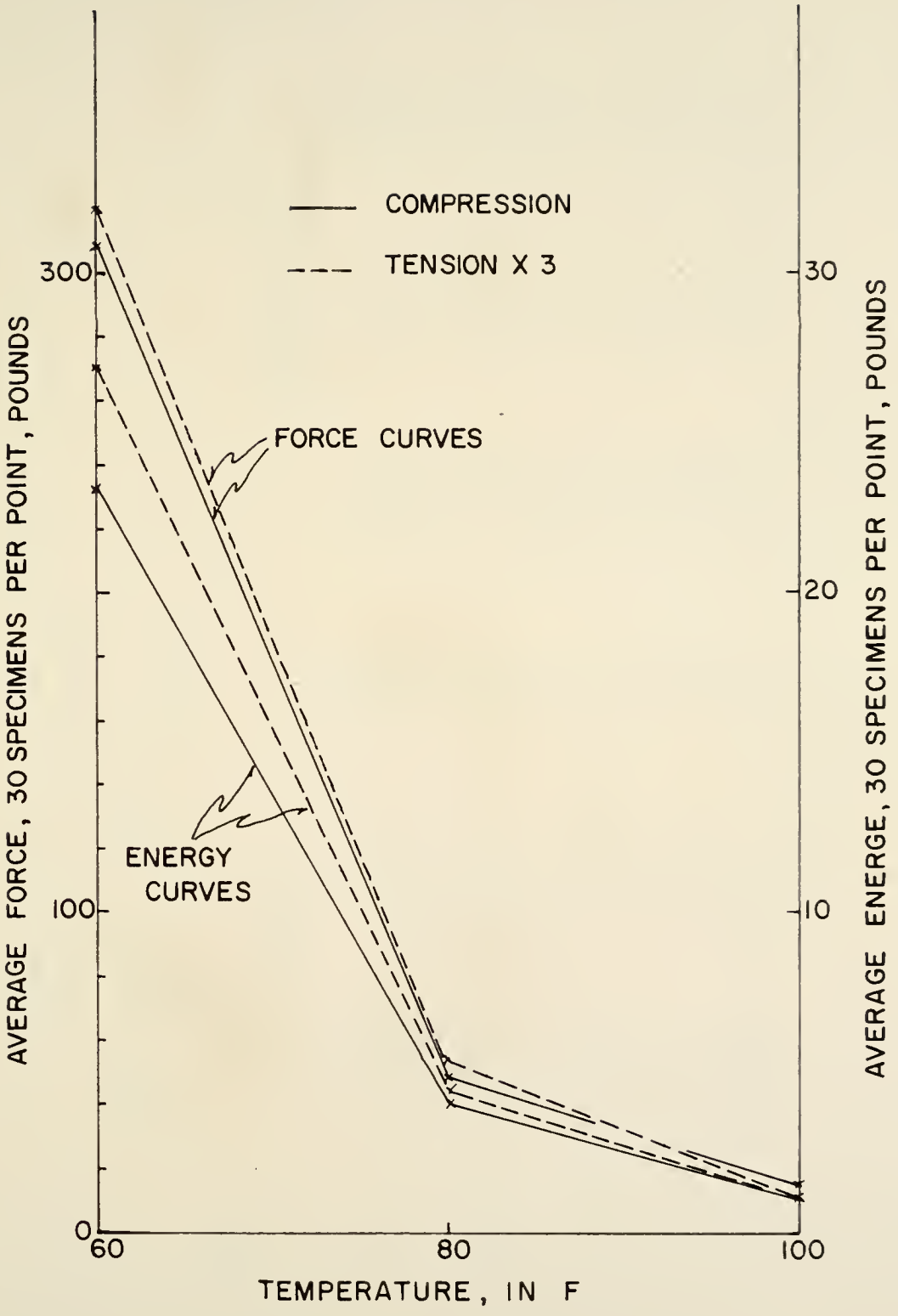

FIGURE 44 FORCE AND ENERGY AVERAGES

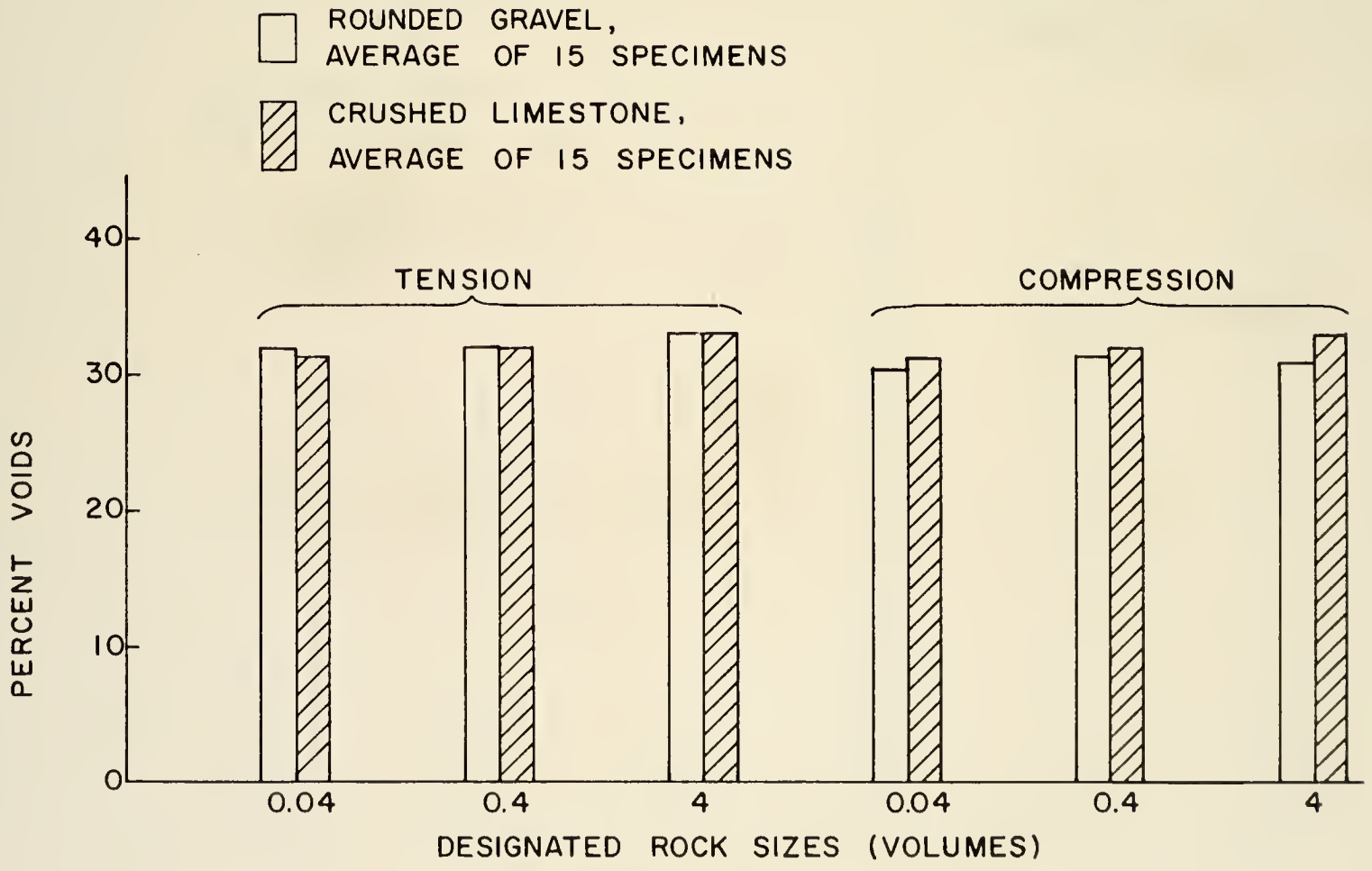

FIGURE 45 AVERAGE VOID COMPARISONS IN MIXES

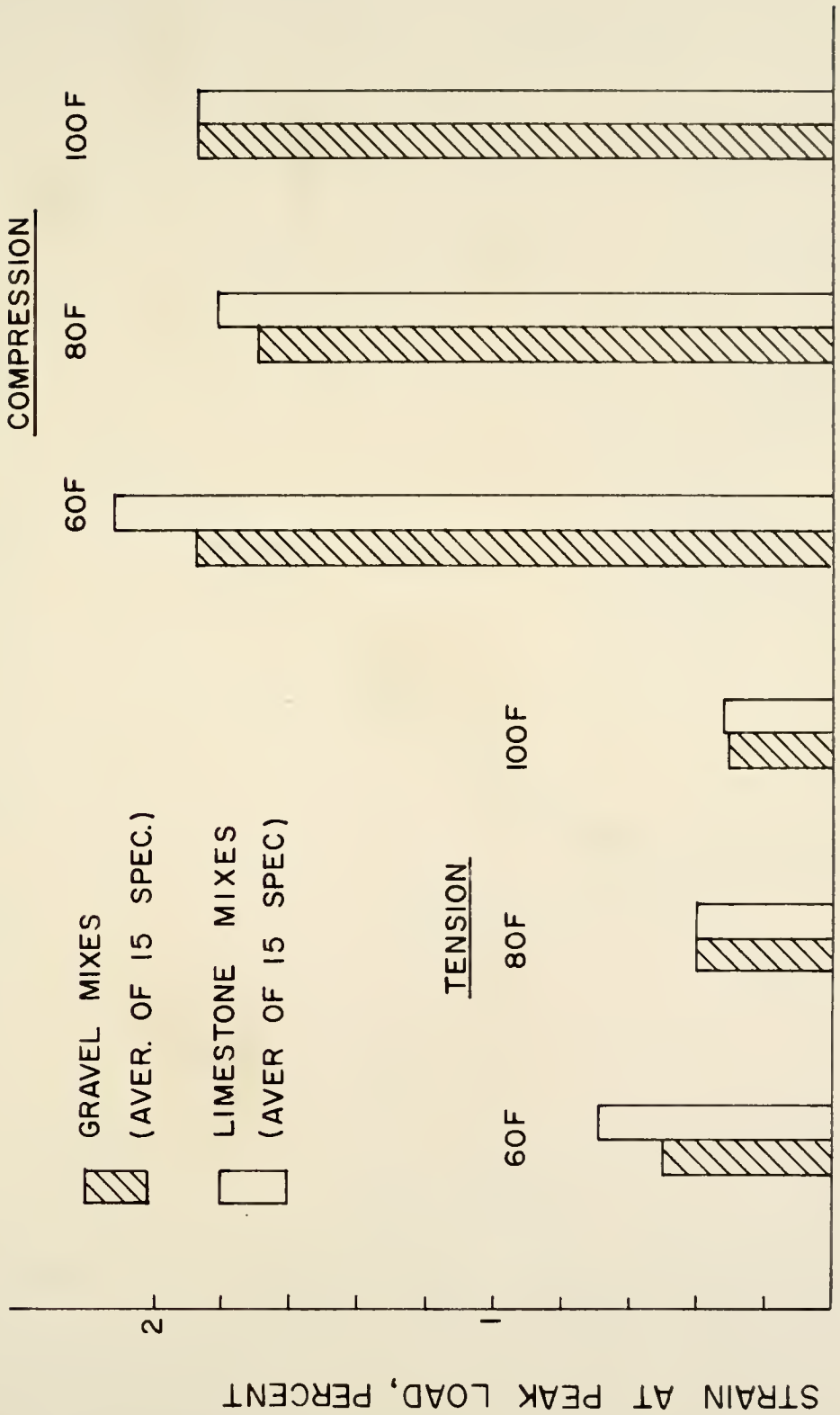

FIGURE 46 AVERAGE VERTICAL STRAIN AT PEAK LOAD

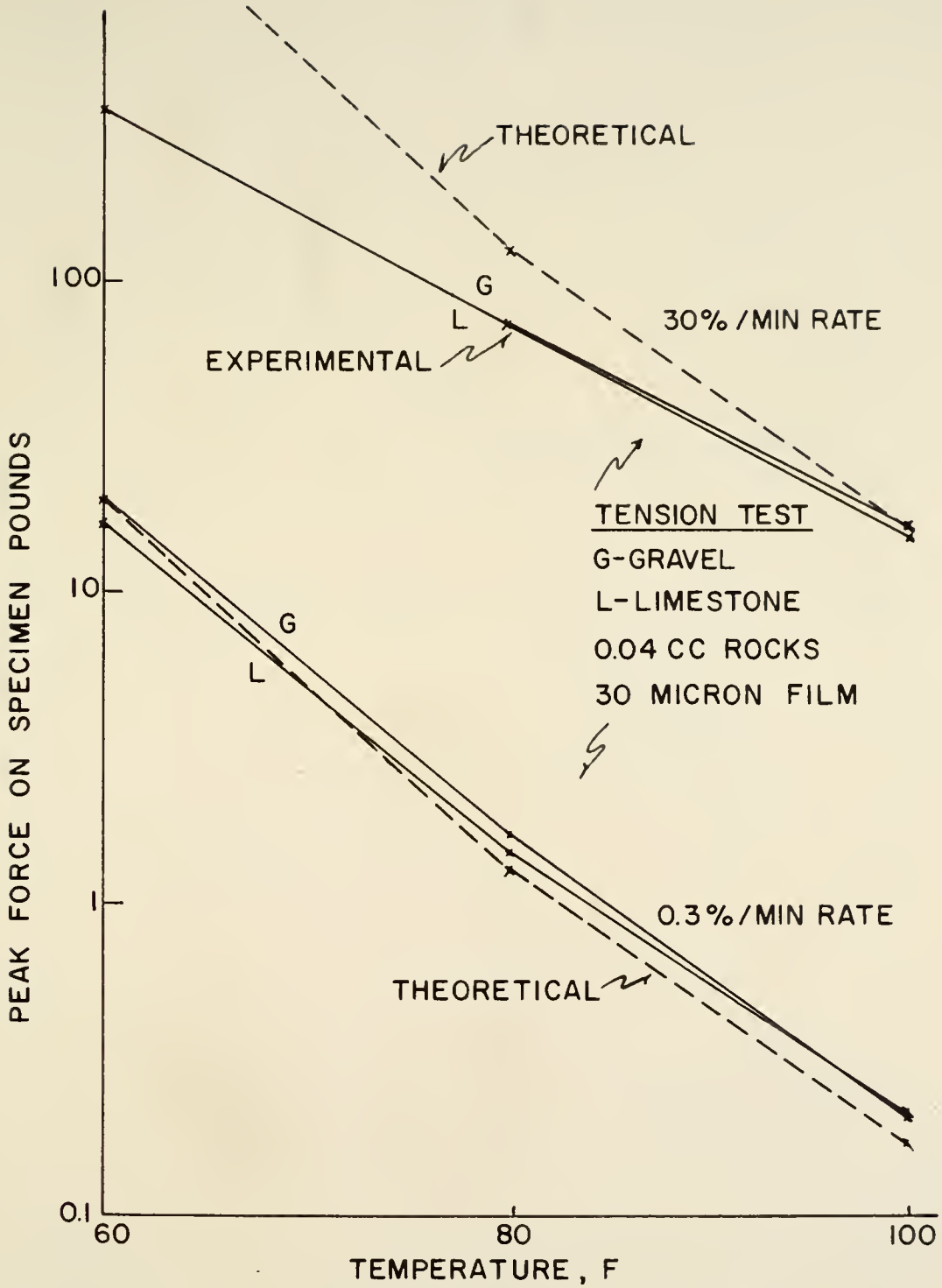

FIGURE 47 THEORETICAL AND EXPERIMENAL TENSILE FORCE, 0.04 CC ROCKS, 30 MICRON FILM

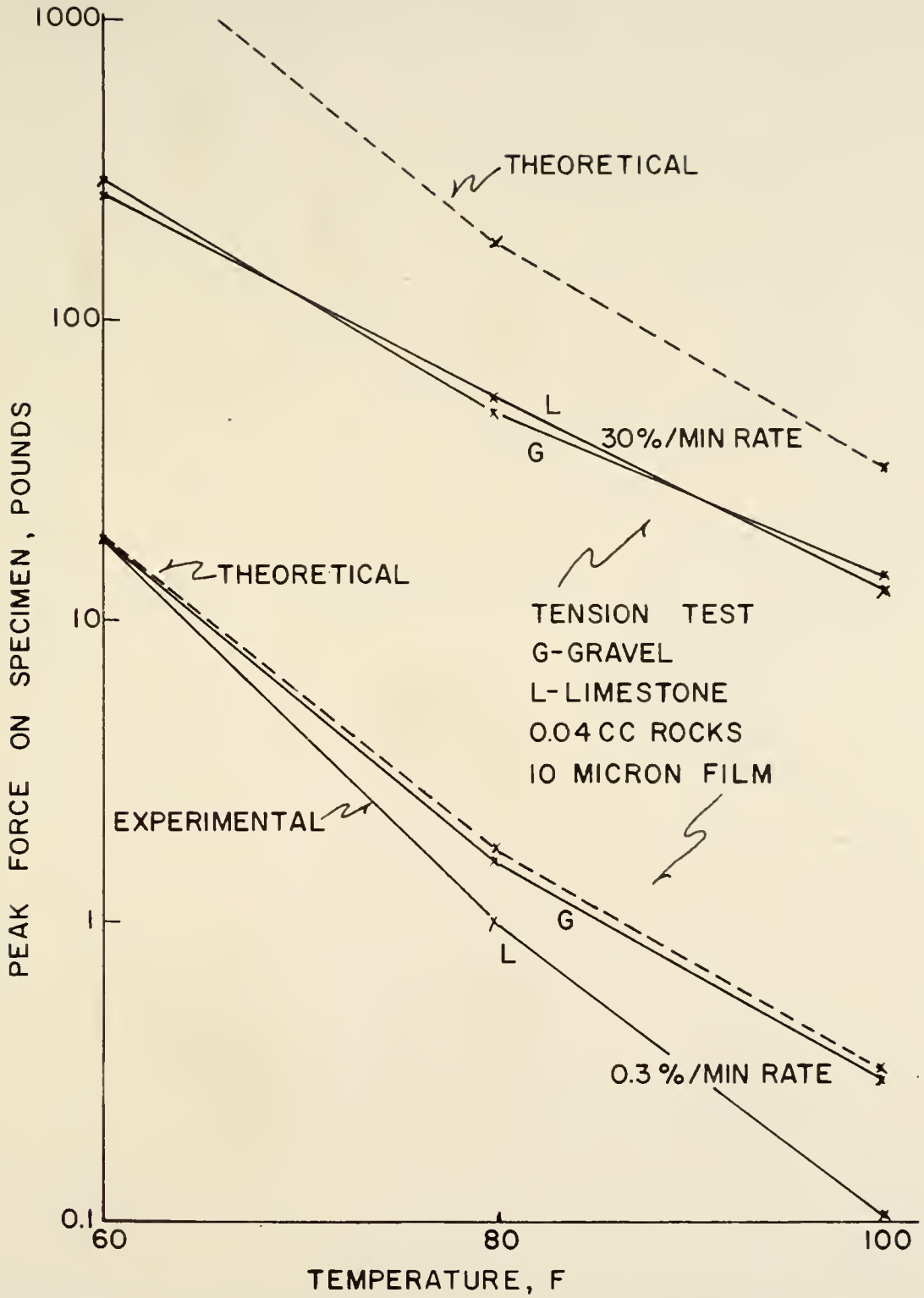

FIGURE 48 THEORETICAL AND EXPERIMENTAL TENSILE FORCE, 0.04 CC ROCKS, 10 MICRON FILM

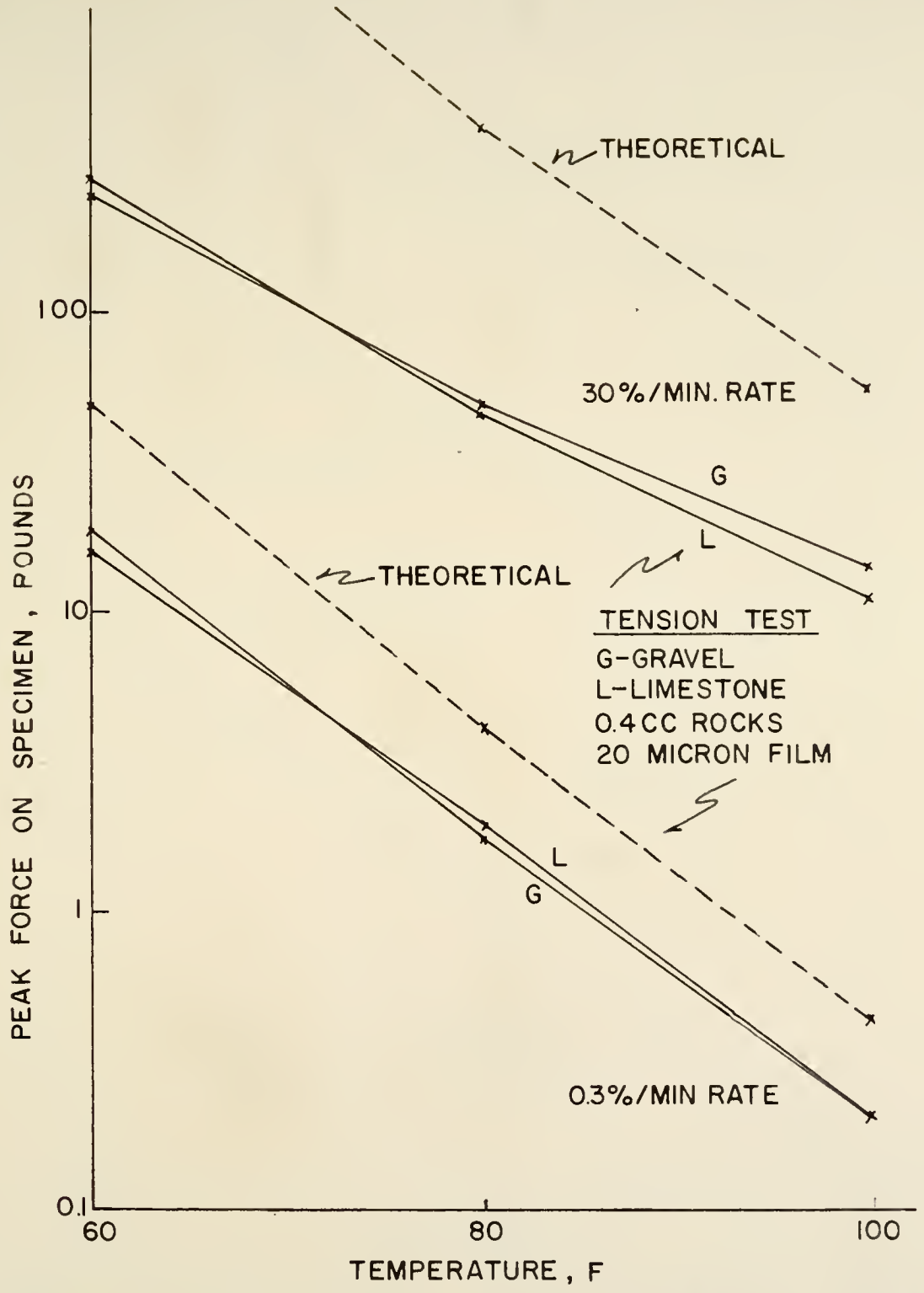

FIGURE 49 THEORETICAL AND EXPERIMENTAL TENSILE FORCE, 0.4CC ROCKS, 20 MICRON FILM

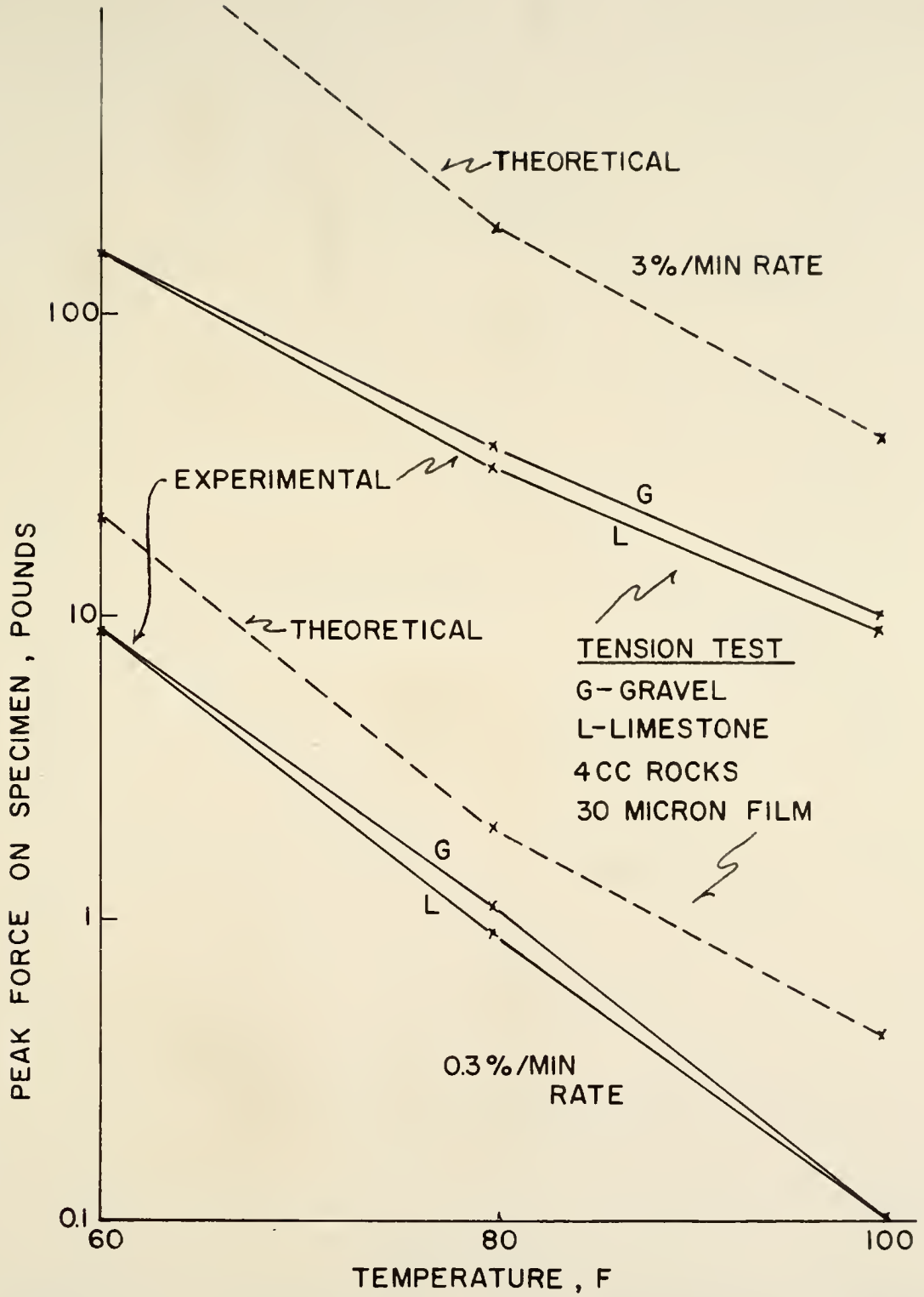

FIGURE 50 THEORETICAL AND EXPERIMENTAL TENSILE FORCE, 4CC ROCKS, 30MICRON FILM

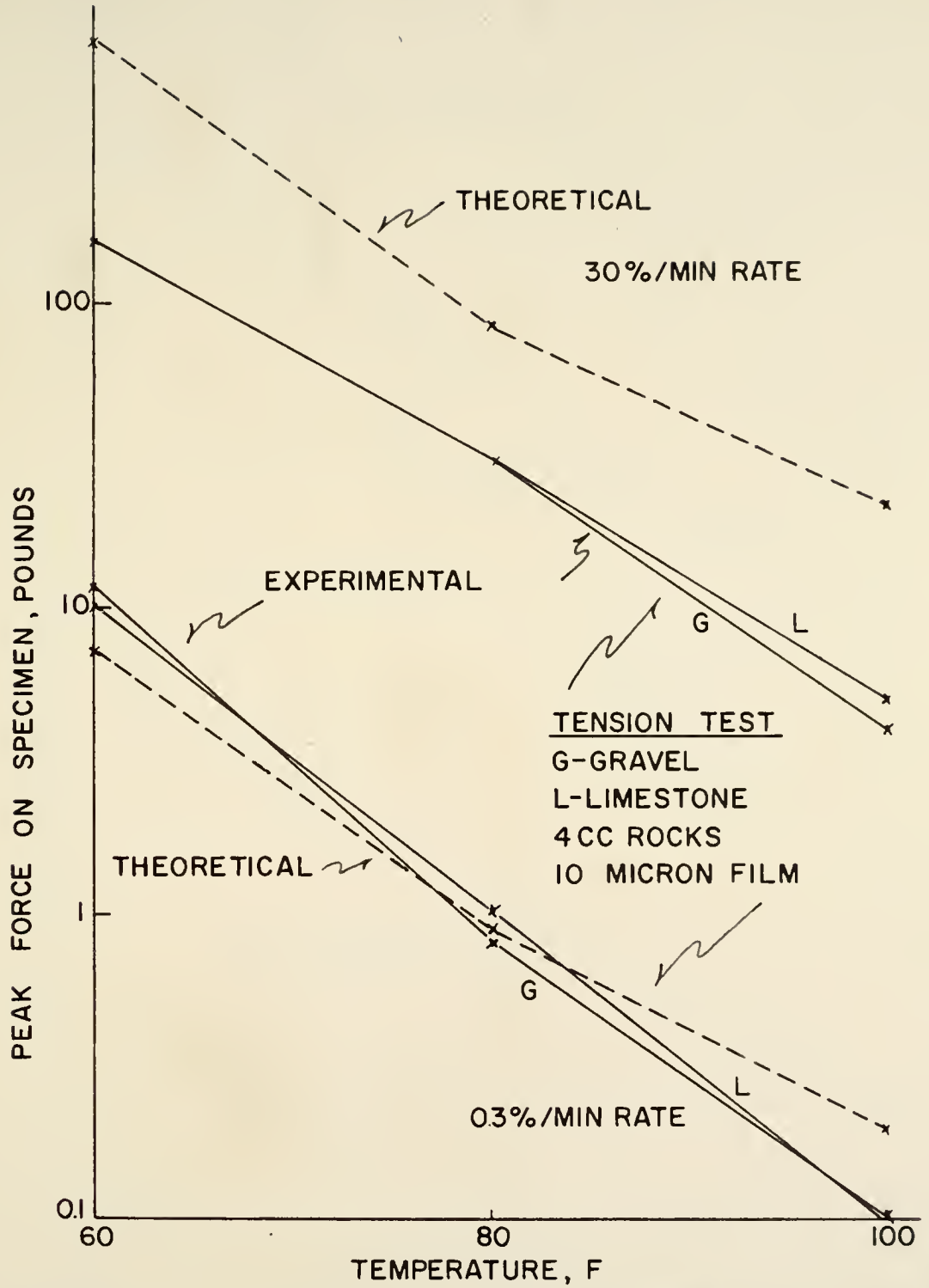

FIGURE 51 THEORETICAL AND EXPERIMENTAL TENSILE FORCE, 4 CC ROCKS, 10 MICRON FILM

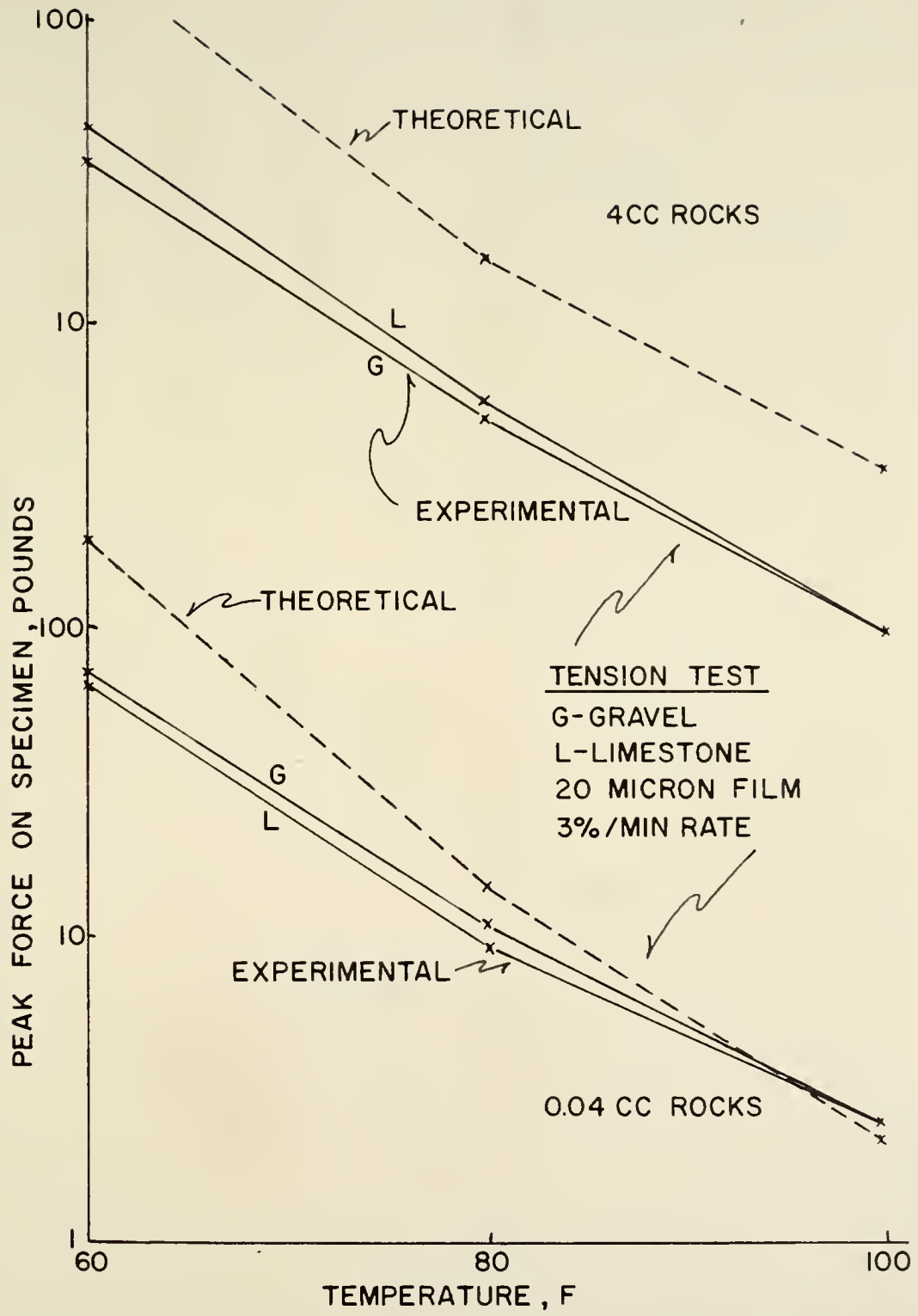

FIGURE 52 THEORETICAL AND EXPERIMENTAL TENSILE FORCE, 20 MICRON FILM, 3%/MIN RATE

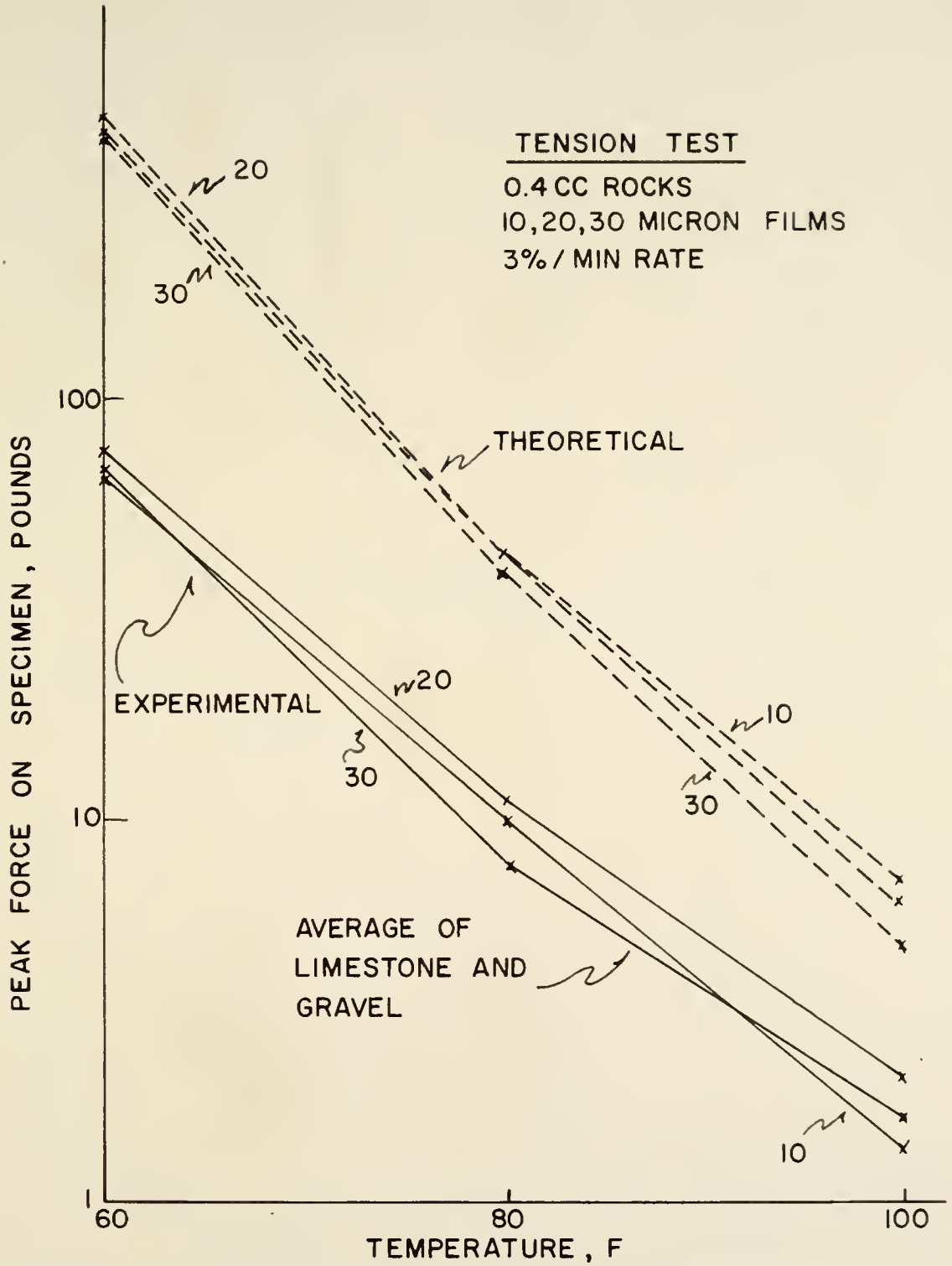

FIGURE 53 THEORETICAL AND EXPERIMENTAL TENSILE FORCE, 0.4 CC ROCKS, 3 FILM THICKNESSES

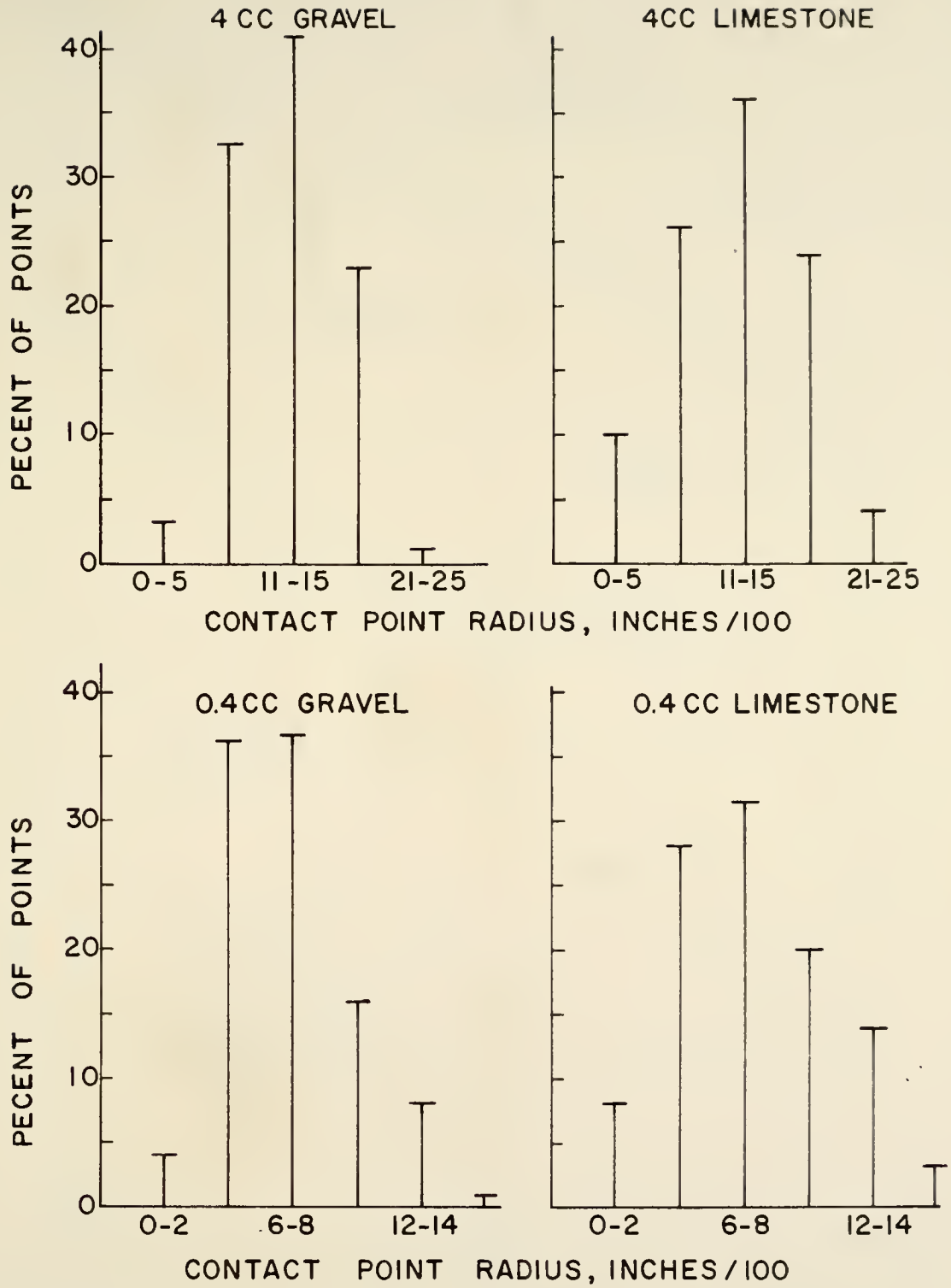

FIGURE 54 DISTRIBUTION OF CONTACT POINT RADII

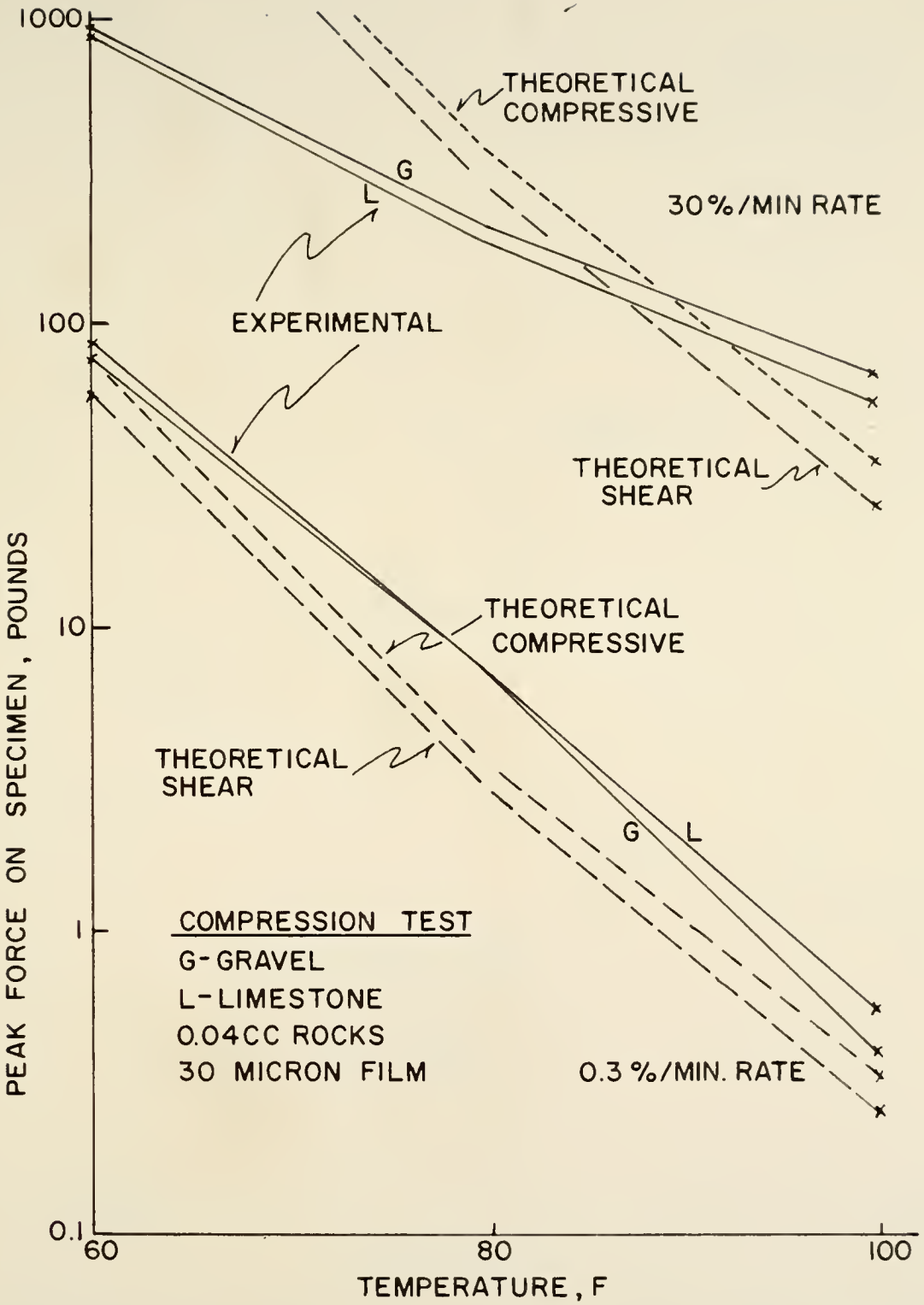

FIGURE 55 EXPERIMENTAL COMPRESSIVE FORCE COMPARED WITH THEORETICAL COMPRESSIVE AND SHEAR FORCES, 0.04 CC ROCKS, 30 MICRON FILM

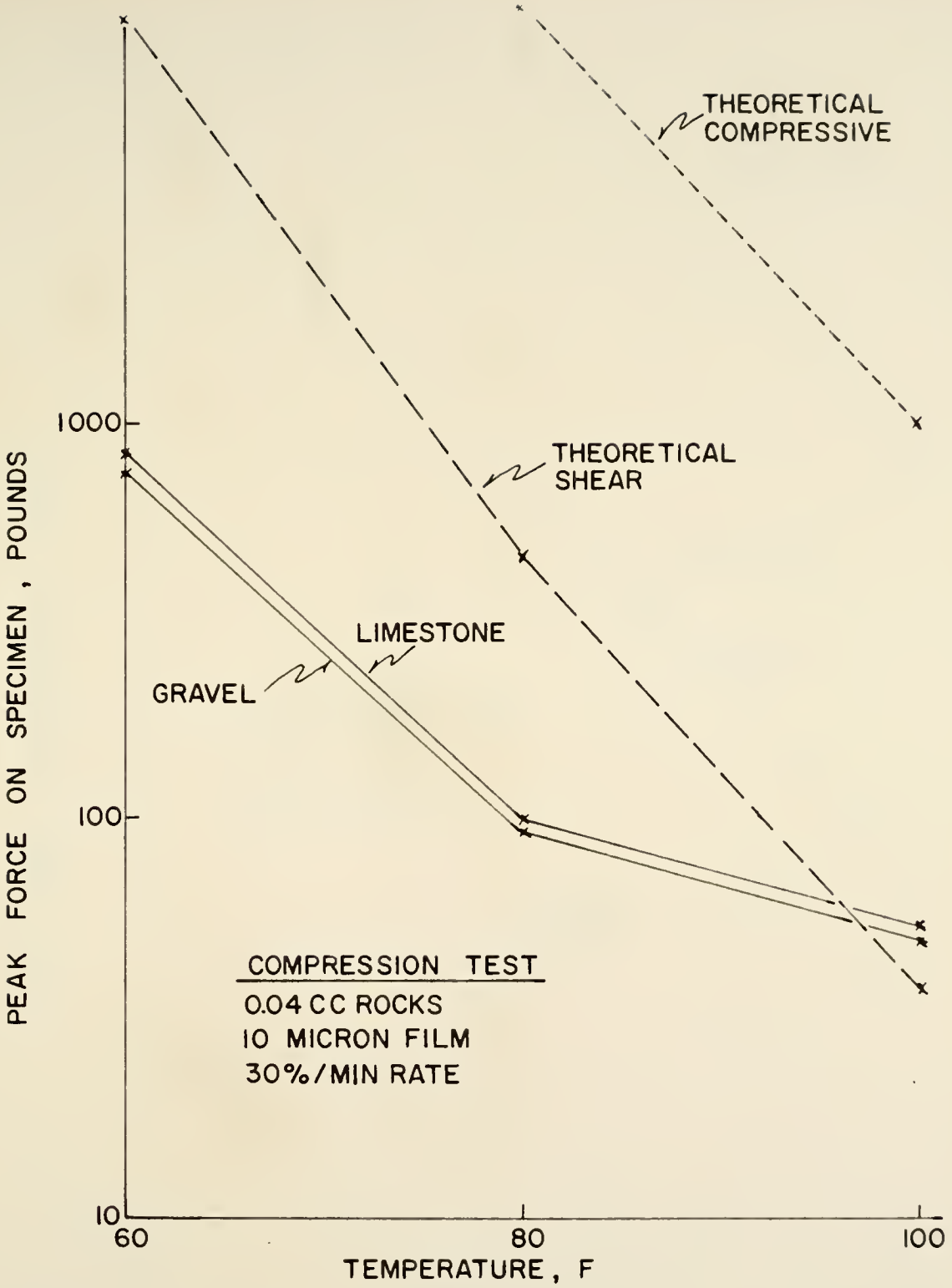

FIGURE 56 EXPERIMENTAL COMPRESSIVE FORCE COMPARED WITH THEORETICAL COMPRESSIVE AND SHEAR FORCES, 0.04CC ROCKS, 30%/MIN RATE

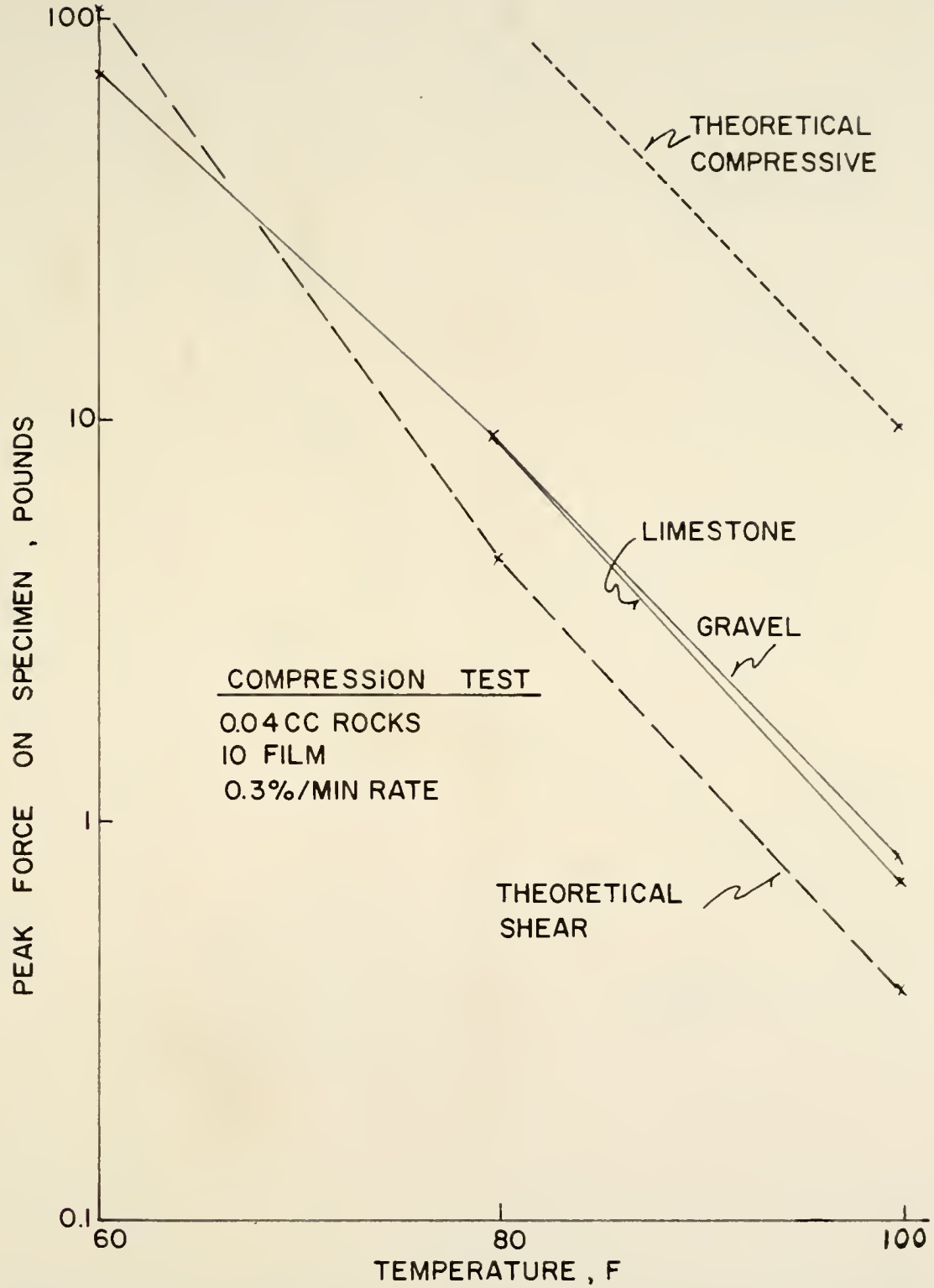

FIGURE 57 EXPERIMENTAL COMPRESSIVE FORCE COMPARED WITH THEORETICAL COMPRESSIVE AND SHEAR FORCES, 0.04CC ROCKS, 0.3%/MIN RATE

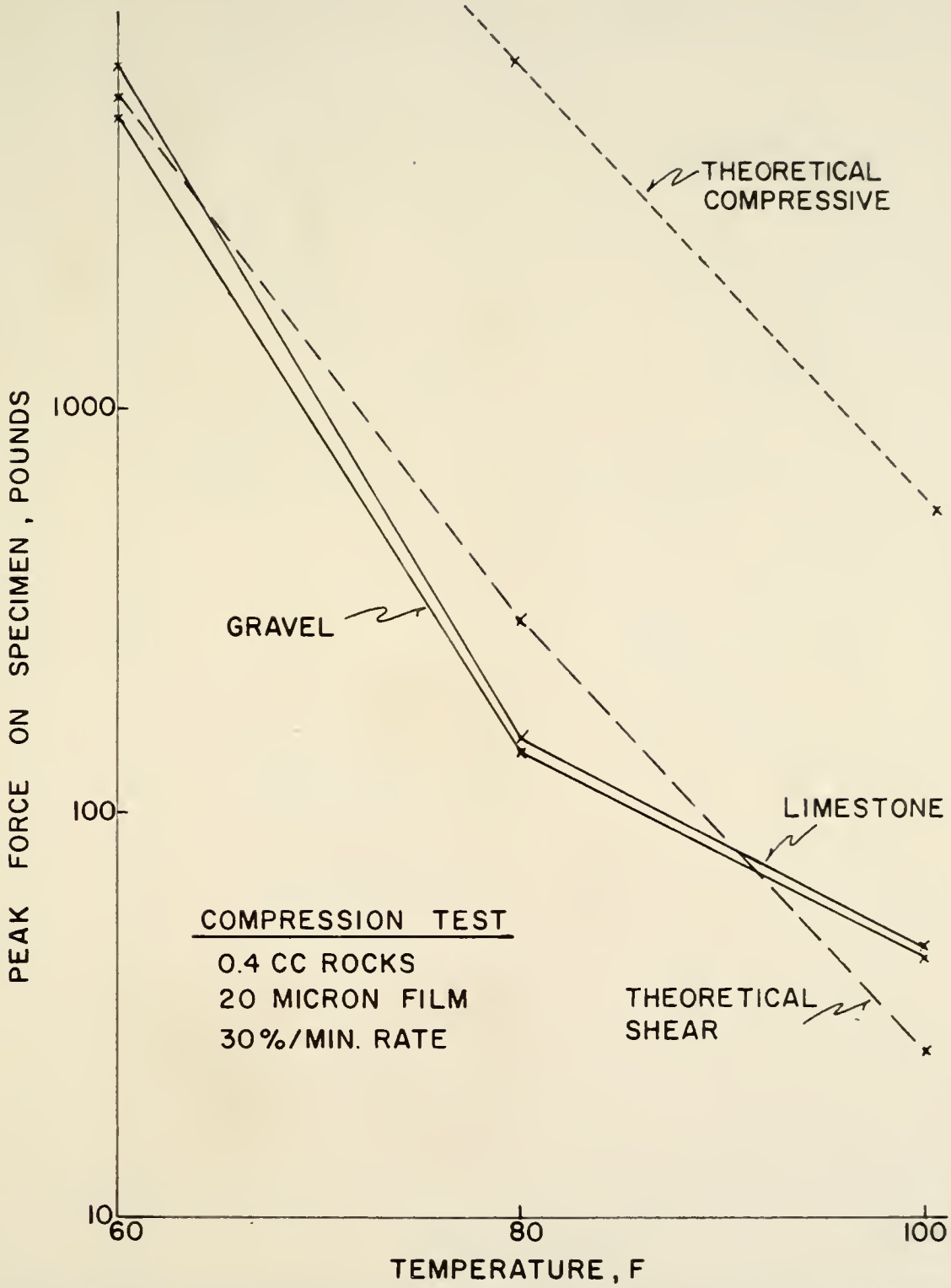

FIGURE 58 EXPERIMENTAL COMPRESSIVE FORCE COMPARED WITH THEORETICAL COMPRESSIVE AND SHEAR FORCES, 0.4CC ROCKS, 30%/MIN RATE

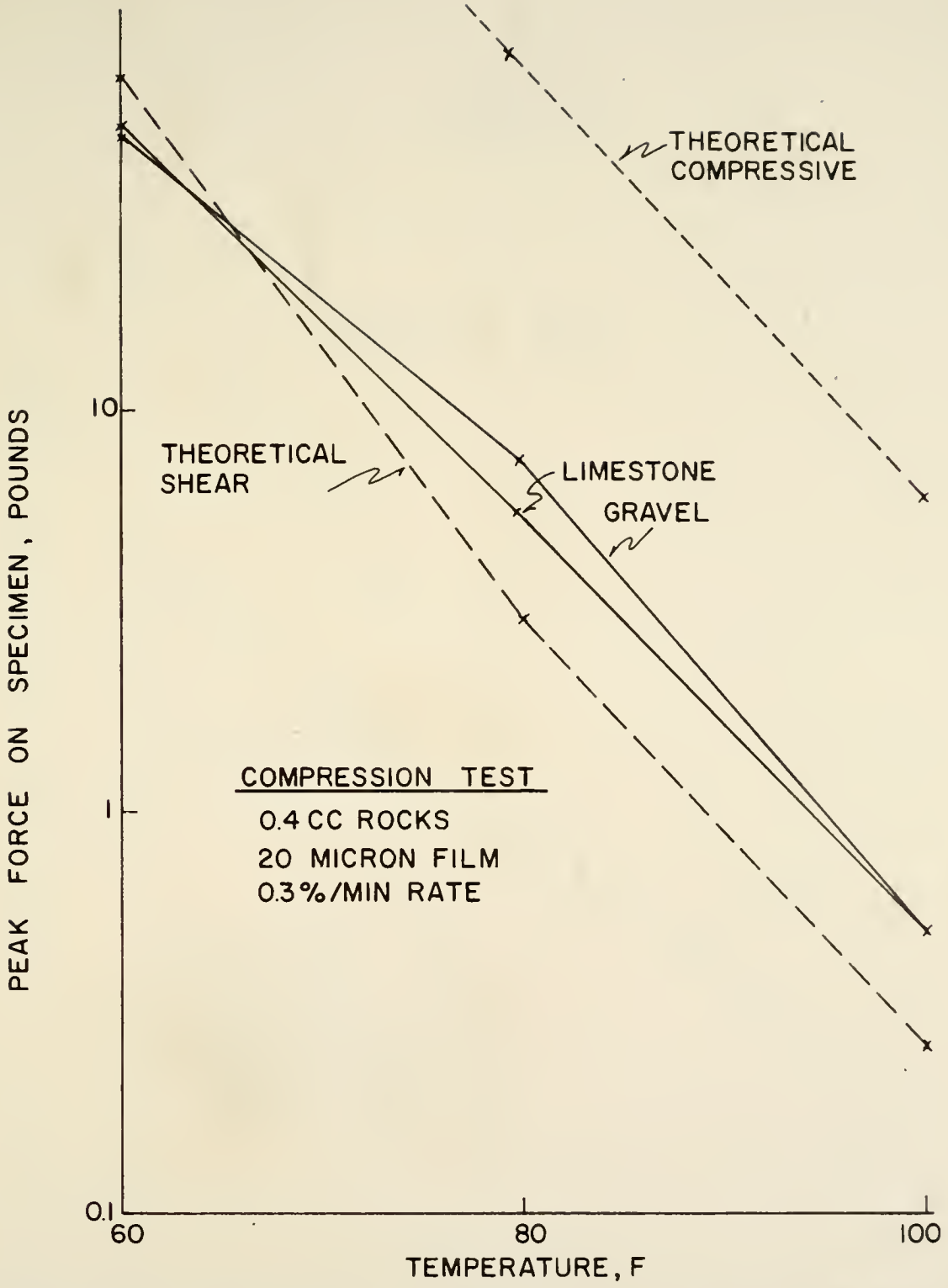

FIGURE 59 EXPERIMENTAL COMPRESSIVE FORCE COMPARED WITH THEORETICAL COMPRESSIVE AND SHEAR FORCES, 0.4CC ROCKS, 0.3%/MIN RATE

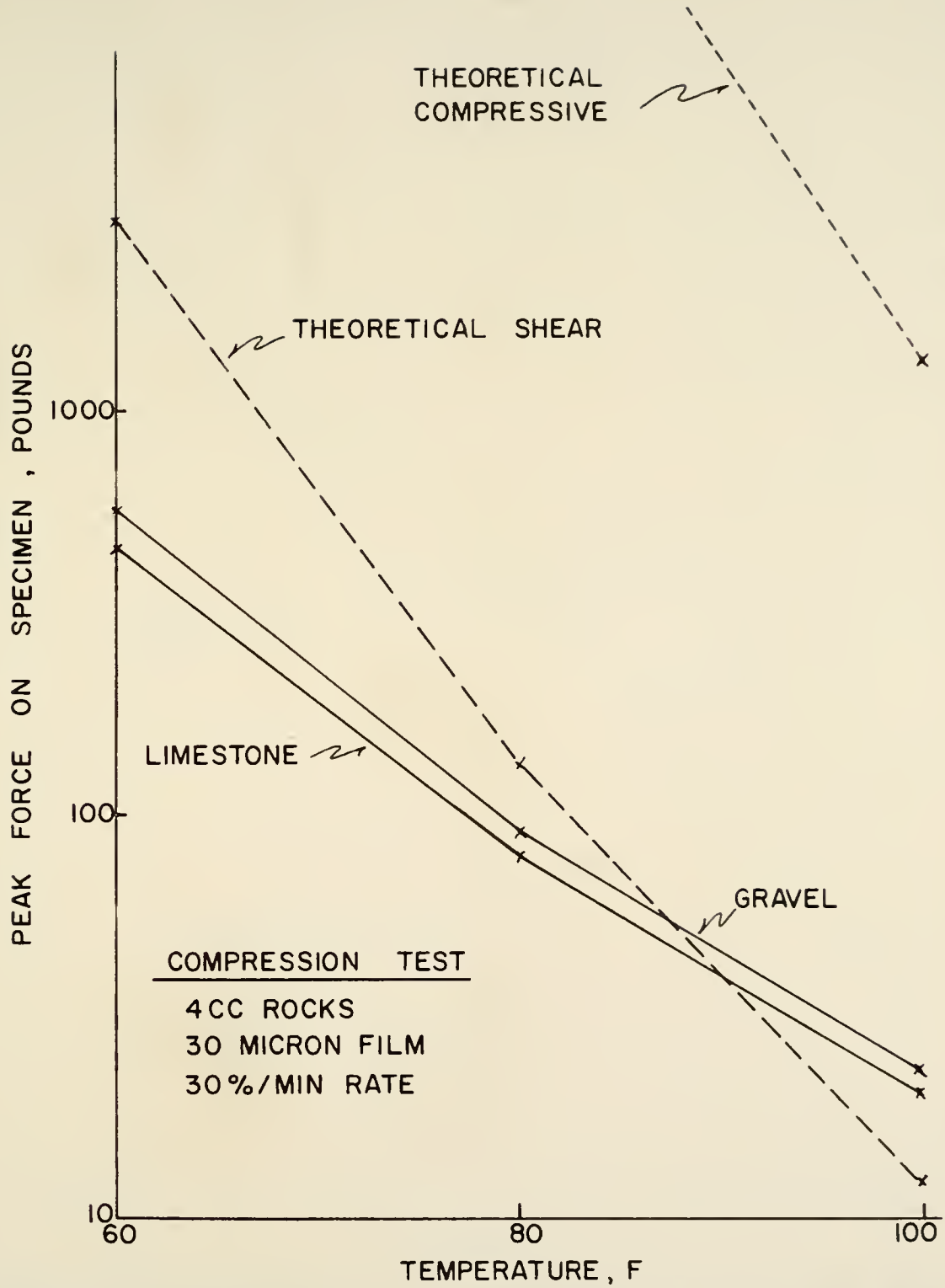

FIGURE 60 EXPERIMENTAL COMPRESSIVE FORCE COMPARED WITH THEORETICAL COMPRESSIVE AND SHEAR FORCES, 4CC ROCKS, 30%/MIN RATE

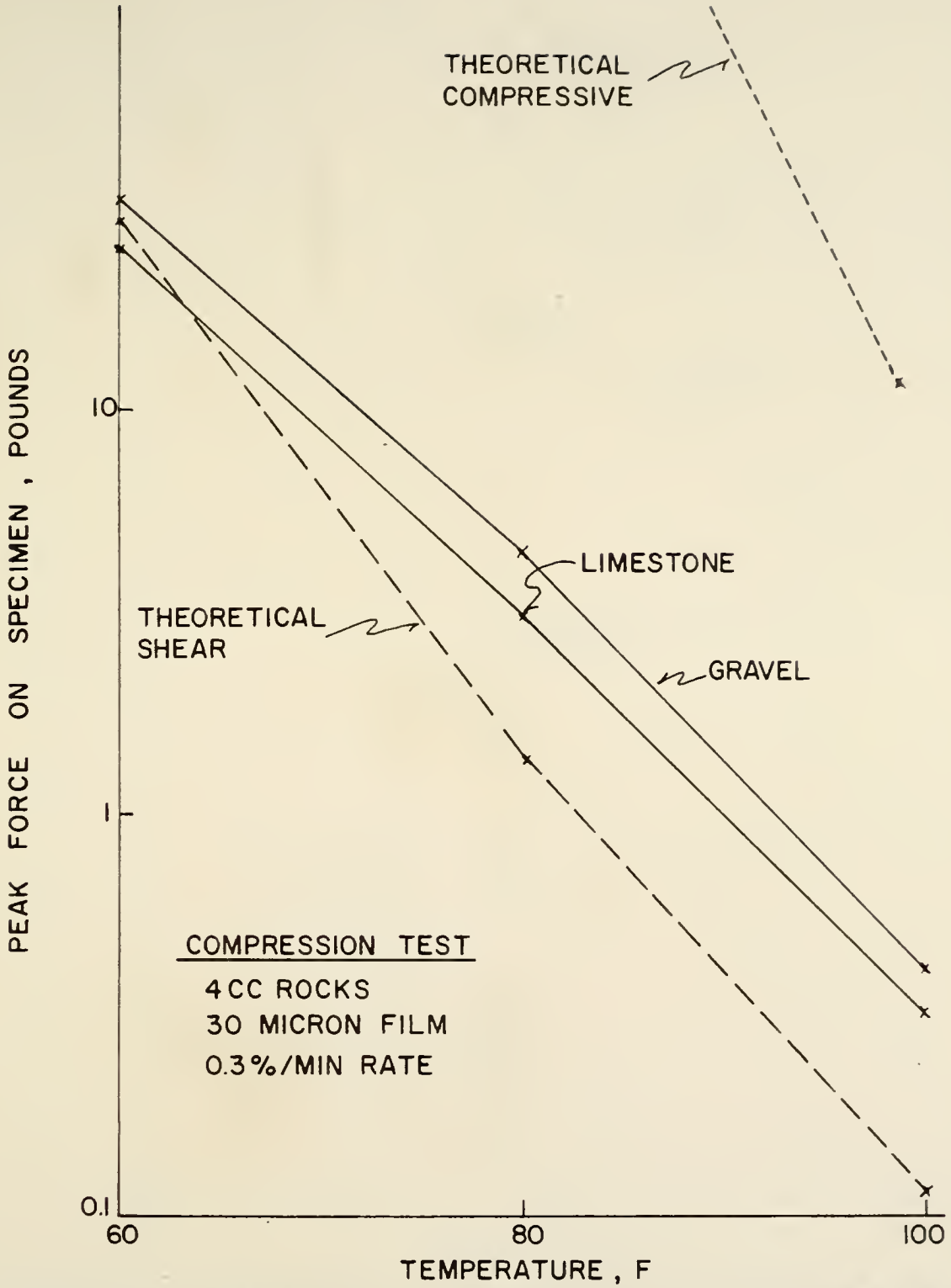

FIGURE 61 EXPERIMENTAL COMPRESSIVE FORCE COMPARED WITH THEORETICAL COMPRESSIVE AND SHEAR FORCES, 4CC ROCKS, 0.3%/MIN RATE

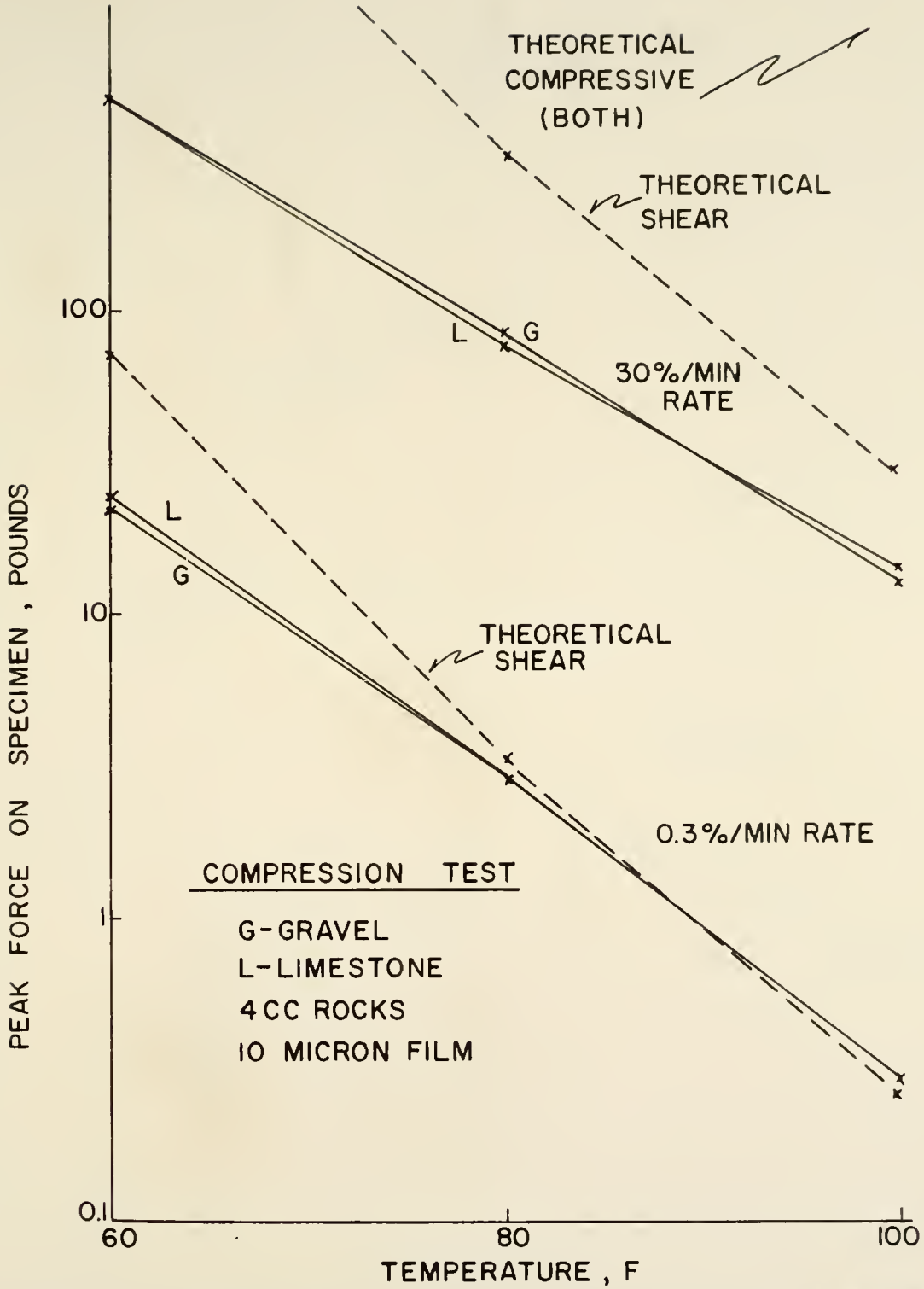

FIGURE 62 EXPERIMENTAL COMPRESSIVE FORCE COMPARED WITH THEORETICAL COMPRESSIVE AND SHEAR FORCES, 4CC ROCKS, 10 MICRON FILM

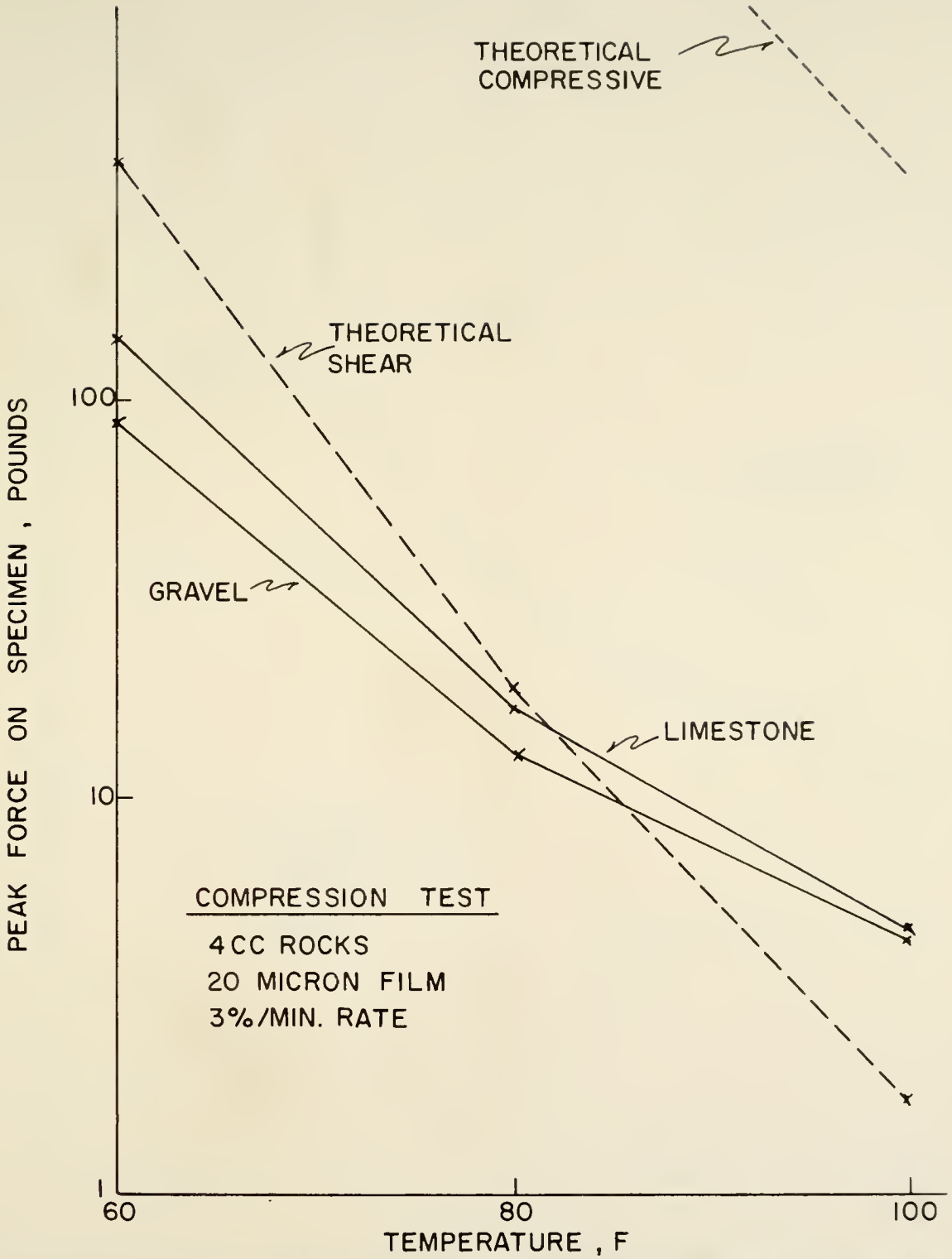

FIGURE 63 EXPERIMENTAL COMPRESSIVE FORCE COMPARED WITH THEORETICAL COMPRESSIVE AND SHEAR FORCES, 4CC ROCKS, 3%/MIN RATE

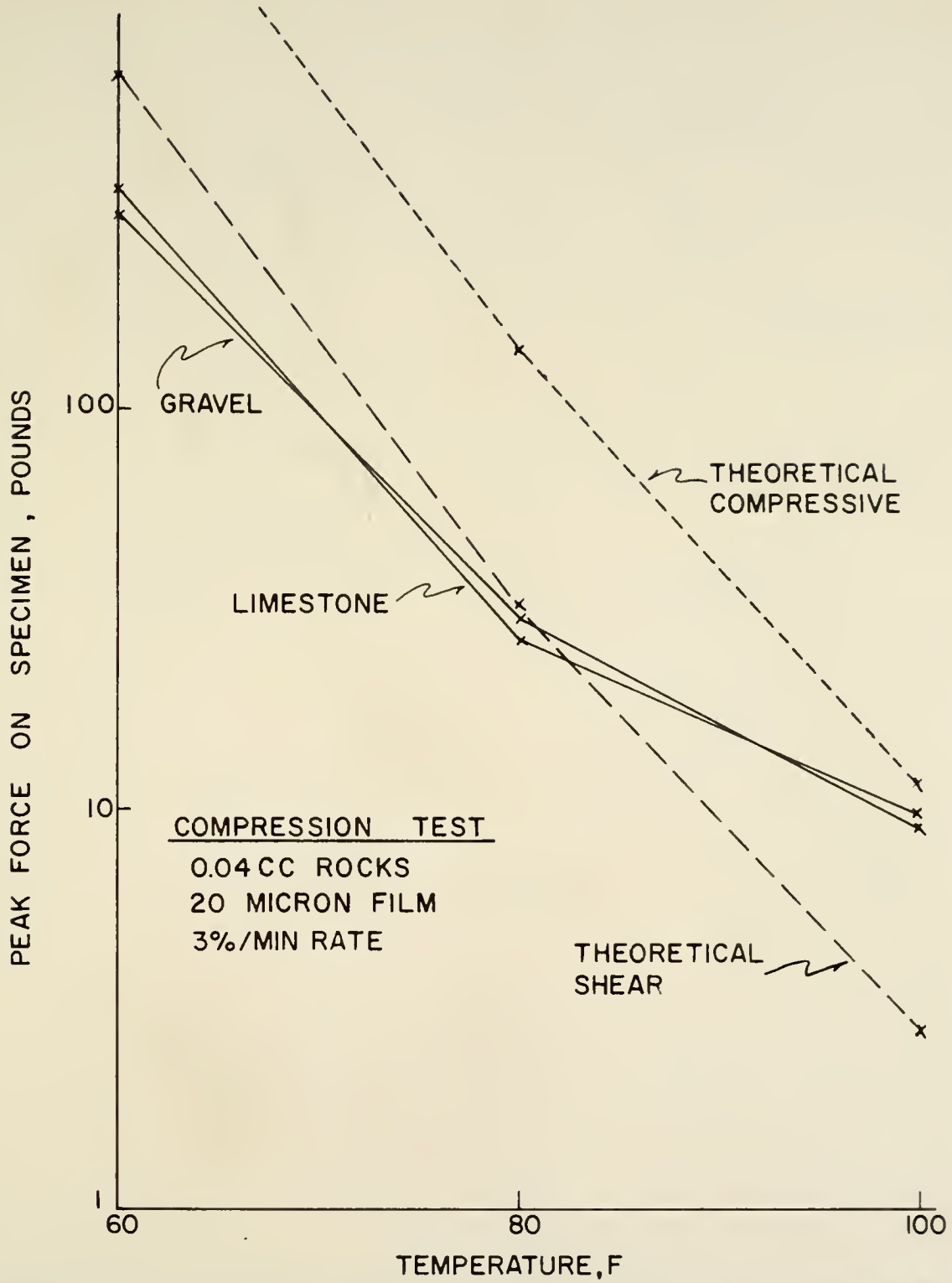

FIGURE 64 EXPERIMENTAL COMPRESSIVE FORCE COMPARED WITH THEORETICAL COMPRESSIVE AND SHEAR FORCES, 0.04CC ROCKS, 3%/MIN RATE

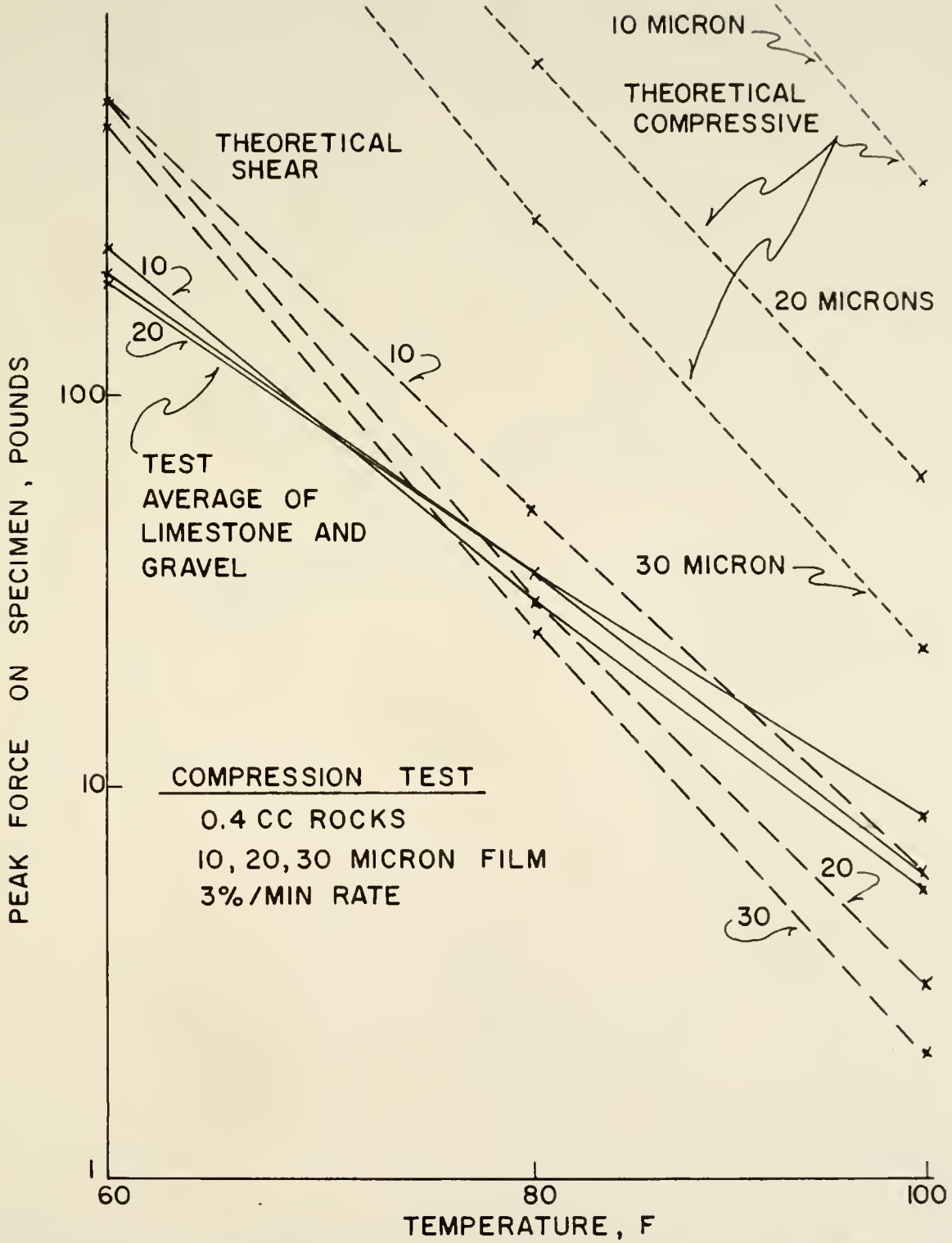

FIGURE 65 EXPERIMENTAL COMPRESSIVE FORCE COMPARED WITH THEORETICAL COMPRESSIVE AND SHEAR FORCES, 0.4 CC ROCKS, 3 FILM THICKNESSES

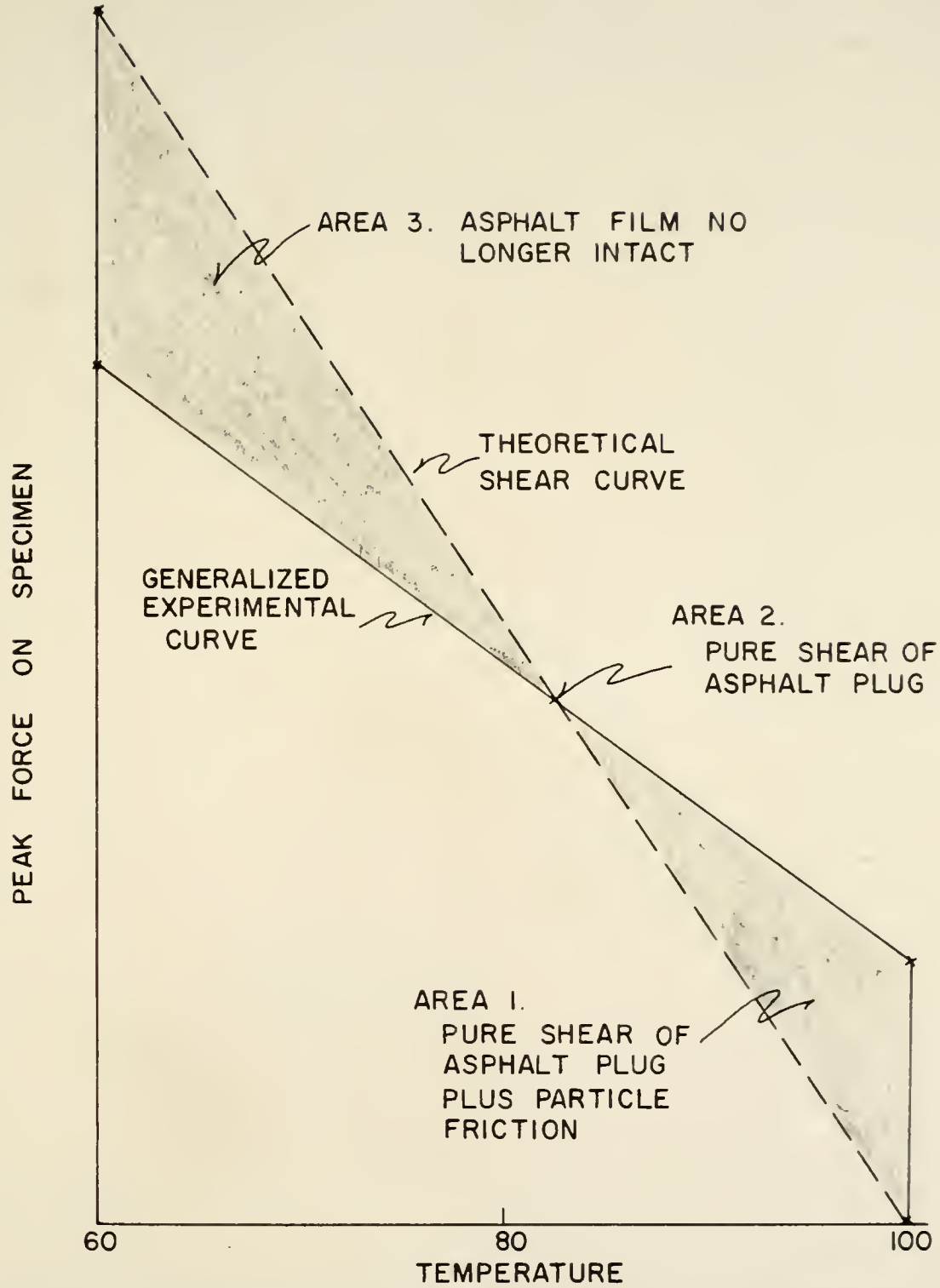

FIGURE 66 CURVES ILLUSTRATING CONCEPTS IN SHEAR FLOW

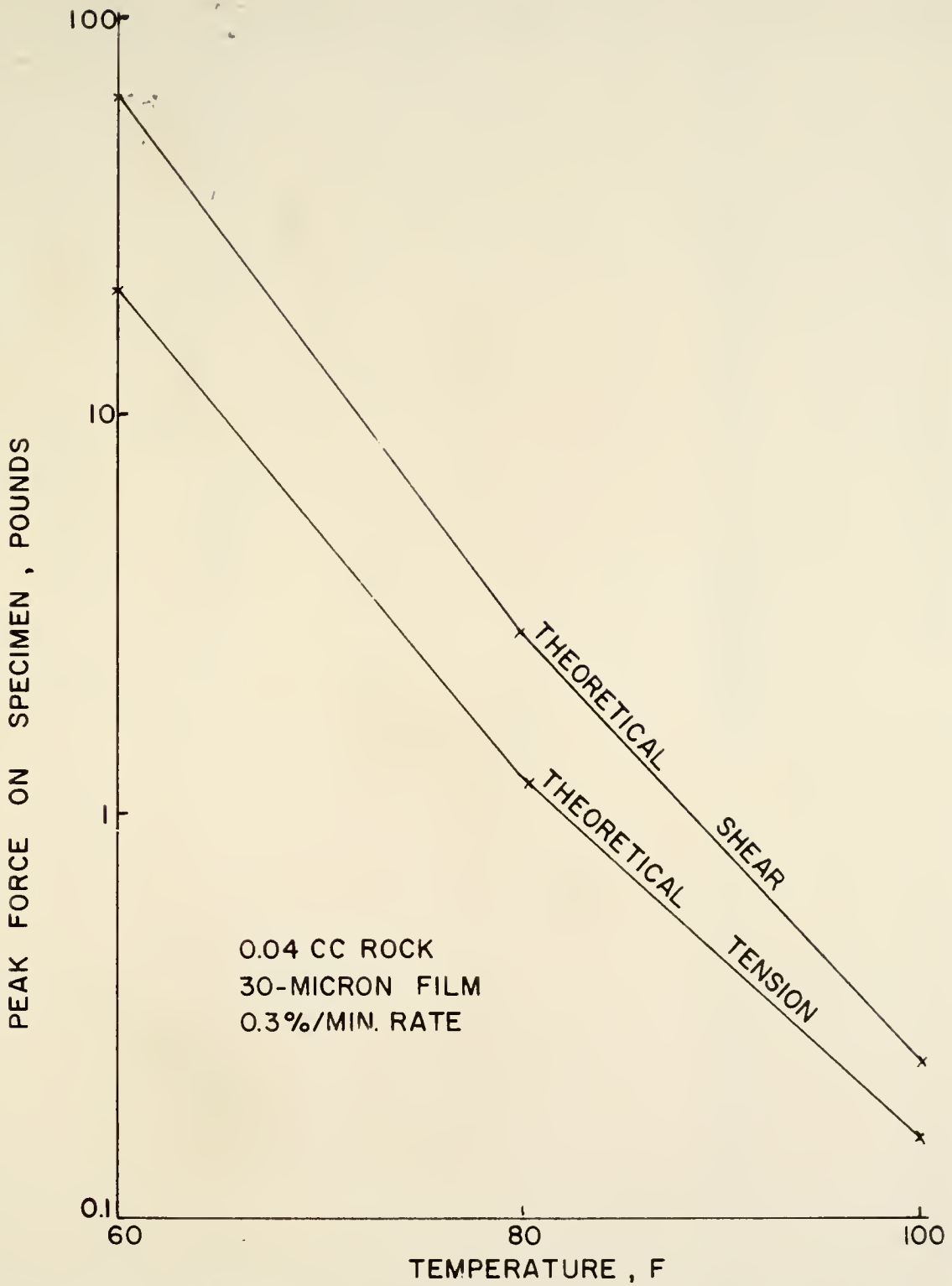

FIGURE 67 THEORETICAL SHEAR AND TENSION CURVES
0.04 CC ROCKS, 30 MICRON FILM, 0.3%/MIN RATE

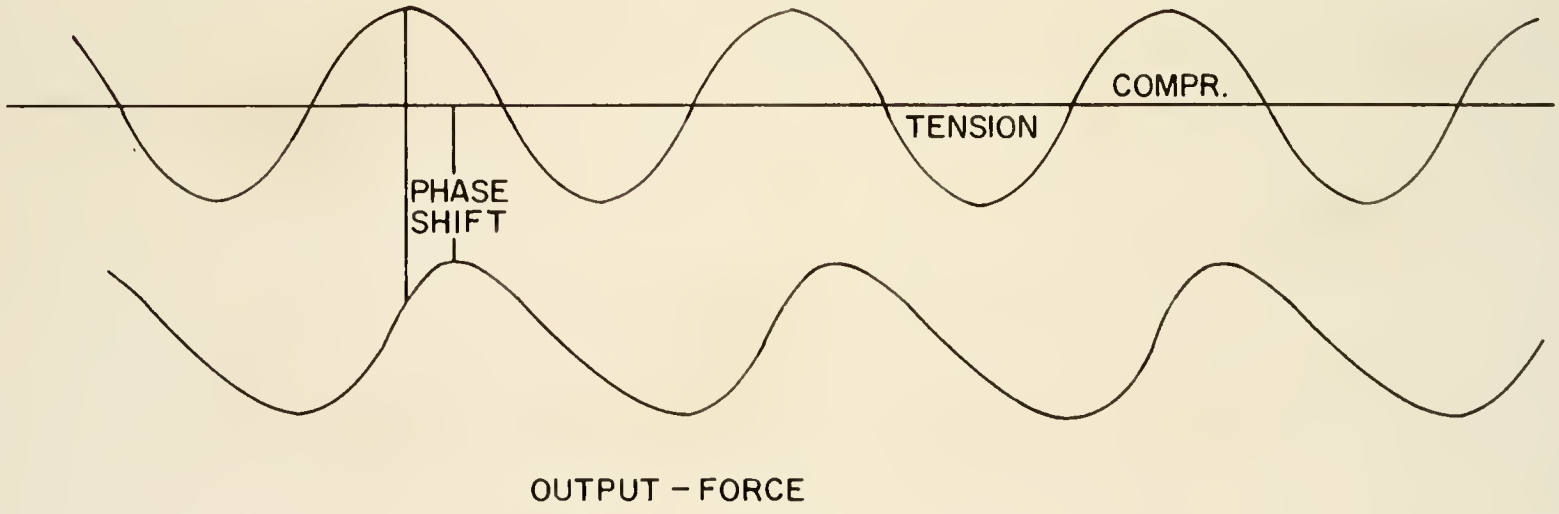

FIGURE 68 SECTIONS OF CYCLIC DEFORMATION AND FORCE RESPONSE CURVES

BIBLIOGRAPHY

BIBLIOGRAPHY

Uncoated Aggregates

1. Gronhaug, A. "Evaluation and Influence of Aggregate Particle Shape and Form." Statens Vegvesen Veglabaratoriet, Oslo, Meddelese Nr. 31, Oslo, 1967.

2. Mather, Bryant. "Shape, Surface Texture and Coatings of Aggregates." U. S. Army Engineer Waterways Experiment Station, Corps of Engineers, Vicksburg, Mississippi, Miscellaneous Paper No. 6-710, 1965.

3. Gaudin, A. M. "An Investigation of Crushing Phenomenon." American Institute of Mining and Metallurgy Engineers, Vol. 73, pp. 253-310, 1926.

4. Coghill, W. H., Holmes. O. W. and Campbell, A. B. "Determination of Flakiness of Ores." Report of Investigation No. 2899, U. S. Bureau of Mines, 1928.

5. Shergold, F. A. "A Study of Granulators Used in the Production of Roadmaking Aggregates." Road Research Technical Paper No. 44, British Road Research Laboratory, 1959.

6. Banning, L. H. and Lamb, F. O. "A Vibratory Screen Surface for Removal of Flat and Elongated Pieces from Crushed Stone." Report of Investigation No. 3781, U. S. Bureau of Mines, September 1949.

7. Wadell, Hakon. "Volume, Shape and Roundness of Rock Particles." Journal of Geology, Vol. 40, pp. 443-451, 1932.

8. Wadell, Hakon. "Sphericity and Roundness of Rock Particles." Journal of Geology, Vol. 41, pp. 310-331, 1933.

9. Zing, T. "Beitrag fuer Schotteranalyse, Schweiz Mineral." Petrog. Mitt. 15, pp. 39-140, 1935.

10. British Standard Institution, Methods of Sampling and Testing of Mineral Aggregates, Sands and Fillers. British Standard 812, pp. 134-136. London, 1960.

11. "Definitions of Terms Relating to Concrete and Concrete Aggregates." ASTM Designation C 125-58, ASTM Standards, Part 4, 1962.

12. Mackey, R. D. "The Measurement of Particle Shape." Civil Engineering and Public Works, Vol. 60, No. 703, pp. 211-214, 1965.

13. Pettijohn, F. J. Sedimentary Rocks, Harper and Brothers, New York, 526 pp. (1949).

14. Wentworth, C. K. "A Method of Measuring and Plotting the Shapes of Pebbles." Bulletin, U. S. Geologic Survey, No. 730, pp. 91-102, 1922.

15. Wadell, H. "Volume, Shape and Roundness of Quartz Particles," Journal of Geology, Vol. 43, pp. 250-280, 1935.

16. Krumbein, W. C. and Sloss, L. L. Stratigraphy and Sedimentation. W. H. Freeman and Company, San Francisco, California, 497 pp., 1951.

17. Bikerman, J. J. The Science of Adhesive Joints. Academic Press, 1961.

18. Broadston, J. A. "Surface Finish Measurement Instrumentation," April and June, 1959.

19. Mikelston, W. "Surface Roughness Measurements of Inspection," Conference of Instrument Society of America, Pittsburgh, Pennsylvania, 1946.

20. Herschmann, H. K. Technical News Bulletin. National Bureau of Standards, Vol. 31, No. 3, March 29, 1947.

21. Kriege, H. F. "Mineral Composition of Aggregates." Report on Significance Tests of Concrete and Concrete Aggregates, 2nd Ed. ASTM STP No. 22-A, 1943.

22. Blanks, R. F. "Modern Concepts Applied to Concrete Aggregates." Transactions, American Society of Civil Engineers, Vol. 115, pp. 403, 1950.

23. Adamson, A. W. Physical Chemistry of Surfaces. Interscience Publishers, Third Printing, 1964.

24. Deresiewicz, H. "Geometry of a Granular Mass." Advances in Applied Mechanics, Vol. V, 1958.

25. D'Appolonia, D. J. "Determination of the Maximum Density of Cohesionless Soils." Advance copy of a paper for the Third Asian Regional Conference on "Soil Mechanics and Foundation Engineering", 1967.

26. Bikerman, J. J. "Adhesion of Asphalt to Stone." Massachusetts Institute of Technology, Civil Engineering, Research Report R 64-3, 1964.

27. Golomb and Shanks Elements of Ordinary Differential Equations. McGraw Hill, 1965.

Aggregates in Mixes

28. Benson, J. R. "Effects of Aggregate Size, Shape and Surface Texture on the Properties of Bituminous Mixtures - A Literature Survey." Paper presented at the 47th Annual Meeting of the Highway Research Board, January 15-19, 1963. Washington, D. C.

29. Fuller, W. B. and Thompson, S. E. "The Laws of Proportioning Concrete", Transactions American Society of Civil Engineers, Vol. 59, 1907, pp. 67-143.

30. Nijboer, L. W. "Elasticity as a Factor in the Design of Road Carpets", Amsterdam Laboratory of the N. V. de Bataafsche Petrosleum Maatschappij (Royal Dutch Shell Group); published by Elsevier Publishing Co., Inc.

31. Goode, J. F. and Lufseg, L. A. "A New Graphical Chart for Evaluating Aggregate Gradations", Proceedings Association of Asphalt Paving Technologists, Vol. 31, 1962, pp. 176-192.

32. Hveem, F. N. "Gradation of Mineral Aggregates for Dense Graded Bituminous Mixtures", Proceedings of Association of Asphalt Paving Technologists, Vol. 12, 1940, pp. 315-330.

33. McNaughton, M. F. Discussion of Paper by W. H. Campen, Proceedings of Association of Asphalt Paving Technologists, Vol. 12, 1940, pp. 309-314.

34. Henderson, G. H. "Application of Present Knowledge in the Construction and Maintenance of Bituminous Macadam and Bituminous Concrete", Proceedings Highway Research Board, Vol. 8, 1928, pp. 184-187.

35. Reagal, F. V. "Factors Governing the Selection of Aggregates; Practice in Missouri", Proceedings Thirteenth National Asphalt Conference, 1940, pp. 181-186.

36. Stanton, Thomas E., Jr. and Hveem, F. N. "Role of the Laboratory in Preliminary Investigations and Control of Materials for Low Cost Bituminous Pavements", Proceedings Highway Research Board, Vol. 14, Part II, 1934, pp. 14-54.

37. Campen, W. H., Smith, J. R., Erickson, L. G., and Mertz, L. R. "Factors that Control Asphalt Requirements of Bituminous Paving Mixtures and a Method for Determining the Proper Asphalt Content", Proceedings Association of Asphalt Paving Technologists, Vol. 32, 1963, pp. 530-544.

38. Herrin, M. and Goetz, W. H. "Effect of Aggregate Shape on Stability of Bituminous Mixes", Highway Research Board Proceedings, Vol. 33, 1954, pp. 293-308.

39. Griffith, John M. and Kallas, B. F. "Influence of Fine Aggregate on Asphaltic Concrete Paving Mixtures", Proceedings Highway Research Board, Vol. 37, 1958, pp. 219-255.

40. Lottman, R. R. and Goetz, W. H. "Effect of Crushed Gravel Fine Aggregate on the Strength of Asphaltic Surfacing Mixtures", National Sand and Gravel Association Circular 63, 1956, Washington, D. C.

41. Shklarsky, E. and Livneh, M. "The Use of Gravels for Bituminous Paving Mixtures", Proceedings Association of Asphalt Paving Technologists, Vol. 33, 1964, 584-610.

42. Field, Frederick. "The Importance of Percent Crushed in Coarse Aggregate as Applied to Bituminous Pavements", Proceedings, Association of Asphalt Paving Technologists, Vol. 27, 1958, pp. 294-320.

43. Lefebvre, J. "Recent Investigations of Design of Asphalt Paving Mixtures", Proceedings Association of Asphalt Paving Technologists, Vol. 26, 1957, pp. 297-309.

44. Campen, W. H. and Smith, J. R. "A Study of the Role of Angular Aggregates in the Development of Stability in Bituminous Mixtures", Proceedings of the Association of Asphalt Paving Technologists, Vol. 17, 1948, pp. 114-135.

45. Puzinauskas, V. P. "Influence of Mineral Aggregate Structure on Properties of Asphalt Paving Mixtures", Highway Research Record Number 51 (papers presented at 43rd Annual Meeting, January 13-17, 1964) pp. 1-15.

46. Wedding, P. A. and Gaynor, R. D. "The Effects of Using Gravel as the Coarse and Fine Aggregate in Dense Graded Bituminous Mixtures", Proceedings Association of Asphalt Paving Technologists, Vol. 30, 1961, pp. 469-488.

47. Lees, G. "The Measurement of Particle Shape and Its Influence in Engineering Materials", Journal of British Granite and Whinstone Federation, Vol. 4, No. 2, Autumn 1964.

48. Hveem, F. N. "Some Basic Factors and Their Effect on the Design of Bituminous Mixtures", Proceedings of the National Bituminous Conference, 1937, pp. 220-228.

49. Vallerga, B. A. "On Asphalt Pavement Performance", Proceedings Association of Asphalt Paving Technologists, Vol. 24, 1955, pp. 79-99.

50. Neppe, S. L. "Mechanical Stability of Bituminous Mixtures: A Summary of Literature", Proceedings of the Association of Asphalt Paving Technologists, Vol. 22, 1953, pp. 383-427.

51. Ryan, A. P. "Discussion of Plant Mixes", Crushed Stone Journal, Vol. 29, No. 1, March 1954, pp. 20-24.

52. Brodnyan, J. E. "Rheological and Adhesion Characteristics of Asphalt, Bulletin 192, Highway Research Board, 1958.

53. Saal, R. N. J. and Lesout, J. W. A. "Rheological Properties of Asphalt", Rheology - Theory and Applications, Ed. by F. R. Eirich, Vol. II, Academic Press Inc., New York, 1958.

54. Papazian, H. S. "Response of Linear Viscoelastic Materials in the Engineering Domain", Transportation Engineering Center, Ohio University Report No. 172-2.

55. Krokosky, E. M. "Rheological Properties of Asphalt-Aggregate Compositions", Massachusetts Institute of Technology, Civil Engineering Report, R 62-16, June 1962.

56. The Asphalt Institute, Mix Design Methods for Asphalt Concrete, Manual Series No. 2 (MS-2).

57. Douglas, A. and Tons, E. "Strength Analysis of Bituminous Mastic Concrete", Proceedings, Association of Asphalt Paving Technologists, Vol. 30, 1961, pp. 238.

58. Csanyi, L. H. "Bituminous Mastic Surfaces", Proceedings, Association of Asphalt Paving Technologists, Vol. 25, 1956.

59. Hardman, R., Buglass, B. F. "A Full Scale Experiment to Compare the Resistance to Deformation of Plastic Asphalt and a Rolled Asphalt at a Bus-Stop in Slough", British Road Research Laboratory, Road Research Note No. RN/3311/October 1958.

60. Meehan, R. L. "Physical Behavior of Mastic Asphalt Concrete Under Tension", Bachelor's Thesis, Massachusetts Institute of Technology, May 1961.

Flow in Porous Media

61. Jacob, C. E. "Radial Flow in Leaky Artesian Aquifer", Transactions, American Geophysical Union, Vol. 27, No. 11, pp. 198, April 1946.

62. Franzini, J. B. "Porosity Factor for Case of Laminar Flow Through Granular Media", Transactions, American Geophysical Union, Vol. 32, No. 3, pp. 443, June 1951.

63. Hudson, H. E., Jr. and Roberts, R. E. "Transition from Laminar to Turbulent Flow Through Granular Media", The Second Midwestern Conference on Fluid Mechanics, Proceedings, pp. 105, 1952.

64. Mavis, F. T. and Wilsey, E. F. "Filter Sand Permeability Studies", Engineering News-Record, Vol. 118, pp. 299, February 1937.

65. Rose, H. E. "An Investigation into the Laws of Flow of Fluids Through Beds of Granular Materials", Proceedings, Institution of Mechanical Engineers, Vol. 153, pp. 141, 1945.

66. Shuster, W. W. "The Effect of Void Fraction on the Pressure Drop Through Beds of Regularly Packed Spheres", Chemical Engineering Department, Ph. D. Thesis, Rensselaer Polytechnic Institute, January 1952.

67. Bulnes, A. C. and Fitting, R. V. "An Introductory Discussion of the Reservoir Performance of Limestone Formations", Transactions, American Institute of Mining and Metallurgical Engineers, Vol. 160, pp. 179, 1945.

68. Cloud, W. F. "Effects of Sand Grain Size Distribution Upon Porosity and Permeability", The Oil Weekly, Vol. 103, No. 8, pp. 26, October 1941.

69. Nelson, W. R. and Baver, L. D. "Movement of Water Through Soils in Relation to the Nature of the Pores", Proceedings, Soil Science Society of America, Vol. 5, pp. 69, 1940.

70. Gratow, L. C. and Fraser, H. J. "Systematic Packing of Spheres with Particular Relation to Porosity and Permeability", Journal of Geology, Vol. 43, pp. 785, 1935.

71. Tickell, F. G. "Permeability of Unconsolidated Rocks", Bulletin of the American Association of Petroleum Geologists, Vol. 19, Part 2, pp. 1233, 1935.

72. Krumbein, W. C. and Monk, G. D. "Permeability as a Function of the Size Parameters of Unconsolidated Sand", Transactions, American Institute of Mining and Metallurgical Engineers, Vol. 151, pp. 153, 1943.

73. Pillsbury, A. F., "Effects of Particle Size and Temperature on the Permeability of Sand to Water", Soil Science, Vol. 70, pp. 299, 1950.

74. Tickell, F. G., Mechem, O. E. and McCurdy, R. C. "Some Studies on the Porosity and Permeability of Rocks", Transactions, American Institute of Mining and Metallurgical Engineers, Vol. 103, pp. 250, 1933.

75. Martin, J. J., McCabe, W. L., and Monrad, C. C. "Pressure Drop through Stacked Spheres", Chemical Engineering Progress, Vol. 47, pp. 91, 1951.

76. Scheidegger, A. E. "Theoretical Models of Porous Matter", Producers Monthly, No. 10, 17, 1953.

77. Smith, W. O. "Capillary Flow Through an Ideal Uniform Soil", Physics (superseded by the Journal of Applied Physics), Vol. 3, pp. 139, September 1932.

78. Terzaghi, C. "Determination of Permeability of Clay", Engineering News Record, Vol. 95, No. 21, pp. 832, 1925.

79. Jacob, C. E. "On the Flow of Water in an Elastic Artesian Aquifer", Transactions, American Geophysical Union, pp. 574, April 1940.

80. Backer, Stanley, "The Relationship Between the Structural Geometry of a Textile Fabric and its Physical Properties", Textile Research Journal, Vol. 21, pp. 703, October 1951.

81. Kozeny, J. "Ueber Kapillare Leitung des Wassers im Boden", Berichte, Wiener Akademie, Vol. 136a, pp. 271, 1927.

82. Fair, G. M. and Hatch, L. P. "Fundamental Factors Governing the Streamline Flow of Water Through Sand", Journal of the American Waterworks Association, Proceedings, Vol. 25, pp. 1551, 1933.

83. Carman, P. C. "Fluid Flow Through Granular Beds", Transactions, Institution of Chemical Engineers, Vol. 15, pp. 150, 1937.

84. Sullivan, R. R. "Specific Surface Measurements on Compact Bundles of Parallel Fibers", Journal of Applied Physics, Vol. 13, pp. 725, November 1942.

85. Hubbert, M. K. "The Theory of Groundwater Motion", Journal of Geology, Vol. 48, Number 8, Part 1, pp. 785, 1940.

86. Childs, E. C. and Collis-George, N. "The Permeability of Porous Materials", Proceedings of the Royal Society, Vol. 201, pp. 392, 1950.

87. Taub, A. H. "The Sampling Method for Solving the Equations of Compressible Flow in a Permeable Medium", Proceedings of the Midwest Conference on Fluid Dynamics, First Conference, pp. 121, May 1950. Published by J. W. Edward, Ann Arbor, Michigan, 1951.

88. Scheidegger, A. E. "Statistical Hydrodynamics in Porous Media", Journal of Applied Physics, Vol. 25, pp. 994, August 1954.

89. Scheidegger, A. E. "The Physics of Flow Through Porous Media", The Macmillan Co., New York, 1957.

90. Irani, R. R. and Collis, C. F. Particle Size: Measurement Interpretation and Application, John Wiley and Sons, Inc., New York, 1963.

91. Herdan, G. "Small Particle Statistics", Academic Press, New York, 1960.

92. Green, Henry "The Effect of Non-Uniformity and Particle Shape on Average Particle Size", Journal of the Franklin Institute, Vol. 204, pp. 713, 1927.

93. Lutz, J. F. and Leamer, R. W. "Pore Size Distribution as Related to the Permeability of Soils", Soil Science Society, American Proceedings, Vol. 4, pp. 28, 1939.

94. Baver, L. D. "Soil Permeability in Relation to Non-Capillary Porosity", Proceedings, Soil Science Society of America, Vol. 3, pp. 52, 1938.

95. Kottler, F. "Distribution of Particle Sizes", Journal of the Franklin Institute, Vol. 250, pp. 419, 1950.

96. Pillsbury, A. F. and Appleman, D. "Factors in Permeability Changes of Soils and Inert Granular Material", Soil Science, Vol. 59, pp. 115, 1945.

97. Dudley, F. L. and Domingo, C. E. "Effect of Water Temperature on Rate of Infiltration", Soil Science Society, American Proceedings, Vol. 8, pp. 129, 1944.

98. Given, C. V. "Flow of Water Through Granular Materials - Initial Experiments with Lead Shot", Transactions, American Geophysical Union, Part 2, Vol. 52, pp. 579, 1934.

99. Rose, H. E. "The Isothermal Flow of Gasses Through Beds of Granular Material", Proceedings, Institution of Mechanical Engineers, Vol. 153, pp. 148, 1945.

100. Haines, W. B. "Studies on the Physical Properties of Soils, IV. A Further Contribution to the Theory of Capillary Phenomenon in Soils", Journal of Agricultural Science, Vol. 17, pp. 264, 1927.

101. Donat, J. "Das Gefuge des Bodens und dessen Kennzeichnung", Transactions, Sixth Committee of the International Society of Soil Science, Vol. B, pp. 423, 1937.

Miscellaneous

102. Stefan, J., (In German), Sitzberichte Kaiserl, Akad., Wiss. Wien, Math - Naturw Klasse, Abt. 2, 69, 713 (1874).

103. Bikerman, J. J. "The Fundamentals of Tackiness and Adhesion", Journal of Colloidal Science, Vol. 2, pp. 163-175 (1947).

104. Bikerman, J. J. "The Rheology of Adhesion", Rheology Theory and Application (ed. by F. R. Eirich) Vol. 3, pp. 479, Academic Press, New York, 1960.

105. Scott, J. R. "Theory and Application of the Parallel Plate Plastometer", Transactions, Institute Rubber Ind., Vol. 7, pp. 169, August 1931.

106. Askew, F. A. "Time and Tack", Paint Technology, Vol. 9 (106), pp. 217, October 1944.

107. Mack C. "Physical Properties of Asphalt in Thin Films", Industrial Eng. Chem., Vol. 49, pp. 422, 1957.

108. Lennard-Jones, J. E. "Cohesion", Proceedings Physical Society of London, Vol. 43, Part I, pp. 461, September 1931.

109. Majidzadeh, K., and Herrin, M. "Methods of Failure and Strength of Asphalt Films Subjected to Tensile Stresses", Highway Research Board, Highway Research Record No. 67, Publication 1251, pp. 98, 1965.

110. Marek, C. R. and Herrin, M. "Tensile Behavior and Failure Characteristics of Asphalt Cements in Thin Films", University of Illinois, Private Communication, 1968.

111. Box, G. E. P. and Wilson, K. B. "On Experimental Attainment of Optimum Conditions", J. Royal Stat. Soc. B., Vol. 13, pp. 1-45, 1951.

112. Hicks, C. R. Fundamental Concepts in the Design of Experiments, Holt, Rinhart and Winston, 1965.

113. Ostle, B. Statistics in Research, Second Edition, The Iowa State University Press, 1963.

114. Tons, E. and Krokosky, E. M. "Tensile Properties of Dense Graded Bituminous Concrete", Proceedings, Association of Asphalt Paving Technologists, Vol. 32, pp. 497, 1963.

APPENDICES

APPENDIX 1

DERIVATION OF EQUATION 42 (SEE TEXT)

From Madjidzadeh and Herrin (109), page 100, Equation 2:

$$F_T = \frac{3\ \eta\ V^2}{2\ \pi\ h^5}\ \frac{dH}{dt} \quad \text{dynes}$$

Since $V^2 = \pi^2\ r^4\ h_o^2$

and $h = h_o + \Delta h$

and $1 \text{ dyne} = \frac{2.25}{10^6}$ pounds

$$F_T = \frac{10.73}{10^6} \times \frac{r^4 h_o^2}{(h_o + \Delta h)^5} \times \frac{dH}{dt} \quad \text{pounds per contact}$$

If the number of contacts across the specimen is L, and the number of contact points vertically down is M

$$F_T = \frac{10.73}{10^6}\ \frac{r^4 h_o^2}{(h_o + \Delta h)^5} \times \frac{dH}{dt} \times \frac{L}{M} \quad \text{pounds per specimen}$$

APPENDIX 2

SAMPLE CALCULATION FOR FIGURE 7 DEFINING MAXIMUM ALLOWABLE STRAIN AT 77 F

Take Figure 5

Minimum film thickness h_o for "flow" = 110 microns

Rate of extension = 10^{-3} in/min

Rate of extension, % of h_o per sec. is:

$$\%/\text{sec} = \frac{(2.54)(10)^{4}(100)}{(1000)(60)(110)} = 0.38\ \%/\text{sec}$$

Since $$\frac{r}{h_o} = \frac{(2.54)(10^{4})}{(2)(110)} = 115$$

and from Figure 8, the strain along the necked-in surface (skin) is approximately directly proportional to the r/h_o ratio, the critical strain rate in the skin is:

$$\epsilon_{critical} = 0.38 \times 115 = 43.5\ \%/\text{sec}$$

This agrees closely with Figure 7.

APPENDIX 2 (continued)

SAMPLE CALCULATION FOR FIGURE 9 DEFINING
FLOW REGION FOR ONE ASPHALT

Majidzadeh and Herrin (109, p. 114) give the following values of critical r/h_o ratios for flow at 0.02 in/min rate and various temperatures (r = 12700 microns)

40 F	critical	r/h_o = .63
60 F	"	" = 6.3
80 F	"	" = 25.4
100 F	"	" = 84.8

Using these values Figure 9 was prepared.

Sample calculation:

Critical rate of widening of h_o at 40 F, W_{crit} :

$$W_{crit} = \frac{(2)(2.54)(10^4)(100)}{(100)\,h_o} = \frac{(2)(2.54)(10^4)}{(2)(10^4)} = 2.54 \text{ \%/min}$$

but $\epsilon_{crit} = W_{crit} \times \frac{r}{h_o} = (2.54)(.63) = 1.6$ %/min

Since $W_{crit} \approx \epsilon_{crit} \times \frac{h_o}{r}$, for $\frac{r}{h_o} = 1$

W_{crit} = 1.6 %/min = rate of h_o widening for 40 F. This checks with Figure 9.

APPENDIX 3

DERIVATION FOR EQUATION 45 (TEXT)

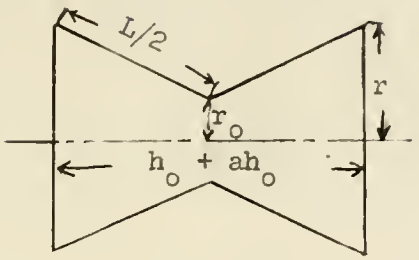

$$\text{unit strain } \epsilon = \frac{L/2 - h_o/2}{h_o/2} = \frac{L - h_o}{T}$$

$$\text{but} \quad \frac{L}{2} = \left[(r - r_o)^2 + \frac{h_o^2 (1 + a)^2}{4} \right]^{\frac{1}{2}}$$

$$L = 2 \left[(r - r_o)^2 + \frac{h_o^2 (1 + a)^2}{4} \right]^{\frac{1}{2}}$$

$$\text{or} \quad \epsilon = \frac{2}{T} \left[(r - r_o)^2 + \left(\frac{h_o + ah_o}{2} \right)^2 \right]^{\frac{1}{2}} - 1 =$$

$$= \left[\frac{4}{T^2} (r - r_o)^2 + (a + 1)^2 \right]^{\frac{1}{2}} - 1 \qquad \text{(I)}$$

$$\text{but} \quad (r - r_o) = r - \frac{(-r - ar + r\sqrt{c})}{2(a + 1)}$$

$$\text{where} \quad c = [3(3 + 2a - a^2)]^{\frac{1}{2}}$$

APPENDIX 3 (continued)

and $$(r - r_o)^2 = \frac{r^2}{4}\left[9 - \frac{6\sqrt{c}}{a+1} + \frac{c}{(a+1)^2}\right]$$

Substituting in (I)

$$\epsilon = \left\{ \frac{r^2}{h_o^2}\left[9 - \frac{6(9 + 6a - 3a^2)^{\frac{1}{2}}}{a+1} + \frac{9 + 6a - 3a^2}{(a+1)^2}\right] + (a+1)^2 - 1 \right\}^{\frac{1}{2}}$$

APPENDIX 4

COMPARISON OF MEASURED ELLIPSOID VOLUMES WITH VOLUMES BY WATER DISPLACEMENT METHOD

Numbers are percentages of difference between the two methods

Rock → / Volume ↓	CL	CG	RG	Ti.	n	X_{ij}^2
	+ 10.8	+ 2.0	+ 5.3			
	- 16.8	- 6.1	- 8.3			
	+ 9.9	+ 1.3	+ 12.6			
	+ .3	- 11.2	- 7.4			764.1
4	- 8.3	- 4.4	+ 10.4	10.1	30	722.0
	- 8.7	+ 2.1	- 11.7			822.7
	- 1.0	- 8.6	+ 9.4			2308.8
	+ 2.8	+ 17.9	- 12.7			
	+ 5.4	+ 11.6	- 0.8			
	+ 9.2	+ 1.0	+ 4.1			
	- 3.2	- 12.1	+ 7.0			
	- 7.1	+ 8.9	- 5.8			
	+ 7.9	+ 10.5	- 11.9			
	- 1.4	+ 6.2	- 0.3			
	+ 1.3	- 2.9	- 6.3			741.2
0.4	- 11.8	- 2.6	+ 13.4	7.7	30	575.9
	- 6.8	+ 7.6	+ 3.8			640.2
	+ 1.4	- 3.6	+ 6.5			1957.3
	+ 4.8	- 10.7	- 10.9			
	+ 20.1	+ 1.1	+ 4.6			

APPENDIX 4 (continued)

	CL	CG	RG	Ti.	n	X_{ij}^2
	+ 9.9	- 8.0	+ 3.5			
	- 18.3	+ 2.2	- 2.8			
	+ 7.6	+ 4.6	+ 16.2			
	- 12.1	- 7.2	+ 3.8			
	- 1.3	+ 11.4	- 6.2			767.6
0.04	+ 3.1	+ 3.2	- 6.5	- 2.4	30	329.2
	- 1.3	- 2.0	- 7.1			601.0
	+ 2.6	+ 2.8	- 6.1			1697.8
	+ 0.6	- 1.3	- 7.4			
	+ 10.5	- 5.8	+ 9.0			

$T._j$	10.1	7.9	- 2.6	$T.. = 15.4$
n	30	30	30	$N = 90$
	764.1	722.0	822.7	
	741.2	575.9	640.2	
ΣX_{ij}^2	767.4	329.2	601.0	
	2272.7	1627.1	2063.9	$\Sigma\Sigma X_{ij}^2 = 5963.7$

Volume Difference Analysis

for CL-4 Stone

Model: $d_i = \bar{D} + \epsilon$ (Correlated Samples)

H: $\bar{D} = 0$ $\bar{D} = .36$

$$S_{\bar{d}} = \sqrt{\frac{s^2}{10}}$$

$$s^2 = \frac{764.1 - \frac{(3.6)^2}{10}}{9} = 84.4$$

$$S_{\bar{d}} = \sqrt{\frac{84.8}{10}} = 2.9$$

APPENDIX 4 (continued)

$$t = \frac{\bar{d}}{S_{\bar{d}}} = \frac{.36}{2.9} = .12$$

$$t_{9\ (5)} = 2.26 \qquad .12 < 2.26 \quad \text{Hypothesis accepted}$$

Similar results were obtained for:

	CG-4	RG-4
CL-0.4	CG-0.4	RG-0.4
CL-0.04	CG-0.04	RG-0.04

In addition, volume difference analyses were performed for:

(1) CL-4, CL-0.4, CL-0.04 combined

(2) CG-4, CG-0.4, CG-0.04 combined

(3) RG-4, RG-0.4, RG-0.04 combined

(4) CL-4, CG-4, RG-4 combined

(5) CL-0.4, CG-0.4, RG-0.4 combined

(6) CL-0.04, CG-0.04, RG-0.04 combined

(7) All nine combinations

No significant differences were found.

APPENDIX 5

ANALYSIS OF ℓ/s RATIOS

Hypothesis: Average ℓ/s ratios for CL are equal (numbers are actual ratios)

Volume of Rock, cc

4	0.4	0.04
3.3	1.9	2.5
2.0	4.3	3.2
2.1	4.3	2.5
2.7	3.5	3.4
3.1	3.7	2.5
2.5	3.7	3.5
2.6	2.4	4.4
2.0	3.7	3.6
2.9	3.4	2.1
1.9	5.5	2.1
$T._j$ 25.1	36.4	29.8
n 10	10	10
ΣX_{ij}^2 65.2	141.5	93.9

$T.. = 91.3$

$N = 30$

$\Sigma\Sigma X_{ij}^2 = 300.6$

$$SS_{total} = \Sigma(X_{ij})^2 - \frac{T..^2}{N} = 300.6 - \frac{(91.3)^2}{30} = 22.8$$

$$SS_{treat} = \Sigma(T._j)^2/n - \frac{(T..)^2}{N} = \frac{(25.1)^2+(36.4)^2+(29.8)^2}{10} - \frac{(91.3)^2}{30} = 6.5$$

$$SS_{err.} = SS_{tot.} - SS_{treat.} = 22.8 - 6.5 = 16.3$$

APPENDIX 5 (continued)

$$F_{2,27} = 5.4$$

$$F_{2,27(.99)} = 5.45$$

$$5.40 < 5.45$$

Hypothesis accepted

Randomly chosen Crushed Gravel (CG) and Rounded Gravel (RG) pieces had the following ℓ/s ratios:

Crushed Gravel

Volume of Rock, cc

4	0.4	0.04
2.8	3.0	1.3
1.9	2.9	3.6
5.6	5.3	1.7
2.3	3.8	3.3
1.8	2.3	4.0
1.8	1.8	2.0
1.8	5.7	2.0
2.5	2.8	1.7
3.3	2.8	2.0
2.7	4.0	2.8

APPENDIX 5 (continued)

Rounded Gravel

Volume of Rock, cc

4	0.4	0.04
1.9	3.5	1.7
3.6	1.4	1.8
1.7	2.6	1.7
1.6	2.4	2.8
3.2	1.7	2.6
1.3	2.6	1.9
1.9	2.3	1.7
1.9	2.2	1.4
2.1	2.1	2.0
2.1	2.6	2.0

For the sake of brevity ℓ/m and m/s ratios are given only in graphical form, Figure 15. Detailed data are available from the author.

APPENDIX 6

ANALYSIS FOR NUMBER OF CONTACT POINTS

Hypothesis: Average number of contact points are equal in the following rocks:

CL-4	CL-0.04	RG-4	RG-0.04	Marbles

(Number of contact points; each number is an average for 10 rocks)

7.6	7.4	7.6	7.0	7.6
8.0	7.8	7.2	7.8	8.2
7.2	8.6	7.4	7.6	7.2
7.6	7.4	7.2	7.6	8.0

Coded $X' = \frac{X-7.6}{.1}$ $\qquad \bar{X} = 7.6$

0	-2	0	-6	0	
4	+2	+4	+2	+6	
-4	+10	-2	0	-4	
0	-2	-4	0	+4	
$T._j$	0	+8	-2	-4	+6	$T.. = +8$
n	4	4	4	4	4	$N = 20$
ΣX_{ij}	32	112	36	40	68	$\Sigma\Sigma X_{ij}^2 = 288$

$$SS_{total} = 288 - \frac{64}{20} = 285$$

$$SS_{treat} = \frac{120}{4} - 3 = 27$$

$$SS_{err} = 261$$

$F_{4,15} = .39$ $\qquad F_{4,15(.95)} = 3.06$ $\qquad .39 < 3.06$

Hypothesis accepted

APPENDIX 7

ANOVA FOR FORCE AT 60 F, TENSION

	Source	df	MS	F
A	(Rocks)	1	30	.35
B	(Rock Size)	1	30800	366.67*
A x B		1	81	.96
C	(Asphalt Cont.)	1	1560	18.57*
A x C		1	81	.96
B x C		1	1936	23.04*
A x B x C		1	132	--
D	(Rate of Def.)	1	210222	2502.64*
A x D		1	4	.04
B x D		1	24646	293.40*
A x B x D		1	12	--
C x D		1	1849	22.01*
A x C x D		1	72	--
B x C x D		1	1892	--
A x B x C x D		1	121	--

Pure error using 5 replications

$$\epsilon_{pure} = 208$$

BCD - significant at the 95% level

Using 4 remaining higher interactions for error:

$$\epsilon = 84 \text{ with } 4 \text{ df}$$

$$F_{1,4(.95)} = 7.71$$

* Significant at the 95% level.

APPENDIX 7 (continued)

ANOVA FOR FORCE AT 80 F, TENSION

Source	df	MS	F
A	1	281	1.13
B	1	86583	347.72*
A x B	1	150	.60
C	1	12266	49.26*
A x C	1	233	.94
B x C	1	8418	33.81*
A x B x C	1	150	--
D	1	845940	3397.35*
A x D	1	175	.70
B x D	1	78821	316.55*
A x B x D	1	315	--
C x D	1	10868	43.65*
A x C x D	1	218	--
B x C x D	1	8696	--
A x B x C x D	1	315	--

Pure error using 5 replications:

$$\epsilon_{pure} = 171$$

BCD - significant at the 95% level

Using 4 remaining higher interactions for error

$$\epsilon = 249 \text{ with } 4 \text{ df}$$

$$F_{1,4(.95)} = 7.71$$

* Significant at the 95% level.

APPENDIX 7 (continued)

ANOVA FOR FORCE AT 100 F, TENSION

Source	df	MS	F
A	1	163	2.86
B	1	7966	139.75
A x B	1	8	.14
C	1	798	14*
A x C	1	150	2.63
B x C	1	8	.14
A x B x C	1	60	--
D	1	41923	735.49
A x D	1	150	2.63
B x D	1	7353	129*
A x B x D	1	5	--
C x D	1	716	12.56
A x C x D	1	162	--
B x C x D	1	5	--
A x B x C x D	1	53	--

Pure error using 5 replications

$$\epsilon_{pure} = 61$$

None of the higher interactions are significant.

Using all 5 higher interactions for error

$$\epsilon = 57 \text{ with } 5 \text{ df}$$

$$F_{1,5(.95)} = 661$$

* Significant at the 95% level.

APPENDIX 7 (continued)

ANOVA FOR FORCE AT 60 F, COMPRESSION

Source	df	MS	F
A	1	18	.03
B	1	162208	298.72*
A x B	1	4456	8.20
C	1	6520	12.00*
A x C	1	2328	4.28
B x C	1	3164	5.82
A x B x C	1	452	--
D	1	1612265	2969.18*
A x D	1	0	0
B x D	1	88358	162.72*
A x B x D	1	1106	--
C x D	1	4128	7.60
A x C x D	1	2678	--
B x C x D	1	2376	--
A x B x C x D	1	76	--

Pure error using 5 replications

$$\epsilon_{pure} = 248$$

BCD and ACD - significant at 95% level.

Using higher interactions, except BCD and ACD, for error:

$$\epsilon = 543 \text{ with } 3 \text{ df}$$

$$F_{1,3(.95)} = 10.1$$

* Significant at the 95% level.

APPENDIX 7 (continued)

ANOVA FOR FORCE AT 80 F, COMPRESSION

Source	df	MS	F
A	1	4	.12
B	1	4225	132.03*
A x B	1	64	2.00
C	1	2704	84.50*
A x C	1	1	.03
B x C	1	2209	69.03*
A x B x C	1	16	--
D	1	49952	1561.00*
A x D	1	6	.18
B x D	1	3906	122.07*
A x B x D	1	100	--
C x D	1	2756	86.12*
A x C x D	1	2	--
B x C x D	1	2352	--
A x B x C x D	1	12	--

Pure error using 5 replications:

$$\epsilon_{pure} = 157$$

BCD - significant at the 95% level

Using 4 remaining higher interactions for error:

$$\epsilon = 32 \text{ with } 4 \text{ df}$$

$$F_{1,4(.95)} = 7.71$$

* Significant at the 95% level.

APPENDIX 7 (continued)

ANOVA FOR FORCE AT 100 F, COMPRESSION

Source	df	MS	F
A	1	1388	1.76
B	1	159800	202.27*
A x B	1	2836	3.58
C	1	9361	11.84*
A x C	1	150	.18
B x C	1	116	.14
A x B x C	1	1444	--
D	1	552421	699.26*
A x D	1	1425	1.80
B x D	1	156223	197.75*
A x B x D	1	2704	--
C x D	1	2730	3.46
A x C x D	1	163	--
B x C x D	1	203	--
A x B x C x D	1	1351	--

Pure error using 5 replications:

$$\epsilon_{pure} = 292$$

ABD - significant at the 95% level

Using 4 remaining higher interactions for error:

$$\epsilon = 790 \text{ with } 4 \text{ df}$$

$$F_{1,4(.95)} = 7.71$$

* Significant at the 95% level.

APPENDIX 8

ANOVA FOR ENERGY AT 60 F, TENSION

Source	df	MS	F
A	1	9168	1.42
B	1	743475	114.96*
A x B	1	27143	4.20
C	1	54873	8.48*
A x C	1	1351	.20
B x C	1	26488	4.09
A x B x C	1	3691	--
D	1	3552283	549.29*
A x D	1	9361	1.44
B x D	1	585608	90.55*
A x B x D	1	16193	--
C x D	1	16606	2.56
A x C x D	1	1661	--
B x C x D	1	23948	--
A x B x C x D	1	4456	--

Pure error using 5 replications:

$$\epsilon_{pure} = 3319$$

BCD - significant at the 95% level

Using 4 remaining higher interactions for error:

$$\epsilon = 6467 \text{ with } 4 \text{ df}$$

$$F_{1,4(.95)} = 7.71$$

* Significant at the 95% level.

APPENDIX 8 (continued)

ANOVA FOR ENERGY AT 80 F, TENSION

Source	df	MS	F
A	1	371	2.92
B	1	24414	192.23*
A x B	1	218	1.71
C	1	3844	30.27*
A x C	1	68	.53
B x C	1	2678	21.08*
A x B x C	1	127	--
D	1	136171	1072.21*
A x D	1	371	2.92
B x D	1	22575	177.75*
A x B x D	1	163	--
C x D	1	4356	34.29*
A x C x D	1	68	--
B x C x D	1	2576	--
A x B x C x D	1	150	--

Pure error using 5 replications:

$$\epsilon_{pure} = 109$$

BCD - significant at the 95% level

Using 4 remaining higher interactions for error:

$$\epsilon = 127 \text{ with } 4 \text{ df}$$

$$F_{1,4(.95)} = 7.71$$

* Significant at the 95% level.

APPENDIX 8 (continued)

ANOVA FOR ENERGY AT 100 F, TENSION

Source	df	MS	F
A	1	390	.82
B	1	88061	187.36*
A x B	1	638	1.35
C	1	2943	6.26
A x C	1	10973	23.34*
B x C	1	6440	13.70*
A x B x C	1	4935	--
D	1	859793	1829.34*
A x D	1	410	.87
B x D	1	85996	182.97*
A x B x D	1	613	--
C x D	1	3108	6.61*
A x C x D	1	11078	--
B x C x D	1	6360	--
A x B x C x D	1	4865	--

Pure error using 5 replications:

$$\epsilon_{pure} = 470$$

Except for ABD - all higher interactions are large

Use ϵ_{pure} for ϵ

$\epsilon = 470$ with 5 df

$$F_{1,5(.95)} = 6.61$$

* Significant at the 95% level.

APPENDIX 8 (continued)

ANOVA FOR ENERGY AT 60 F, COMPRESSION

Source	df	MS	F
A	1	1208	1.41
B	1	41108	48.07*
A x B	1	410	.48
C	1	430	.50
A x C	1	2475	2.89
B x C	1	946	1.10
A x B x C	1	410	--
D	1	803264	939.49*
A x D	1	1242	1.45
B x D	1	13748	16.07*
A x B x D	1	390	--
C x D	1	86	.10
A x C x D	1	2525	--
B x C x D	1	856	--
A x B x C x D	1	95	--

Pure error using 5 replicates:

$$\epsilon_{pure} = 642$$

None of the higher interactions are significant at the 95% level

Using all 5 higher interactions for error:

$$\epsilon = 855 \text{ with } 5 \text{ df}$$

$$F_{1,5(.95)} = 6.61$$

* Significant at the 95% level.

APPENDIX 8 (continued)

ANOVA FOR ENERGY AT 80 F, COMPRESSION

Source	df	MS	F
A	1	742	2.82
B	1	45903	174.53*
A x B	1	653	2.48
C	1	34689	131.89*
A x C	1	298	1.13
B x C	1	28646	108.92*
A x B x C	1	248	--
D	1	762566	2899.49*
A x D	1	588	2.23
B x D	1	43786	166.48*
A x B x D	1	439	--
C x D	1	35063	133.31*
A x C x D	1	203	--
B x C x D	1	30363	--
A x B x C x D	1	162	--

Pure error using 5 replicates

$$\epsilon_{pure} = 1456$$

BCD - significant at the 95% level

Using 4 remaining higher interactions for error:

$$\epsilon = 263 \text{ with } 5 \text{ df}$$

$$F_{1,4(.95)} = 7.71$$

* Significant at the 95% level.

APPENDIX 8 (continued)

ANOVA FOR ENERGY AT 100 F, COMPRESSION

Source	df	MS	F
A	1	4	.05
B	1	17956	224.45*
A x B	1	306	3.82
C	1	1369	17.11*
A x C	1	6	.08
B x C	1	12	.15
A x B x C	1	36	.45
D	1	30490	381.12*
A x D	1	4	.05
B x D	1	17424	217.80*
A x B x D	1	306	3.82
C x D	1	1369	17.11*
A x C x D	1	6	.08
B x C x D	1	12	.15
A x B x C x D	1	36	.45

Pure error using 5 replicates:

$$\epsilon_{pure} = 426$$

None of the higher interactions are significant

Using all 5 higher interactions for error:

$$\epsilon = 80 \text{ with } 5 \text{ df}$$

$$F_{1,5(.95)} = 6.61$$

* Significant at the 95% level.

APPENDIX 9

CALCULATED VALUES FOR THEORETICAL "STRENGTH"

(a) Size of Contact Radius "r", Microns

	Average Height, h_o, Microns		
	2 x 10 = 20	2 x 20 = 40	2 x 30 = 60
0.04 cc Rocks	310	370	430
0.4 cc Rocks	740	800	857
4 cc Rocks	1430	1520	1600

(b) Values for L and M

	L	M	L/M
0.04 cc Rocks	650	28	23
0.4 cc Rocks	130	13	10
4 cc Rocks	20	4.5	4.5

(c) Sample Calculation of Theoretical Peak Tensile Force for:

0.04 cc rocks
30 - micron film
0.3 %/min. rate
100 F temperature

APPENDIX 9 (continued)

Take Equation 42

$$F_t = \frac{10.73}{10^6} \eta \times \frac{r^4 h_o^2}{(h_o + \Delta h)} \times \frac{L}{M} \times \frac{dH}{dt} \text{ (Pounds)}$$

η = 1.7 x 10^5 poises at 100 F

r = 430 microns = 0.043 cm

h_o = 60 microns = 0.006 cm

$\Delta h = \frac{\text{strain at peak force}}{\text{number of films}} = \frac{(0.003)(4)(2.54)}{28} = 0.001$ cm

$\frac{L}{M}$ = 23

$\frac{dH}{dt} = \frac{(0.003)(4)(2.54)}{60} = 5.08 \times 10^{-4}$ cm/sec

Placing all the values in Equation 42:

$$F_t = \frac{(10.73)(1.7)(10)^5(4.3)^4(6^2)(10^{15})(5.08)(23)}{10^6 \quad (10)^8 \ (10^6)(7)^5 \ (10^4)} = 0.16 \text{ Pounds}$$

This value is shown in Fig. 47

(d) Sample Calculation of Theoretical Shear Force for:

0.04 cc rocks

30 - micron film

0.3 %/min. rate

100 F temperature

APPENDIX 9 (continued)

Take Equation 58:

$$F_s = \frac{2.248}{10^6} \times \eta \times \frac{dx}{dh_o} \times A$$

$\eta = 1.7 \times 10^5$ poises at 100 F

Assuming 45^o sliding angle, shear rate

$$\frac{dx}{dh} = \frac{(5.08)(10^3)(2)}{(10^4)(6)} = 0.17 \text{ sec}^{-1}$$

A = Total asphalt cross-sectional area under shear for 45^o sliding angle

$$A = (3.14)(.043)(.043)(650)(2)$$

Thus finally

$$F_s = \frac{2.248}{10^6} \times \frac{(1.7)(10^5)}{1} \times \frac{(3.14)(4.3)(.43)(650)(2)}{(10)\quad(10^2)} = 0.25 \text{ Pounds}$$

This value is shown in Fig. 55

(c) Sample Calculation of Theoretical Compressive Force

Using Equation 57

$$F_c = \frac{10.73}{10^6} \times \eta \times \frac{r^4}{h_o^3} \times \frac{L}{M} \times \frac{dH}{dt}$$

Calculations are similar to Part C, Appendix 9.

APPENDIX 10

DATA FOR CYCLIC TESTS

(1) Sinusoidal Deformation (see Fig. 68)

(2) Max. Deformation 1%

(3) Temperature 80 F

(4) Total 20 cycles each specimen

(5) Asphalt film - 20 microns

(6) Type rocks - gravel and limestone

(7) Size rocks - 0.04 cc and 4 cc

(8) Cycles per min. - 0.6 and 6

(9) Statistical design - 2^3

(10) Factorial, 2 units per cell

(11) The response variable chosen was average peak force, in pounds obtained by averaging 40 peak forces (20 cycles) from each specimen.

AVERAGE FORCE, CYCLIC TESTS, POUNDS x 10

		Gravel		Limestone	
		0.04 cc	4 cc	0.04 cc	4 cc
Cycles per Second	0.01	49 65	17 29	58 51	27 24
	0.1	342 367	188 174	318 317	185 188

APPENDIX 10 (continued)

ANOVA FOR AVERAGE FORCE, CYCLIC TESTS

Source	df	MS	F
R (Rocks)	1	248	3.06
S (Size)	1	33764	416
R x S	1	564	6.92
C (Frequency)	1	193380	2380
C x R	1	248	3.06
C x S	1	14581	179
C x R x S	1	351	4.34
Error	8	81	

Since $F_{(.95)\ 1,8} = 5.32$, Rocks are not "significant."

VITA

VITA

Egons Tons was born on April 26, 1925, in Eleja, Latvia, where he received his primary and secondary education. In 1944 he left Latvia and spent the following five years as a refugee in Germany. In 1948 he enrolled in the Baltic University in Hamburg.

In 1949 he came to the United States as an immigrant and has since become a United States citizen.

In the United States Egons Tons continued his education at Antioch College where he had a full scholarship and from which he received a B.S. in Civil Engineering. After a year's work as laboratory engineer at the National Crushed Stone Association, he went on to the Massachusetts Institute of Technology and earned his M.S. in 1954.

For the following ten years he was associated with the Massachusetts Institute of Technology, first as research engineer and, during the final five years, as assistant professor. During this time he carried out research in the Institute's bituminous laboratory and published numerous professional papers. His teaching assignments were mostly in the field of bituminous as well as other materials used in the construction of highways.

In 1964 Egons Tons came to Purdue University as instructor and graduate student and began work toward his doctorate.

Egons Tons is married and has three children.